TFA

ACTA FACULTATIS TECHNICAE

TECHNICAL UNIVERSITY IN ZVOLEN

2

ISSUE: XXIX ZVOLEN 2024

Medzinárodný zbor recenzentov / International Reviewers Board

TABLE OF CONTENTS

SCIENTIFIC PAPERS

SCIENTIFIC PAPERS

ACTA FACULTATIS TECHNICAE
ZVOLEN – SLOVAKIA

XXIX
2024

APPLICATION OF FMEA FOR FAILURE ANALYSIS IN MICROBREWERY PRODUCTION TECHNOLOGY

APLIKACE METODY FMEA PRO ANALÝZU PORUCH VE VÝROBNÍ TECHNOLOGII MINIPIVOVARŮ

Tomáš Vaško[1], Zdeněk Aleš[2]

[1] *Department of Quality and Dependability of Machines, Faculty of Engineering, Czech University of Life Sciences Prague, 165 00 Prague - Suchdol, Czech Republic, vaskot@tf.czu.cz*
[2] *Department of Quality and Dependability of Machines, Faculty of Engineering, Czech University of Life Sciences Prague, 165 00 Prague - Suchdol, Czech Republic, ales@tf.czu.cz*

ABSTRACT: The global beer production industry has seen a rise in demand for craft beers in recent years, necessitating their production in microbreweries, which represent a significant manufacturing segment. Beer production is a complex process requiring sophisticated equipment. To achieve optimal production outcomes, it is crucial for microbreweries to maintain a well-managed quality control of the production equipment. Downtimes due to mechanical failures not only lead to production losses but can also adversely affect the final product. In this context, the application of the Failure Mode and Effects Analysis (FMEA) method proves particularly useful, helping to identify potential failures in the production equipment. This allows brewery staff to proactively address issues that could negatively impact the performance and lifespan of the equipment. This article examines the implementation of the FMEA method in the microbrewery setting to address concerns not only about the reliability of the production equipment but also about the safety and quality of the final product. After conducting a literature review on the application of the FMEA method in other food industries, a case study was carried out in a microbrewery operation. Specifically, the FMEA method was applied to the mash copper, which, from a long-term perspective, represents the weakest link in terms of reliability in the studied operation. The evaluation of critical points in the mash copper led to the calculation of the Risk Priority Number (RPN). The inability to expel brewing vapors through the chimney during the mashing and wort boiling process was identified as the most severe failure with the highest RPN, particularly threatening the qualitative parameters of the final product. The failure of isolated steam conduits to transfer heat to the mash copper was deemed the most severe failure in terms of executing the brewing process with the most significant impact on the operation's economy. Preventive, predictive, and proactive maintenance emerged as the effective measures. Thanks to these approaches, it is ensured that there will be a minimization of major failures that will result in the outage of the entire technology.

Key words: food safety and quality; machine dependability; mash copper; risk priority number

ABSTRAKT: Výroba piva je globálně rozšířená. V posledních letech roste poptávka po řemeslném pivu, což souvisí s nutností jeho výroby v minipivovarech, které představují významný výrobní segment. Výroba piva je složitý proces, pro jehož realizaci je nutné využít sofistikované výrobní zařízení. Pro dosažení co nejlepších výrobních výsledků je podstatné, aby minipivovary měly dobře nastaven management jakosti výrobního zařízení. Prostoje způsobené mechanickými poruchami vedou nejen ke ztrátám ve výrobě, ale mohou také negativně ovlivnit finální produkt výroby. V tomto kontextu je zvláště užitečná aplikace metody FMEA (Failure Mode and Effects Analysis), která pomáhá identifikovat potenciální poruchy na výrobním zařízením. Zaměstnanci pivovaru tedy mohou preventivně řešit problémy, které by mohly negativně ovlivnit výkon a životnost výrobního zařízení. Tento článek zkoumá implementaci metody FMEA v prostředí minipivovarů s cílem řešit nejen obavy o spolehlivost výrobního zařízení, ale také obavy o bezpečnost a kvalitu finálního produktu. Po provedení literární rešerše o aplikaci metody FMEA v jiných potravinářských odvětví byla provedena případová studie v provozu minipivovaru. Konkrétně byla metoda FMEA aplikována na rmutomladinovou pánev, která z dlouhodobé perspektivy představuje ve zkoumaném provozu z hlediska spolehlivosti nejslabší místo. Na základě popsání a posouzení kritických míst ve rmutomladinové pánvi bylo vypočítáno rizikové číslo RPN (Risk Priority Number). Jako nejzávažnější porucha s nejvyšším RPN byla vyhodnocena neschopnost odvodu brýdových par komínem během rmutování a chmelovaru. Tato porucha ohrožuje zejména kvalitativní parametry výsledného produktu. Neschopnost izolovaného parního vedení přenášet teplo do rmutomladinové pánve byla vyhodnocena jako nejzávažnější porucha z hlediska realizace samotného varného procesu s nejzásadnějším dopadem na ekonomiku provozu. Jako účinné opatření se zdá být preventivní, prediktivní a proaktivní údržba. Díky těmto přístupům je zajištěno, že dojde k minimalizaci havarijních poruch, které budou mít za následek výpadek celé technologie.

Klíčová slova: bezpečnost a kvalita potravin; spolehlivost strojů; rmutomladinová pánev; rizikové číslo

INTRODUCTION

Beer is among the most widespread alcoholic beverages worldwide (Kunze, 2010). For example, in the European Union, according to European Beer Trends Statistics Report (2023), 358,230,000 hl of beer was produced in 9,684 breweries in 2022. Of this, 20,550,000 hectoliters were produced in the Czech Republic, where the consumption of this beverage per person in the world has long been the highest. In 2022, it was 136 liters. Not only in the Czech Republic the demand for craft beer has been growing in recent years. This is related to the necessity of producing such beer by microbreweries, which thus represent a non-negligible production segment. For instance, in 2016 there were more than 19,000 breweries worldwide, with 94% of them considered microbreweries. As of 2018, there were more than 400 microbreweries in the Czech Republic, whose share in the total beer production in the country was 2% (Baiano, 2021). Beer production is a complex food technology (Briggs et al., 2004). This is logically related to the necessity of using sophisticated technical equipment in its production, and thus also the knowledge and application of reliability tools.

Reliability of machines and equipment is essential for ensuring consistent production quality and operational efficiency in all companies. Downtime due to mechanical failures not only leads to production losses but can also affect the quality of the brew. Therefore, implementing rigorous maintenance strategies and ensuring the life span of machinery are critical considerations. The application of Failure Modes and Effects Analysis (FMEA) is particularly useful in this context. FMEA helps identify potential failures in the machin-

ery and equipment. By analyzing failure modes, their causes, and their potential effects, FMEA allows brewery employees to preemptively address issues that could impact machine performance and lifespan (Sharma and Srivastava, 2018). This proactive approach logically not only helps in optimizing the operational life of the equipment but also ensures the consistent quality and taste of the beer produced.

One of the authors examines the use of the FMEA method in a small and medium-sized enterprise in the food industry. FMEA is used to identify potential risks in the bread production process that could endanger worker safety. The method assesses risks based on three criteria: severity, occurrence probability, and detection capability. Data was collected through questionnaires filled out by three bakery workers, based on which Risk Priority Number (RPN) was calculated. The highest RPN was obtained for the risk of overheating and dehydration of workers due to high temperatures in the production area. The results showed that seven risk factors exceeded the critical value and require priority intervention. This case study article highlights the importance of implementing safety and health measures in the workplace to ensure safety and increase worker productivity (Fithri et al., 2021).

Application FMEA and cause and effect analysis can be applied on processing of ready to eat vegetables. Focus is aimed on enhancing the safety protocols in the manufacturing of ready-to-eat vegetables through the systematic application of FMEA. It identifies critical control points in the processes such as receiving, storage, distribution, packaging, and cooling, where the initial Risk Priority Numbers indicated high risks. Implementing corrective actions significantly reduced these RPN values, demonstrating the effectiveness of the interventions. Additionally, the study by Varzakas and Arvanitoyannis (2009) utilized Ishikawa diagrams to support the FMEA findings, reinforcing the reliability of the risk assessments. The research underscores the importance of integrating FMEA and cause and effect analysis within the ISO22000 standards to ensure comprehensive risk management in food processing. This integration not only helps in identifying potential failures proactively but also ensures that the manufacturing process adheres to safety standards, thereby safeguarding consumer health. The reduction in RPN post-correction highlights the necessity of such structured analyses in maintaining the integrity and safety of food production processes. Result of research strongly recommends the mandatory inclusion of FMEA in the ISO22000 system for systematic risk identification and mitigation in the production of ready-to-eat vegetables (Varzakas and Arvanitoyannis, 2009).

The results of other study showed that the highest RPN were recorded during the stages of cold smoking, drying-ripening, reception, shredding, and raw material storage, as well as during leakage and strengthening of meat. These findings led to the formulation of recommendations for improving and expanding the application of the FMEA method within food safety management systems. The study effectively demonstrated how integrating FMEA with HACCP principles allows for a more accurate quantitative assessment and prioritization of risks, thereby enhancing the control measures and corrective actions in the food safety management of raw-dried salami production (Pop et al., 2019). The search for problem areas in food production in small enterprises was also dealt with by Liong et al. (2016), who identified the last stage of production, i.e. filling into packaging, as the most critical point in terms of time consumption.

It follows that applying the FMEA method in microbreweries might significantly help

in identifying and mitigating potential risks associated with equipment failures, inconsistencies in brewing processes, and maintenance issues, thereby ensuring equipment reliability and consistent product quality. The presented article aims to apply the FMEA method within the environment of microbrewery technology.

MATERIAL AND METHODS

When assessing individual microbreweries, it can be stated that the technological process and technical equipment are similar across microbreweries. However, it may vary slightly across individual operations, for example depending on the level of automation or the type of product range produced.

The following text describes the general and basic process of beer production (as evidenced by the relevant citations), however, it is identical to the process of beer production in the Research and Training Microbrewery – Suchdolský Jeník (RTM), which is the subject of this article. It is a brewery that belongs to Department of Technological Equipment of Buildings (Faculty of Engineering, Czech University of Life Sciences Prague) and has been in operation since 2006. In addition to research and training purposes, it is also used for commercial beer production. The volume of one batch is 10 hl of wort, while the annual production is around 150 hl. A diagram of the main technical equipment of the RTM is shown in Fig. 1. This equipment is almost identical to microbreweries of a similar size and focus.

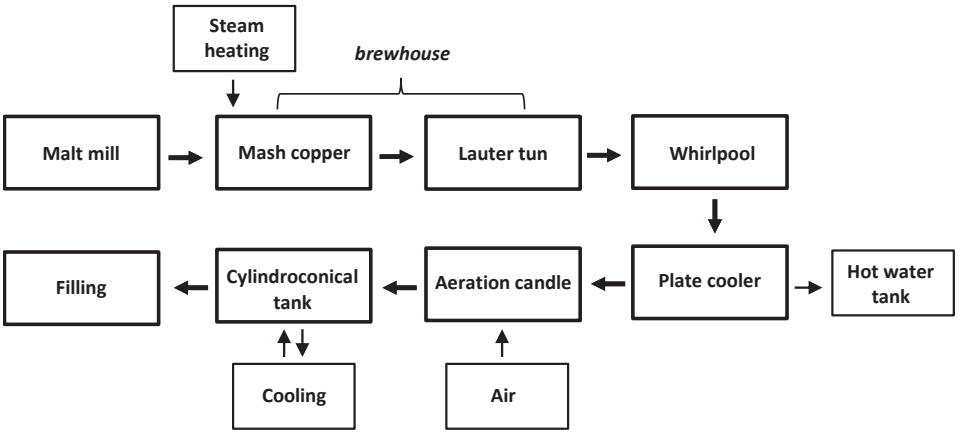

Fig. 1 Diagram of the main technical equipment in microbreweries
Obr. 1 Schéma hlavního technického vybavení minipivovarů

First, the malt is ground using a malt mill. The resulting malt grist is poured into the water prepared in the mash copper. The resulting mash is heated here to the given technological temperatures, at which enzymatic splitting of the stored malt substances takes place (Kunze, 2010). The mash is then pumped into a lauter tun, where the sweet wort (hydrolyzed malt liquor) is separated from the spent grains (malt coating layers). The sweet wort is pumped back into the mash copper, where it is brought to a boil and boiled with hops to form the production intermediate, which is wort (Basařová et al., 2010). The

wort contains coarse hop sludge, which must be removed using a whirlpool. The hot wort, freed from coarse hop sludge, is further cooled using a plate cooler to the fermentation temperature (Kosař and Procházka, 2000).

The cooled wort without coarse hop sludge is pumped into the cylindroconical tank (CCT) through an aeration candle located in a stainless-steel pipe, which ensures saturation of the wort with oxygen. In CCT, the wort is mixed with yeast, which starts the main fermentation process (Bamforth, 2006). During the main fermentation, which lasts about a week, the yeast metabolizes fermentable sugars into ethanol, carbon dioxide and other products. During the main fermentation, it is necessary to regulate the temperature of the fermenting wort. The resulting intermediate product is young beer, which is then maturated at low temperature and overpressure for several weeks (Hardwick, 1995). Maturation can take place either in the same CCT as the main fermentation or in a separate storage tank. After maturation, we get fresh beer, which is already intended for consumption. However, some breweries further filter and pasteurize the beer to increase shelf life. Subsequently, the beer is filled into consumer packaging and stored (Briggs et al., 2004).

It follows from the previous text that FMEA might be principally useful in microbreweries, where process reliability and product quality are crucial. Applying FMEA within this context helps identify potential failures in the brewing process, filling and packaging systems, which can impact product quality, safety, and production efficiency. The scope of FMEA in a microbrewery can include the entire brewing, from raw material intake to final product distribution.

The FMEA begins with the identification of the scope, concentrating on these key areas. Subsequently, it is important to define the functional requirements for each process component, such as ensuring accurate temperature control during fermentation or maintaining high purity levels during filtration. Once the framework is established, potential failure modes for each component are listed. The next step involves a failure effects analysis, where the impact of each failure mode is assessed. Each identified effect is then rated for severity on a scale from 1 to 10, with 10 indicating a catastrophic impact on safety or product quality. For each cause of failure is assigned a likelihood of occurrence, rated from 1 - unlikely to 10 - highly likely. The effectiveness of failure detection is subsequently rated on a scale from 1 -highly effective to 10 – ineffective (ČSN EN IEC 60812).

Calculation of Risk Priority Number (RPN) for each failure mode is according to formula (1)

$$RPN = S \cdot O \cdot D \tag{1}$$

Where S - Severity - measures the seriousness of the consequences of a failure,
O - Occurrence - estimates the frequency at which the failure is likely to occur,
D - Detection - assesses the likelihood that the failure will be detected before it affects the customer or the final product (ČSN EN IEC 60812).

In the framework of this article, we focused on the part of production that is carried out in the mash copper (Fig. 2), specifically, it involves mashiving in, mashing and wort boiling, i.e. operations that lead to the creation of the intermediate product of beer production, which is wort. Based on long-term experience, this technological section seems to be the most problematic in the entire production.

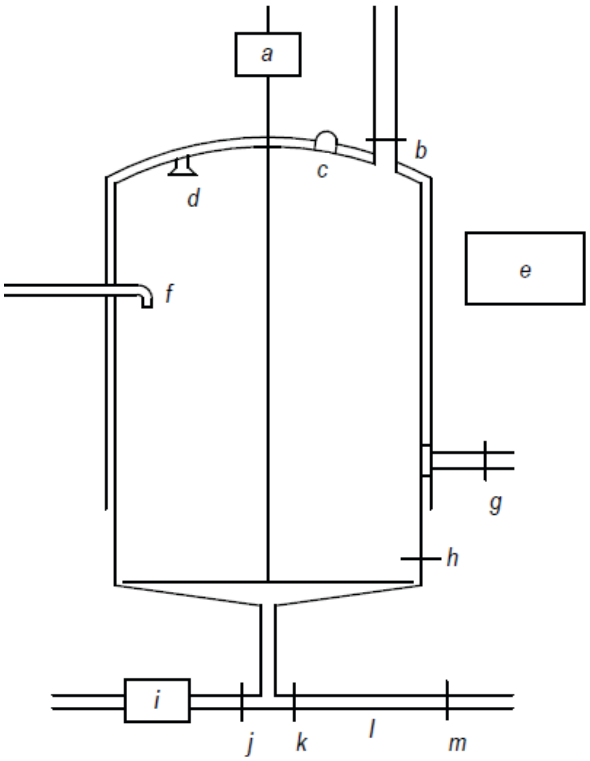

a) – engine of stirrer, b) – chimney valve, c) – light source, d) – shower head, e) – control panel, f) – lauter tap, g) – steam heating, h) – temperature sensor, i) – mash pump, j) – valve, k) – valve, l) – stainless-steel pipe, m) – ball valve (water source)

Fig. 2 Schematic drawing of the rated mash copper
Obr. 2 Schématický nákres hodnocené rmutomladinové pánve

RESULTS

When applying the FMEA method to the RTM mash copper, a total of 8 main failures were identified (see Table 1), which manifested themselves during the 18 years of beer production at this workplace.

Table 1 Application of the FMEA method to the mash copper

	Description of Failure	Potential Failure Effects	SEVERITY	Potential Failure Causes (Mechanisms)	OCCURRENCE	Current Prevention Measures	DETECTABILITY	RPN
1	the stirrer cannot be turned on	necessity of manual mixing; final product nearly unchanged	**5**	engine failure	**4**	without preventive measures	**2**	**40**
2	the chimney does not remove vapour	the vapour condenses back into the mash/wort; negative impact on the final product	**8**	deposits, clogged valve	**5**	without preventive measures	**8**	**320**
	Description of Failure	**Potential Failure Effects**	**SEVERITY**	**Potential Failure Causes (Mechanisms)**	**OCCURRENCE**	**Current Prevention Measures**	**DETECTABILITY**	**RPN**
3	malfunctioning light source	necessity to use a replacement light source; final product unchanged	**1**	broken bulb filament	**7**	without preventive measures	**1**	**7**
4	the insulated steam line does not transfer heat to the mash copper	production cannot be carried out	**10**	wear of control valves	**5**	without preventive measures	**5**	**250**
5	the control panel displays an error message of the temperature sensor	necessity to use a mobile thermometer; final product unchanged	**6**	mechanical damage to the temperature sensor itself	**7**	without preventive measures	**5**	**210**
6	the mash pump does not pump	need to use a mobile pump; time consuming, final product unchanged	**7**	engine failure	**6**	without preventive measures	**4**	**168**
7	flowing threaded flaps of stainless-steel pipes ensuring the movement of the mash	replacement of the seal, tightening of the thread; time consuming, final product unchanged	**3**	damaged seal, loose thread	**8**	without preventive measures	**3**	**72**
8	torn control lever of the ball valve ensuring water supply	need to replace the ball valve; time consuming, final product unchanged	**5**	corrosion of the control mechanism	**4**	without preventive measures	**4**	**80**

In terms of severity, the inability of the insulated steam line to transfer heat to the mash copper was evaluated as the most critical failure. On the contrary, the lowest severity was assigned to the malfunctioning mash copper lighting. When assessing the occurrence of the failure, the flowing threaded flaps of stainless-steel pipes ensuring the movement of the mash can be considered the most critical. On the contrary, the least common failure is the inability to turn on the stirrer and the broken control lever of the ball valve ensuring the water supply. In the detectability rating, the biggest risk is non-functioning lighting, while the best detectable failure is the chimney‘s inability to vent vapour.

However, considering the severity, occurrence and detectability of individual failures and simultaneously calculating their RPN, the 4 most risky failures with RPN above the threshold value of 100 were identified. According to the rising value of RPN, the following failures are involved: “the mash pump does not pump” (168), “the control panel displays an error message of the temperature sensor” (210), “the insulated steam line does not transfer heat to the mash copper” (250), and “the chimney does not remove vapour” (320).

DISCUSSION

From a practical point of view, it is important to be prepared for a potential failure during the production process, i.e. to have alternative solutions available, the application of which will allow the technological process of production to be completed as soon as possible and with as few deficiencies as possible. Under this assumption, the severity of the failures was evaluated in this research. Otherwise, the severity of the selected failures would be assessed more critically, and therefore the RPN would also reach higher values.

This case concerns the first mentioned failure (see Table 1). In a situation where the stirrer cannot be turned on, manual stirring is necessary. If the mash was not stirred during the decoction mashing (when the mash must be boiled), the husks of the malt would burn on the wall of the mash copper, and thus the transfer of unwanted aromatic substances into the wort. At the same time, the demand for sanitation of the mash copper would be increased, as the fired husks would create a substrate for microbial contamination (Kunze, 2010). When a manual stirrer is available, it is possible to minimize these consequences, although not completely, because manual stirring usually cannot homogenize the mash as intensively as with an automatic stirrer. In the case of boiling the sweet wort with hops (wort boiling), this problem no longer exists, as the hop mash is not prone to burning and in practice, there is often no stirring during the wort boiling, for example for reasons of energy saving. Several possible causes of agitator failure can be encountered in the wort production process. From the simple, such as a tripped circuit breaker, to irreparable failures in the operation of microbreweries, such as engine burnout.

From the point of view of the negative impact on the quality parameters of the final product, the second examined failure seems to be very serious. In the course of technological operations during the production of wort, such as boiling the mash and wort boiling, the formation of vapours. This is water vapor, which can contain substances that are technologically desirable, but also undesirable. Among the technologically desirable substances, hop essential oils can be mentioned, which give the beer the desired aroma and which partially release the vapours through the chimney into the atmosphere during the wort boiling. For this reason, hops with a high content of essential oils are added only at the end of the wort boiling. Unwanted dimethyl sulfide also escapes through steam vapors. It is a compound that arises from the thermal decomposition of precursors that are already present in the malt. If the dimethyl sulfide does not escape through the chimney into the atmosphere during the hop process, it causes undesirable sensory sensations in the

beer, specifically the aroma of "cooked vegetables" (Basařová et al., 2010). The advantage is that this failure is relatively easy to detect and can be partially solved acutely during operation, for instance by opening the top of the mash copper or activating the safety fan in the brewhouse.

On the contrary, the lowest risk for the implementation of the production process is a frequent failure, which is a malfunctioning light source of the mash copper. Here, the cause is almost always a broken bulb filament. In the event of a defect occurring during the production of wort, the problem can be provisionally easily solved with a mobile light source. Indeed, it is necessary to observe the mash in the mash copper during the production of wort, for example in order to evaluate the performance of the pump during mash transfer.

The most fundamental impact on the actual implementation of beer production is a failure in which heat is not transferred to the mash copper through an insulated steam line. If the steam generator generates heat as standard and transfers it through an insulated steam line to the control valve, where the heat transfer is stopped due to wear of the valve, it is possible to solve the problem in operating conditions at least partially by reactive maintenance. In case of more complicated failures, it is not possible to implement the production process, which results in negative effects on the economy of operation. In case of manifestation of the failure only during the brewing process, for instance at the beginning of the wort boiling, significant negative impacts on the quality parameters of the final product can be expected. We can mention, for example, insufficient isomerization of hop alpha bitter acids resulting in low sensory bitterness, non-precipitation of malt proteins with hop tannins resulting in turbidity and insufficient sterilization of the wort with the subsequent risk of microbial contamination (Briggs et al., 2004). For instance, some species of Enterobacterales bacteria are involved not only in the production of sensory undesirable substances in beer, but also in the production of toxic N-nitrosamines (Matoulková et al., 2018).

During the production of wort, it is necessary to carefully control the temperature of the batch, especially during mashing. Malt enzymes are activated at defined temperatures, which break down complex malt storage substances into simpler ones. For example, at 72°C, the enzyme alpha amylase, which breaks down starch into fermentable sugars, is best used, and therefore it is necessary to keep the mash at this temperature for a few minutes. If this temperature is exceeded, even if only by 4 °C, the alpha amylase will be denatured, so that the starch will not be split into fermentable sugars, thereby limiting the fermentation process (Kosař and Procházka, 2000). In the event of a failure of the temperature sensor, it is therefore absolutely necessary to use a replacement thermometer. The failure can also consist in a distortion of the actual temperature, which worsens the detectability and thus increases the RPN of the failure, and therefore it is advisable to check the temperature of the mash with two thermometers.

During the production of wort in RTM, the mash is transferred from the mash copper to the lauter tun and the resulting wort from the mash copper to the whirlpool using a mash pump. The mash pump thus pumps a thick suspension with temperatures of 50 to 100 °C and a volume of at least 12 hl within one batch, which puts it under considerable stress. The mash pump must also withstand acids and alkalis during its sanitation. The probability of a pump failure is therefore high. If the pump is destroyed during the batch, for instance due to a burned-out engine, it is necessary to have a mobile pump and the appropriate hoses available. Otherwise, the batch cannot be completed. A repair of such a scale is time-consuming and spoilage of the intermediate product of production would be inevitable.

Leaking threads of stainless-steel pipe flaps due to a damaged seal or loose threads due to shocks are a problem that can be solved easily. In most cases, it is sufficient to manually tighten the threads. Otherwise, production losses would be very small anyway. A slightly more serious failure occurs when the control lever of the ball valve, which ensures the water supply, breaks off. Here, it depends in which position the tear out occurs and whether it is possible to manipulate the valve at least to a limited extent, for example with pliers. In the most serious case, the ball valve must be replaced, which is a relatively simple and time-saving repair.

RTM is controlled manually, like most current microbreweries in the Czech Republic. However, the use of automation and other modern technologies such as augmented reality is becoming more and more important. Peciar (2024) presents the application of these technical solutions to a smart microbrewery (PCT – WO2022144763A1), which enables a remotely controlled automatic beer production process and the optimization of several production parameters. The constant collection of diagnostic data is absolutely essential here, which can facilitate and improve the application of FMEA for failure analysis in microbrewery production technology.

A combination of predictive, proactive, but especially preventive maintenance seems to be a suitable strategy for eliminating the occurrence of production failures and increasing the reliability of production equipment (Gackowiec, 2019). However, it is necessary to consider the economic aspect of the application of these measures, especially for small enterprises. Failures showing low severity, which are also easy to repair, should not be the subject of sophisticated maintenance. The combined approach of maintenance should be applied especially to failures that, due to their severity, make it impossible to implement the production process and thus cause large financial losses.

To ensure the highest possible product quality, as well as employee and consumer safety, it is advisable to combine the implementation of FMEA with other quality control methods such as Hazard Analysis and Critical Control Points (HACCP). As stated by (Hulebak and Schlosser, 2002), this system increases product safety by monitoring biological, chemical and physical risks during food production and at the same time implementing preventive measures. This would bring an integrated approach to risk management, which would include both the prevention of technical failures and the prevention of the occurrence of contaminants affecting the safety of the product and thus the health of the consumer. However, it is necessary to take into account the high administrative and logistical requirements or the difficulty of staff training, which, especially in the operation of microbreweries with limited resources, can represent a significant burden.

CONCLUSION

When applying the FMEA method to the RTM mash copper, out of a total of 8 failures that were observed during the 18 years of beer production in this operation, a total of 4 failures were identified with an RPN above the critical value of 100. The failure with the greatest impact on the quality parameters of the final product was identified as the inability to remove vapours through the chimney during mashing and wort boiling. However, the biggest impact on the implementation of the production process itself, or the safety of the final product, is the inability of the insulated steam line to transfer heat to the mash copper. An appropriate measure is the use of preventive, predictive and proactive maintenance. These methods have not yet been applied due to the focus of RTM. As part of further research, it is desirable to evaluate in detail the impact on the safety and quality parameters of the product.

ACKNOWLEDGMENT

The paper was created with the grant support – CZU: 31190/1414|1633/4134; TAČR FW – TREND: FW06010124 - Predictive maintenance of machinery using statistical and operational data in Industry 4.0.

REFERENCES

BAIANO, A., 2021. Craft beer: An overview. Comprehensive Reviews in Food Science and Food Safety. vol. 20, p. 1829-1856.

BAMFORTH, C.W., 2006. Brewing: new technologies. Boca Raton: CRC Press.

BASAŘOVÁ, G.; ŠAVEL, J.; BASAŘ, P. and LEJSEK, T., 2010. Pivovarství: teorie a praxe výroby piva. Praha: VŠCHT.

BRIGGS, D.E.; BOULTON, Ch.A.; BROOKES, P.A. and STEVENS, R., 2004. Brewing: science and practice. Boca Raton: CRC Press.

FITHRI, P.; RAFI, M.; PAWENARY and PRABUWONO, A.S., 2021. Risk analysis of production process for food SMEs using FMEA method: a case study. In: E3S Web of Conferences. 331, 02010. Available at: https://doi.org/https://doi.org/10.1051/e3sconf/202133102010.

GACKOWIEC, P., 2019. General overview of maintenance strategies – concepts and approaches. Multidisciplinary Aspects of Production Engineering. vol. 2, p. 126-139.

HARDWICK, W.A., 1995. Handbook of Brewing. New York: Dekker.

HULEBAK, Karen L and SCHLOSSER, Wayne, 2002. Hazard Analysis and Critical Control Point (HACCP) History and Conceptual Overview. *Risk Analysis*. Roč. 22, pp. 547-552.

INTERNATIONAL ELECTROTECHNICAL COMMISSION, 2019. ČSN EN IEC 60812, Failure modes and effects analysis (FMEA and FMECA). Ed. 2.

KOSAŘ, K. and PROCHÁZKA, S., 2000. Technologie výroby sladu a piva. Praha: Výzkumný ústav pivovarský a sladařský.

KUNZE, W., 2010. Technology Brewing & Malting. Berlin: VLB.

LIONG, Ch.-Y.; HAMID, S.H. Ab and IBRAHIM, I.M., 2016. Improving the Performance of Chili Sauce Manufacturing Process using Simulation Approach. In: AIP Conference Proceedings. American Institute of Physics, 1750, 030026. Available at: https://doi.org/10.1063/1.4954562.

MATOULKOVÁ, D.; VONTROBOVÁ, E.; BROŽOVÁ, M. and KUBIZNIAKOVÁ, P., 2018. Microbiology of brewery production – bacteria of the order Enterobacterales. Kvasný Průmysl. vol. 64, p. 161-166.

PECIAR, Peter, 2024. Využitie rozšírenej reality pri prevádzke unikátneho smart pivovaru. *ATP Journal*. Pp. 14-15. ISSN 1335-2237.

POP, C.; FRUNZĂ, G. and CIOBANU, M.M., 2019. Study regarding application of the FMEA method within a food safety management system. Scientific Papers-Animal Science Series. vol. 71, p. 189-196.

SHARMA, K.D. and SRIVASTAVA, S., 2018. Failure Mode and Effect Analysis (FMEA) Implementation: A Literature Review. Journal of Advance Research in Aeronautics and Space Science. vol. 5, p. 1-17.

THE BREWERS OF EUROPE, 2023. European Beer Trends Statistics Report 2023 Edition. Online. Brussels: The Brewers of Europe. Available at: https://brewersofeurope.eu/wp-content/uploads/2023/11/european-beer-trends-2023-web.pdf.

VARZAKAS, T.H. and ARVANITOYANNIS, I.S., 2009. Application of failure mode and effect analysis and cause and effect analysis on processing of ready to eat vegetables – part II. International Journal of Food Science and Technology. vol. 44, p. 932-939.

Corresponding author:
Tomáš Vaško, +420 736 691 503, vaskot@tf.czu.cz

MODIFICATION OF EXPOSED SURFACES OF TOOLS FOR CRUSHING UNWANTED GROWTHS TO INCREASE THEIR LIFETIME

ÚPRAVA EXPONOVANÝCH PLÔCH NÁSTROJOV NA DRVENIE NEŽIADUCICH NÁRASTOV PRE ZVÝŠENIE ICH ŽIVOTNOSTI

Monika Vargová[1], Richard Hnilica[2]

[1,2] Department of Manufacturing Technology and Quality Management, Faculty of Technology, Technical University in Zvolen, Študentská 26, 960 01 Zvolen
e-mail: [1]xvargovam1@tuzvo.sk, [2]hnilica@tuzvo.sk

ABSTRACT: Tools for crushing unwanted growths operate in a strongly heterogeneous environment. After a short time, the tungsten carbide (WC) tip is lost due to the heterogeneity of the environment and the tool body wears further. The article deals with the possibilities of increasing the lifetime of tools for crushing unwanted growths by grooving with subsequent welding of additional materials. To preserve the shape and weight of the tool, the grooves were prepared by grinding on the face and back surfaces. For hardfacing by welding into these grooves, two types of electrodes were chosen, namely OK 84.58 and UTP 690. Subsequently, the tool was cut, and samples were taken for light microscopy. Subsequently, the Rockwell hardness test was performed. Furthermore, an abrasion resistance test was performed according to GOST 23.208-79. The best results were achieved by UTP 690 compared to the base material 16MnCr5. Based on the results, we can conclude that the appropriate choice of pre-treatment of tools with subsequent hardfacing by welding is the premise of increasing their service life while maintaining their original shape and weight.

Key words: unwanted growth crusher, grooving, hardfacing by welding, abrasive resistance

ABSTRAKT: Nástroje na drvenie nežiaducich nárastov pracujú v silne heterogénnom prostredí. Po krátkom čase dôjde vplyvom heterogenity prostredia k strate volfrám-karbidovej (WC) špičky a telo nástroja sa ďalej opotrebúva. Článok sa zaoberá možnosťami zvyšovania životnosti nástrojov na drvenie nežiaducich nárastov drážkovaním s následným naváraním prídavných materiálov. Pre zachovanie tvaru a hmotnosti nástroja, boli drážky pripravené brúsením na čelnej a chrbtovej ploche. Pre naváranie do týchto drážok, boli zvolené dva druhy elektród, a to OK 84.58 a UTP 690. Následne bol nástroj rozpílený, a boli odobraté vzorky pre svetelnú mikroskopiu. Následne bola vykonaná Rockwellova skúška tvrdosti. Ďalej bola vykonaná skúška oteruvzdornosti podľa GOST 23.208-79. Najlepšie výsledky dosiahol návar UTP 690 v porovnaní so základným materiálom 16MnCr5. Na základe výsledkov môžeme konštatovať, že vhodnou voľbou predúpravy nástrojov s následným naváraním, je predpoklad zvýšenia ich životnosti pri zachovaní ich pôvodného tvaru a hmotnosti.

Kľúčové slová: drvič nežiaducich nárastov, drážkovanie, naváranie, abrazívna odolnosť

INTRODUCTION

A significant role in forestry is related to the regular removal of unwanted woody growth, e.g. in landscape areas intended for planting new forests, in areas near forest roads and especially in areas under overhead power lines.

The tools involved in removing unwanted growths operate in a heterogeneous environment. This environment is made up not only of wood, but also of soil, which contains rocks and minerals of varying sizes and irregular shapes. They are subject to rapid wear as a result of this working environment. This leads to frequent tool changes, which causes technical and economic problems for companies working in the forestry sector. The permanent requirement to extend the lifetime of working tools working in forestry represents a strong impetus for the search for economical and effective material-technological solutions aimed at significantly suppressing the mechanical degradation of the functional surfaces of tools (Kalincová et al. 2016).

Abrasive wear is one of the dominant and commonly occurring tribological wear processes, leading to significant costs for repairing worn mechanisms and replacing parts (Doluk et al. 2021, Jankauskas et al. 2020, Singh et al. 2020, Stawicki et al. 2018). Abrasive wear is characterised by the separation of particles and damage to the functional surface of the worn body by gouging and cutting by these particles or by the hard and rough surface of the other body, which occurs when the relative motion of the two bodies introduces irregularities of the surface of the harder body into the surface of the softer body. The material from the grooves is usually removed in the form of free particles (Ťavodová et al. 2020a, Javaheri et al. 2018, Petrů et al. 2015).

There are several methods for increasing tool life. Among the very effective measure for increasing tool life is to cover their functional surfaces with a suitable additive material by hardfacing by welding (Müller & Hrabě 2013). Hardfacing by welding is a commonly used method to improve the surface properties of agricultural tools, mining components, land preparation equipment and other (Buchely et al. 2005). The alloy is homogeneously applied to the surface of the base material (usually low-carbon or medium-carbon steels) by welding in order to increase hardness and wear resistance without significant loss of ductility and toughness of the base material (Müller & Hrabě 2013, Buchely et al. 2005).

Particle size, shape and intensity are factors that determine resistance to abrasive wear. These also include hardness, shape, size and number of hard phases and their distribution in the parent metal. Wear resistance increases with the hardness of the hard structural components (carbides, borides, etc.) and with increasing proportion in the structure (Ťavodová et al. 2020a; Balla et al. 2003).

Iron-based hardfacing alloys are the most cost-effective group of hardfacing alloys. They are mostly used for applications where resistance to abrasive wear, impact and thermal fatigue is required (Okechukwu et al. 2017). Transverse surface cracks may form in iron-based alloys containing Cr carbides. Despite these cracks, these hardfacing materials are suitable for use in the mining and earthmoving industries (Tandon et al. 2023). Wang et al. studied the microstructure and wear resistance of Fe-based alloys by adding the elements ferrotitanium (Fe–Ti), ferromolybdenum (Fe–Mo), ferrovanadium (Fe–V) and graphite deposited by the SMAW process. The results showed good resistance to wear and cracking when the amount of Fe–Ti, Fe–Mo, Fe–V was in the range of 12–15%, 2–4%, 10–12% and 8–10% (Wang, X. et al. 2008; Wang, Z. H. et al. 2008).

Cobalt-based hardfacing alloys are used for applications where high resistance to wear, oxidation, corrosion and heat combined with high hot hardness is required. The primary compositional elements of these weld alloys are Co (typically 60%) and Cr (typically 30%). A high Cr content ensures resistance to corrosion and high temperatures, Ni ensures good ductility, and W, Mo and C provide higher strength and wear resistance (Tandon et al. 2023; Ahn 2013).

Nickel-based hardfacing alloys are mainly used where resistance to wear and corrosion at high temperatures is required (Digambar & Choudhary 2014). Studies indicate that W and Mo elements in nickel-based weld alloys improve hardness and strength at high temperatures, C, B and Nb elements provide excellent resistance to abrasive wear, and Cr and Al elements provide better corrosion resistance (Tandon et al. 2023; Ahn 2013).

Tungsten-based hardfacing alloys are used where extreme resistance to abrasive wear is required. Tungsten carbide is one of the hardest materials used in industry, but it is also brittle. In order to create a uniform distribution of tungsten carbides in weld deposits, it is necessary to use lower heat inputs, as higher heat inputs can lead to the decrease of these carbides towards the build-up zone (Tandon et al. 2023).

By selecting a suitable additive material whose structure is better able to withstand the effects of the working environment, the lifetime of the tools for crushing unwanted growths can be increased.

MATERIAL AND METHODS

Tool modification and hardsurfacing by welding

Based on the research so far, it has been found that the body of the tool for crushing unwanted growth is made of chromium-manganese steel 16MnCr5. It has a tungsten carbide (WC) tip soldered with silver solder (Ťavodová et al. 2018). The chemical composition of this steel is in Tab. 1. Two surfaces were identified on these tools that are most exposed to wear during their work. These surfaces are the back and face of the tool (Fig. 1). However, after hardfacing by welding the additional material on the exposed surfaces of the functional parts of the tools, without their prior treatment, the total weight will increase, and the shape of the tool will change. This will also change the load dynamics of the rotor on which the tools are attached. Such a change is then one of the causes that contributes to faster tool wear. One way to prevent such a change is to pre-prepare the exposed surfaces of the tools by removing material from the body of the tool.

The original tool has only one surface modified (strengthened), namely the WC tip. A tool modified by hardfacing by welding will, while preserving the original shape and composition (body and tip), have other surfaces reinforced with such welding that will increase their lifetime.

The surfaces were prepared on the face and back of the tool by grinding. On these pre-prepared surfaces the additional material OK 84.58 and UTP 690 was welded.

The electrode OK 84.58 is an electrode for hardfacing by welding wear-resistant functional surfaces under simultaneous impact stresses with the necessary partial corrosion resistance. Machining of the deposit is possible by grinding. After hardfacing by welding, it forms a martensitic structure. The chemical composition of this electrode is in Tab. 1. It is used as a coating for parts of agricultural and forestry machinery, mixers, transport

equipment, etc. The hardness of the deposit in the second layer is 52-59 HRC (HBT-weld, 2024, Rapidwelding, 2024).

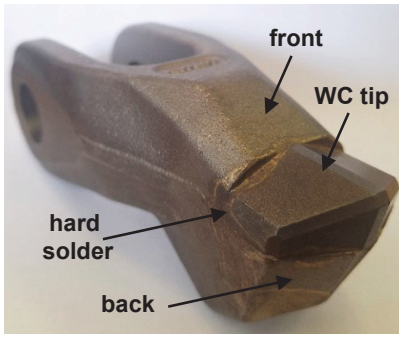

Fig. 1 Tool for crushing unwanted growths
Obr. 1 Nástroj na drvenie nežiaducich nárastov

UTP 690 is used for repair and production of cutting tools, particularly for building-up cutting edges and working surfaces. The deposit is highly resistant to friction, compression and impact, also at elevated temperatures up to 550°C. The production of new tools by welding on non-alloy and lowalloy base metals is also possible (cladding of cutting edges). The chemical composition of this electrode is in Tab. 1. It is used for repair and production of cutting tools, particularly for building-up cutting edges and working surfaces. The hardness of the deposit in the second layer is (Valtec, 2024).

Tab. 1 Chemical composition of base material 16MnCr5 and weld deposit OK 84.58 and UTP 690 (HBT-weld 2024, Valtec 2024)
Tab. 1 Chemické zloženie základného materiálu 16MnCr5 a návarov OK 84.58 a UTP 690 (HBT--weld 2024, Valtec 2024)

Element wt. [%][1]	C	Si	Mn	Cr	Mo	V	W	P	S	Fe
16MnCr5	0.14-0.19	0.17-0.37	1.10-1.40	0.80-1.10	-	-	-	max. 0.035	max. 0.035	balance
OK 84.58	0.7	0.6	0.7	10	-	-	-	-	-	balance
UTP 690	0.9	0.8	0.5	4.5	8.0	1.2	2.0	-	-	balance

[1]Prvok hm [%]

Experimental methods of light microscopy

Specimens for microscopic analysis were prepared in dentacryl, ground on 240, 400, 600 and 800 grit sandpaper, moistened with water, polished with 1/0 grit diamond paste on satin, moistened with kerosene, washed and rinsed with petroleum alcohol. To induce the microstructure for observation of the build zone, 2% Nital etchant (2 ml HNO3, 98 ml ethyl alcohol) was used.

For light microscopy, an OLYMPUS GX71 light microscope with an OLYMPUS DP12 camera was used. The microscope used accessories for observation in polarized light and using differential interference contrast.

Testing methods

The Rockwell hardness was measured according to ISO 6508-1 (ISO 6508-1:2016) and the Universal Hardness Gauge UH250 was used, with a loading force of F=1 471 N.

The test of resistance to abrasive wear was performed according to GOST 23.208-79. The essence of this test is a comparison of the weight loss of the tested material and the weight loss of the reference material under the same test conditions. Electrocorundum with a grain size of 16-P according to GOST 3647-80 with a relative moisture content of no more than 0.15% is used as an abrasive material. Its hardness corresponds to the 9th degree according to the Mohs scale. When assessing wear resistance under specific wear conditions, it is allowed to use abrasive material corresponding to the material that acts during operation, but with a grain size of no more than 1.0 mm.

The TESTER T-07, ITE PIB device was used for the test together with the BT-16 Controller, ITE PIB cycle recording device (Fig. 2).

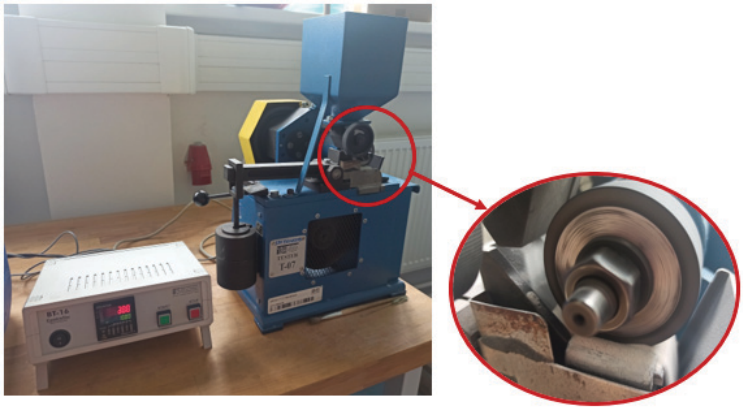

Fig. 2 Device for testing according to GOST 23.208-79 with detail
Obr. 1 Prístroj pre skúšku podľa GOST 23.208-79 s detailom

Prior to the test, the sample was weighed 3 times on a Kern ABS analytical balance with a sensitivity of e=0.1 mg. The arithmetic mean was then calculated and entered in a table. After the initial weighing of the sample, the sample was placed firmly in the instrument between the sample holder and the rubber disc. The abrasive supply was then started, and the instrument started. The test parameters are given in Tab. 2.

Tab. 2 Test parameters according to GOST 23.208-79
Tab. 2 Parametre skúšky podľa GOST 23.208-79

Parameters of the device[1]	
Number of cycles[2]	11
Length of friction path in one cycle R[3]	153.6 m
Rubber disc diameter D[4]	48.9 mm

Pressing force F[5]	15.68 N
Disc speed in one cycle[6]	1 000 RPM
Abrasives[7]	silica sand OTTAWA with a grain size of 0.1 to 0.2 mm
Parameters of the test sample[8]	
Dimensions of the sample[9]	30 x 30 x 5 mm

[1]Parametre skúšobného stroja, [2]Počet cyklov, [3]DÍžka trecej dráhy v jednom cykle R, [4]Priemer gumeného kotúča, [5]Prítlačná sila F, [6]Otáčky kotúča v jednom cycle, [7]Abrazívum, [8]Parametre skúšobnej vzorky, [9]Rozmery vzorky

After each cycle, the sample was removed and weighed 3 times to determine the weight loss of the material. Subsequently, the arithmetic mean was calculated, and this data was entered in the table. After the end of the last cycle and the weighing of the sample, the average weight loss was calculated from the measured values After calculating the average weight loss for each sample - base material and deposits, the relative resistance to abrasive wear was calculated according to formula (1) (GOST 23.208-79:1981):

$$\Psi_{abr} = \frac{W_{hE}}{W_{hV}} \; [-] \tag{1}$$

where: W_{hE} - weight loss of the comparative test body - standard [g],
W_{hV} - weight loss of test body - samples [g].

RESULTS AND DISCUSSION

Grinding wheels with a thickness of 1 mm, 2 mm, 4 mm and 8 mm were used to adjust the tool by grinding. A disc with a thickness of 1 mm was used to define the size of the groove and to grind several grooves, which further served to grind the required surface with a gradual increase in the thickness of the wheel. In Fig. 3a we can see the grooves that were sanded successively with sanding discs with a thickness of 1 mm, 2 mm and 4 mm.

An area of 20 x 30 mm (Fig. 3b) was ground on the face of the tool, and two areas of 20 x 15 mm (Fig. 3c) were ground on the back surface to preserve the shape of the tool. It was ground to a depth of 5 mm. Additional materials were subsequently welded onto the surfaces prepared in this way.

Electrodes with a diameter of 2.5 mm were used for the OK 84.58 deposit. The welding surfaces were cleaned by hand using a wire brush and were degreased with an industrial solvent. Subsequently, the electrodes had to be dried at a temperature of 200°C for 2 hours in a Zepacomp drying oven. The tool was preheated to a temperature of 200°C. Before the hardfacing by welding, the welding parameters were set on the welding device. The set welding current was and voltage . During hardfacing by welding, it was important to minimize the heat input of welding. After every 20 mm section, it was necessary to measure the interpass temperature using a touch thermometer. The interpass temperature is prescribed by the manufacturer at 200°C. If the tool exceeded this temperature, it was necessary to wait until the temperature of the tool fell below the specified interpass tem-

perature in order to continue with the hardfacing by welding. After hardfacing by welding, the tools were allowed to cool freely in air to ambient temperature and were subsequently cleaned (Fig. 4a).

a b c

Fig. 3 Tool prepared by grinding
a – primary grinding phase, b – front surface, c - back surface
Obr. 3 Nástroj upravený brúsením
a – primárna fáza brúsenia, b – čelná plocha, c – chrbtová plocha

Electrodes with a diameter of 2.5 mm were used for the UTP 690 deposit. The welding surfaces were cleaned by hand using a wire brush and were degreased with an industrial solvent. Subsequently, the electrodes had to be dried at a temperature of 300°C for 2 hours in a Zepacomp drying oven. The tool was preheated to a temperature of 250°C. Before the hardfacing by welding, the welding parameters were set on the welding device. The set welding current was and voltage .

The hardfacing by welding procedure was identical to the hardfacing by welding procedure with the OK 84.58 electrode. In Fig. 4b we can see a tool with a OK 84.58 with a UTP 690 weld deposit.

a b

Fig. 4 Modified tools
a – tool with OK 84.58 weld deposit, b – tool with UTP 690 weld deposit
Obr. 4 Upravený nástroj
a – nástroj s návarok OK 84.58, b – nástroj s návarom UTP 690

After cooling, the tools were weighed to determine if the weight of the tool, after pre-modifying the exposed surfaces by removing the tool material and then hardfacing

by welding the additional material, was the same as the weight of the new tool. A digital weighing balance AG2000C with a weighing range of 0.5 to 2 000 g was used for weight determination. Table 3 summarises the results from the tool weight measurements.

Tab. 3 Weight values of the original tool and of the tools with OK 84.58 and UTP 690 weld deposit
Tab. 3 Hodnoty hmotnosti pôvodného nástroja a nástrojov s návarom OK 84.58 a UTP 690

	Unmodified tool[1]	A tool with a ground groove[2]
OK 84.58	1 730	1 709
UTP 690	1 730	1 733

[1]Neupravený nástroj, [2]Nástroj s vybrúsenou drážkou

On the basis of the data obtained, we can conclude that the pre- modified of the exposed surfaces of the tool and the subsequent hardfacing by welding of the additional material did not lead to a significant change in weight. The difference in weight of the new unmodified tool compared to the modified tool with OK 84.58 is approximately 21 g and with UTP 690 is approximately 3 g.

Subsequently, the tools were cut and the samples taken were subjected to microscopic analysis, testing of hardness and abrasion resistance.

Microscopic analysis was performed for the purpose of detecting the mixing of the base material (BM)with the deposit and also to detect the presence of possible defects in the melting zone. In Fig. 5a we can see the ferritic-pearlitic structure of the base material, the melting zone - the connection of the base material and the deposit, and the unetched deposit OK 84.58 on a sample that was taken from a pre-modified tool by grinding. Sufficient diffusional mixing between individual materials is present. There are no defects, cracks or pores that would reduce the quality of mixing base material with the deposit.

The ferritic-pearlitic structure of base material, the melting zone and the unetched deposit of UTP 690 on the sample, which was taken from the pre-modified tool by grinding, can be seen in Fig. 5b. We can conclude that there was a sufficient diffusion mixing of both materials. There are also no visible defects that could affect the cohesion of both materials.

Studies devoted to the resistance of materials to wear differ in their opinions on the suitability of the microstructure that would best withstand the effects of the working environment (Tandon et al. 2023; Rojacz et al. 2022; Nagentrau et al. 2019; Badisch et al. 2009; Coronado et al. 2009). Therefore, it was necessary to carry out further tests that would confirm or ruled out the suitability of using selected depositing materials.

Next, a Rockwell hardness test was performed. The comparison of the measured hardnesses can be seen in Fig. 6. We can state that both coatings reached a higher hardness than the hardness of the base material. The UTP 690 weld reached the highest hardness, namely 62 HRC. The OK 84.58 coating reached a hardness of 52 HRC.

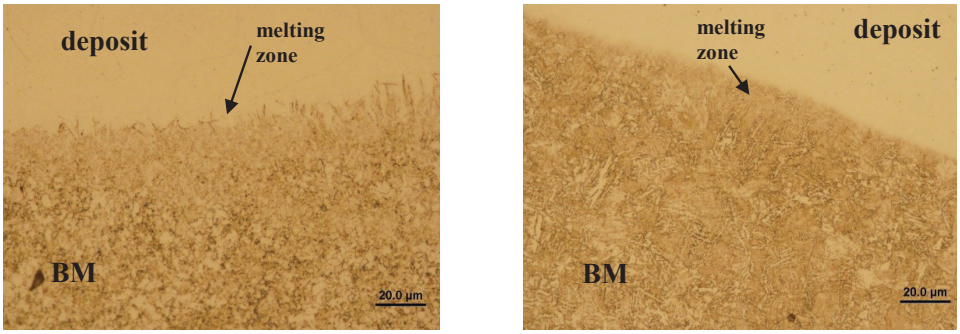

a b

Fig. 5 Microstructure interface base material – weld deposit
a – BM – melting zone – deposit OK 84.58, b - BM – melting zone – deposit UTP 690
Obr. 5 Mikroštruktúra rozhranie základný materiál – návar
a – ZM – zóna stavenia – návar OK 84.58, b – ZM – zóna stavenia – návar UTP 690

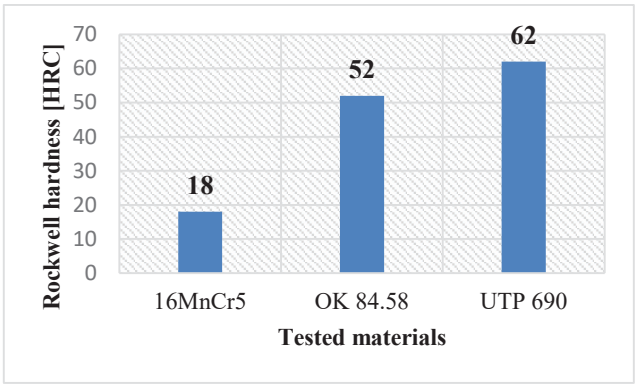

Fig. 6 Comparison of Rockwell hardness
Obr. 6 Porovnanie tvrdostí podľa Rockwella

Some authors report that hardness is strongly correlated with resistance to abrasive wear (Kováč et al. 2022, Slota et al. 2022). Based on the hardness measurement results, we can therefore predict that coatings with the highest hardness will best resist the effects of an abrasive environment. However, other authors state in their studies that hardness has no effect on wear resistance (Falat et al. 2019, Balla et al. 2003, Brziak et al. 2003). Therefore, it was necessary to perform an abrasive wear test for base material and for individual deposit materials. The results from the abrasion resistance test are summarized in Tab. 4.

Tab. 4 Summary of abrasion resistance test results
Tab. 4 Zhrnutie výsledkov zo skúšky oteruvzdornosti

	16MnCr5	OK 84.58	UTP 690
[g]	0.0343	0.0066	0.0014
[-]	1	5.20	24.5

In Fig. 7 we can see a comparison of the results from the abrasion resistance test. We

can conclude that both coatings achieved a higher value of relative resistance to abrasive wear. The OK 84.58 coating achieved five times better results than the base material tool. The UTP 690 coating achieved up to a 24.5-fold increase in relative resistance to abrasive wear Ψ_{abr}.

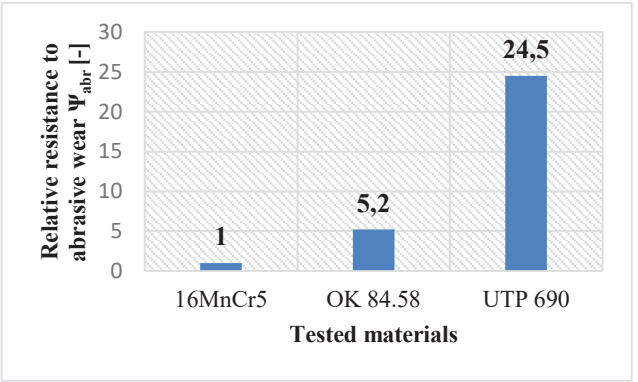

Fig. 7 Comparison of results from the abrasion resistance test
Obr. 7 Porovnanie výsledkov zo skúšky oteruvzdornosti

Based on the obtained results, we can conclude that both weld deposits should better withstand the effects of an abrasive environment than the base material of the tool.

However, it is also necessary to consider the disadvantages of tool modification by manual arc-hardfacing by welding. The main disadvantages include the large heat-affected area and the possible introduction of human fail. Fails created in this way can result in various defects such as cracks. These can further affect not only the wear resistance of the weld deposit but can also cause parts of the material to break off due to the impact load (Ťavodová et al. 2020b).

For the correct evaluation of the performed laboratory tests, it is necessary to carry out operational tests in further research. This will determine the appropriateness of the adjustments made in real working conditions.

CONCLUSION

Tools for crushing unwanted growths operate in a heterogeneous environment. Due to this environment, the WC of the tip is lost after a short time and the tool body is further worn out. By selecting a suitable pre-preparation of the tool, followed by the hardfacing by welding of additive materials that are better able to withstand the effects of the working environment, the tool's lifetime can be increased.

The article analyses two ways to modify crusher for unwanted growth. Based on the results, it is possible to state the following:

a) The weld deposit OK 84.58 achieved better results compared to the base material 16MnCr5. Its Rockwell hardness was almost three times higher and the relative resistance to abrasive wear Ψ_{abr}. was 5.2 times higher compared to base material 16MnCr5.

b) The UTP 690 weld deposit reached 3.4 times higher Rockwell hardness than the base material of tool 16MnCr5 and its relative resistance to abrasive wear Ψ_{abr} was 24.5 times higher.

At the same time, we can state that with both weld deposits there was sufficient diffusion mixing of base material with the weld deposit. Also, no defects were visible that would affect the quality of the coating. The original shape of the tool was also preserved.

In further research it would be advisable to carry out field tests to determine the behaviour of the tool so modified also under real working conditions.

ACKNOWLEDGMENT

This work was supported by "Vedecká grantová agentúra MŠVVaŠ SR a SAV" under the grants numbers VEGA 1/0073/24

REFERENCES

AHN, D. G. 2013. Hardfacing technologies for improvement of wear characteristics of hot working tools: A Review. In International Journal of Precision Engineering and Manufacturing. vol. 14, pp. 1271-1283. ISSN 2005-4602.

BADISCH, E., ILO, S., POLAK, R. 2009. Multivariable modeling of impact-abrasion wear rates in metal matrix-carbide composite materials. In Tribology letters. vol. 36, pp. 55-62. ISSN 1573-2711.

BALLA, J., MIKUŠ, R., CVIKOVÁ, H. 2003. Náuka o Materiáloch: Návody Na Cvičenia. Nitra: Slovenská Poľnohospodárska Univerzita. 158 s. ISBN 80-8069-217-3

BUCHELY, M.F., GUTIERREZ, J.C., LEON, L.M., TORO, A. 2005. The effect of microstructure on abrasive wear of hardfacing alloys. In Wear. vol. 259, no. 1-6, pp.52-61. ISSN 0043-1648. DOI: 10.1016/j.wear.2005.03.002

BRZIAK, P. a kol. autorov. 2003. Materiály a ich správanie sa pri zváraní. Bratislava: VÚZ. 355 s. ISBN 80-88734-10-X

CORONADO, J. J., CAICEDO, H. F., GÓMEZ, A. L. 2009. The effects of welding processes on abrasive wear resistance for hardfacing deposits. In Tribology International. vol. 42, no. 5, pp. 745-749. ISSN 0301-679X. DOI: doi.org/10.1016/j.triboint.2008.10.012

DIGAMBAR, B., CHOUDHARY, D. 2014. A review paper on hardfacing processes, materials, objectives and applications. In International Journal of Science and Research (IJSR). vol. 3, no. 6, pp. 2400-2402. ISSN 2319-7064.

DOLUK A., RUDAWSKA A., STANČEKOVÁ, D., MRÁZIK, J. 2021 Influence of surface treatment on the strength of adhesive joints. In Manufacturing Technology. vol. 21, no. 5. pp. 585-591. ISSN 2787-9402. DOI: 10.21062/mft.2021.068

FALAT, L., DŽUPON, M., ŤAVODOVÁ, M., HNILICA, R., ĽUPTÁČIKOVÁ, V., ČIRIPOVÁ, L., HOMOLOVÁ, V., ĎURIŠINOVÁ, K. 2019. Microstructure and abrasive wear resistance of various alloy hardfacings for application on heavy-duty chipper tools in forestry shredding and mulching operations. In Materials. vol. 12, no. 13, pp. 2212. ISSN 1996-1944. DOI: 10.3390/ma12132212

GOST 23.208-79:1981. Ensuring of wear resistance of products. Wear resistance testing of materials by friction against loosely fixed abrasive particles. [online]. [cit. 2022-01-24]. Available on: http://docs.cntd.ru/document/gost-23-208-79

ISO 6508-1:2016. Metallic Materials—Rockwell Hardness Test—Part 1: Test Method. International Organization for Standardization: London. 2018.
JANKAUSKAS, V., KATINAS, E., PUSVAŠKIS, M. LEIŠYS, R. 2020. A Study of the Durability of Hardened Plough Point. In Journal of Friction and Wear. vol. 41, pp. 78–84. ISSN 1934-9386. DOI:10.3103/S1068366620010171
JAVAHERI, V., PORTER, D., KUOKKALA, V. T. 2018. Slurry erosion of steel–Review of tests, mechanisms and materials. In Wear. vol. 408, pp. 248-273. ISSN 0043-1648. DOI: 10.1016/j.wear.2018.05.010
KALINCOVÁ, D., ŤAVODOVÁ, M., HNILICOVÁ, M., VEVERKOVÁ, D. 2016. Machinery for forest cultivation - Increase of resistance to abrasive wear of the tool. In MM Science Journal. 2016, 5, pp.1269–1272. ISSN 1805-0476. DOI: 10.17973/MMSJ.2016_11_201684
KATALÓG PRÍDAVNÝCH MATERIÁLOV. [online]. [cit. 2024-03-28]. Available on: https://hbt-weld.cz/app/uploads/2019/02/Katalog_CZ_2012.pdf
KOVÁČ, I., MIKUŠ, R., ŽARNOVSKÝ, J., DRLIČKA, R., HARNIČÁROVÁ, M., VALÍČEK, J., KADNÁR, M. 2022. Increasing the wear resistance of surface layers of selected steels by TIG electric arc surface remelting process using a powder based on CaCN2. In The International Journal of Advanced Manufacturing Technology vol. 123, no. 5, pp. 1985-1997. ISSN 1433-3015.
MÜLLER, M., HRABĚ, P. 2013. Overlay materials used for increasing lifetime of machine parts working under conditions of intensive abrasion. In Research in Agricultural Engineering. vol. 59, no. 1, pp.16-22. ISSN 1805-9376.
NAGENTRAU, M., TOBI, A. M., SAMBU, M., JAMIAN, S. 2019. The influence of welding condition on the microstructure of WC hardfacing coating on carbon steel substrate. In International Journal of Refractory Metals and Hard Materials. vol. 82, pp. 43-57. ISSN 0263-4368. DOI: 10.1016/j.ijrmhm.2019.03.029
OKECHUKWU, C., DAHUNSI, O. A., OKE, P. K., OLADELE, I. O., DAUDA, M. 2017. Review on hardfacing as method of improving the service life of critical components subjected to wear in service. In Nigerian Journal of Technology. vol. 36, no. 4, pp. 1095-1103. ISSN 2467-8821. DOI: 10.4314/njt.v36i4.15
PETRŮ, J., ZLÁMAL, T., ČEP, R., STANČEKOVÁ, D., PAGAČ, M., VORTEL, O. 2015. Mechanism of cutting insert wear and their influence on cutting ability of the tool during machining of special alloys In Manufacturing Engineering and Technology for Manufacturing Growth (METMG 2015) : 3rd international conference, Vancouver, Canada, 2015. pp. 36-40. ISBN 978-1-61275-074-3. DOI 10.12913/22998624/64074
RAPIDWELDING. OK 84.58. [online]. [cit. 2024-03-28]. Available on: https://www.rapidwelding.com/files/8458504020.pdf
ROJACZ, H., KATSICH, C., KIRCHGAßNER, M., KIRCHMAYER, R., BADISCH, E. 2022. Impact-abrasive wear of martensitic steels and complex iron-based hardfacing alloys. In Wear. vol. 492-493, p. 204183. ISSN 0043-1648. DOI: 10.1016/j.wear.2021.204183
SINGH, J., CHATHA, S.S., SIDHU, B.S. 2020. Abrasive wear behavior of newly developed weld overlaid tillage tools in laboratory and in actual field conditions. In Journal of Manufacturing Processes. vol. 55, pp. 143-152. DOI:10.1016/j.jmapro.2020.03.040
SLOTA, J., KUBIT, A., GAJDOŠ, I., TRZEPIECIŃSKI, T., KAŠČÁK, Ľ. 2022. A Comparative Study of Hardfacing Deposits Using a Modified Tribological Testing Strategy. In Lubricants. vol. 10, no. 8, p. 187. ISSN 2075-4442. DOI: 10.3390/lubricants10080187
STAWICKI T, KOSTENCKI P, BIAŁOBRZESKA B. 2018. Roughness of Ploughshare Working Surface and Mechanisms of Wear during Operation in Various Soils. In Metals. vol. 8, no. 12, pp. 1042. ISSN 2075-4701. DOI:10.3390/met8121042

TANDON, D., LI, H., PAN, Z., YU, D., PANG, W. 2023. A Review on Hardfacing, Process Variables, Challenges, and Future Works. In Metals. vol. 13, no. 9, pp.1512. ISSN 2075-4701. DOI: 10.3390/met13091512

TAVODOVA, M., FALAT, L., SKULTETYOVA, V. 2020a. Laboratory analysis od hardfacing material applies by plasma and TIG welding. In MM Science Journal. 2020. pp. 3826-3831 ISSN 1803-1269.

ŤAVODOVÁ, M., KALINCOVÁ, D., KOTUS, M., PAVLÍK, Ľ. 2018. The possibility of increasing the wearing resistance of mulcher tools. In Acta technologica agriculturae. vol. 21, no. 2, pp. 87-93. ISSN 1338-5267. DOI: 10.2478/ata-2018-0016

ŤAVODOVÁ, M., VARGOVÁ, M., FALAT, L. 2020b. Possibilities of modification of ploughshares used for winter maintenance of forest roads. In Manufacturing Technology. vol. 20, no. 6, pp. 834-844. ISSN 2787-9402. DOI: 10.21062/mft.2020.111

VALTEC. UTP 690. [online]. [cit. 2024-03-28]. Available on: https://www.valtec.sk/obchod_homedir/data/2616/prilohy/L1_22771_en__UTP%20690.pdf

WANG, Z. H., WANG, Q. B., CUI, L., YANG, A. D., HE, D. Y. 2008. Influence of cooling rate and composition on orientation of primary carbides of Fe–Cr–C hardfacing alloys. In Science and Technology of Welding and Joining. vol. 13, no. 7, pp. 656-662. ISSN 1743-2936. DOI: 10.1179/174329308X37017

WANG, X., HAN, F., LIU, X., QU, S., ZOU, Z. 2008. Microstructure and wear properties of the Fe–Ti–V–Mo–C hardfacing alloy. In Wear. vol. 265, no. 5-6, pp. 583-589. ISSN 0043-1648. DOI: 10.1016/j.wear.2007.12.001

Corresponding author:
Monika Vargová, 045/5206026, xvargovam1@tuzvo.sk

ACTA FACULTATIS TECHNICAE XXIX
ZVOLEN – SLOVAKIA 2024

COMPUTATION OF THE NUSSELT NUMBER IN CHANNEL FLOW ON THE BASIS OF THE MESH SENSITIVITY TEST

VÝPOČET NUSSELTOVHO ČÍSLA PRE PRÚDENIE V KANÁLI NA ZÁKLADE TESTU CITLIVOSTI SIETE

Stanislav Kotšmíd[1]

[1] *Department of Mechanics, Mechanical Engineering, and Design, Faculty of Technology, Technical University in Zvolen, Študentská 26, 960 01, Zvolen, Slovak Republic, stanislav.kotsmid@tuzvo.sk*

ABSTRACT: The paper presents an approach to compute the Nusselt number in a channel flow on the basis of the CFD computation and mesh sensitivity test. A rectangular duct and a circular tube are chosen as a channel type since the exact values of the Nusselt number can be analytically reached. Overall, five various mesh distributions are used for the simulation while a dependence of the Nusselt number on the mesh size is shown. On the basis of the data extrapolation using a power function, the value is calculated for infinite number of elements that has a negligible discrepancy from the exact one. Concerning the approach, a possibility to estimate the Nusselt number without using a large number of elements is given while a time-consuming calculation is eliminated.

Key words: Nusselt number, CFD, heat transfer, extrapolation, mesh sensitivity test

ABSTRAKT: Článok popisuje postup výpočtu Nusseltovho čísla pre prúdenie v kanáli na základe CFD simulácie a testu citlivosti siete. Pre tvar kanála bol zvolený obdĺžnikový a kruhový prierez z dôvodu možnosti analytického výpočtu exaktnej hodnoty Nusseltovho čísla. Celkovo bolo pre výpočet použitých päť rôznych veľkostí siete, pričom sa zisťovala závislosť medzi hodnotou Nusseltovho čísla a počtom elementov. Na základe extrapolácie hodnôt bola prostredníctvom mocninovej funkcie vypočítaná jeho hodnota pre teoreticky nekonečný počet elementov, ktorá má zanedbateľnú odchýlku od exaktnej hodnoty. Pomocou tohto postupu je možné odhadnúť hodnotu Nusseltovho čísla bez použitia veľkého počtu elementov, čo prináša šetrenie výpočtového času.

Kľúčové slová: Nusseltovo číslo, CFD, prenos tepla, extrapolácia, test citlivosti siete

INTRODUCTION

When performing the CFD simulation to obtain the heat transfer parameters, the volume element method is used where the computational domain has to be divided into elements. Besides the element aspect ratio, angle, skew, warpage, or chordal deviation, the element size has a significant effect on the computed values as well [1]. Therefore, a mesh sensitivity test is usually carried out where a dependence of any heat transfer parameter on the mesh size is investigated. The main goal of the analysis is to bring an optimal mesh size so that the result accuracy is appropriate and simultaneously the computational time is not so high. When the number of elements approaches infinity, a theoretically exact value is achieved when remaining the mesh quality. Obviously, it cannot be reached due to lack of time and round-off errors.

The presented paper offers a way to compute the value of a heat transfer parameter for the infinite number of elements using the values obtained at finite element size with subsequent data extrapolation. As an analysed heat transfer parameter, the Nusselt number is considered since it describes the ratio of total heat transfer to conductive heat transfer across a boundary. As a channel type, a rectangular duct of infinite width and a circular tube are chosen since the exact values of the Nusselt number can be analytically reached. As it is shown, the values of the Nusselt number obtained for a small number of elements can be modelled by a power function with a negative exponent. Considering the variable approached infinity, the absolute term determines a theoretically exact value of the Nusselt number. The approach can prevent the time-consuming computation not only for presented cases, but also for other computational domains, heat transfer parameters, and heat loads.

MATERIAL AND METHODS

To perform the CFD computation, a straight channel of a rectangular duct and circular tube shape with the height (diameter) of 50 mm and the length of 2 000 mm were considered as a domain. Since the rectangular duct is of infinite width, the domain is considered as a planar two-dimensional while the circular tube is defined as an axisymmetric. As an element type, the quadrilateral elements, structured into the orthogonal mesh with a defined wall-normal bias, were used where five different numbers of elements (4, 8, 12, 16, and 20) were applied on the half-vertical edge (Fig. 1). For all domains, the element longitudinal size remained the same.

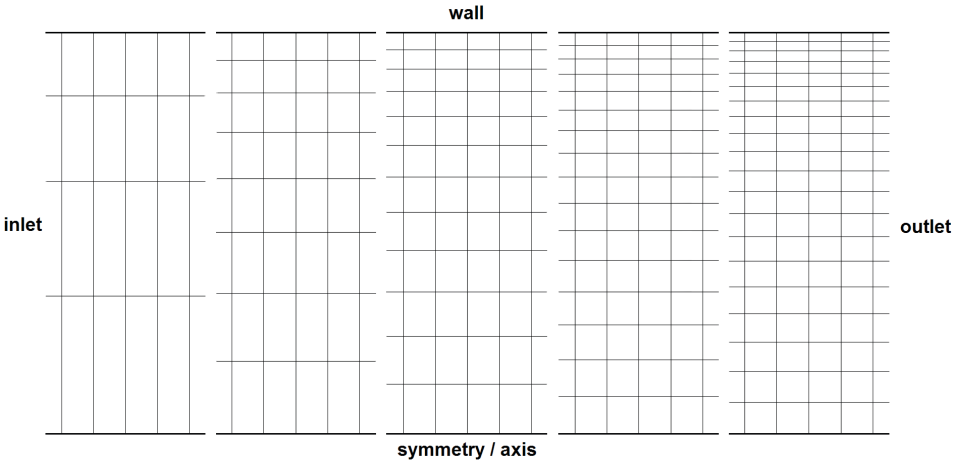

a) b) c) d) e)

Fig. 1 The mesh distribution
a) 4 elements, b) 8 elements, c) 12 elements, d) 16 elements, e) 20 elements
Obr. 1 Rozloženie výpočtovej siete
a) 4 elementy, b) 8 elementov, c) 12 elementov, d) 16 elementov, e) 20 elementov

The channel flow is considered as a steady with constant parameters of the air since the exact values of the Nusselt number are calculated for such conditions. The governing equations of mass, momentum, and energy conservation were solved by the Ansys Fluent software in the following forms [2]:
– continuity equation:

$$\nabla \cdot \mathbf{v} = 0 \tag{1}$$

– momentum equation:

$$\rho \nabla \cdot (\mathbf{v}\mathbf{v}^{\mathrm{T}}) = -\nabla p + \eta \nabla \cdot \left\{ \left[\nabla \mathbf{v} + (\nabla \mathbf{v})^{\mathrm{T}} - \frac{2}{3}(\nabla \cdot \mathbf{v})\mathbf{I} \right] \right\} \tag{2}$$

– energy equation:

$$\rho c_p \nabla \cdot (\mathbf{v}T) = \lambda \nabla \cdot (\nabla T) \tag{3}$$

where ρ is the fluid density ($\rho = 1.225$ kg·m^{-3}),
η is the fluid dynamic viscosity ($\eta = 1.7894 \cdot 10^{-5}$ kg·m^{-1}·s^{-1}),
c_p is the fluid specific heat capacity ($c_p = 1006.43$ J·kg^{-1}·K^{-1}),
λ is the fluid thermal conductivity ($\lambda = 0.0242$ W·m^{-1}·K^{-1}),
p is the fluid pressure (Pa),
T is the fluid temperature (K),
v is the fluid velocity vector,
I is the identity tensor.

To perform the numerical analyses, the Direct Numerical Simulation solver was used for the laminar flow where the pressure-velocity coupling was handled by the coupled scheme with the pseudo transient formulation. For the steady pressure-based analyses, the

QUICK schemes were used as a spatial discretization. The solution was considered to be fully converged when the residuals of continuity, x-velocity, y-velocity, and energy parameters met the convergence criterion 10^{-6}. From the wall boundary condition point of view, the constant heat flux and constant temperature values were defined. For the rectangular duct and circular tube, 2D planar and axisymmetric analysis were performed respectively where the domain boundary conditions are described as follows:

- velocity inlet – left side:

$$v_x = const., \;\; v_y = v_r = 0, \;\; T = T_\infty = const. \tag{4}$$

- pressure outlet – right side:

$$\frac{\partial v_x}{\partial x} = \frac{\partial v_y}{\partial x} = \frac{\partial v_r}{\partial x} = \frac{\partial T}{\partial x} = 0 \tag{5}$$

- wall – upper side:

$$v_x = v_y = v_r = 0, \;\; T = T_w = const. \;\; \vee \;\; q = q_w = const. \tag{6}$$

- symmetry, axis – lower side:

$$\frac{\partial v_x}{\partial y} = \frac{\partial v_x}{\partial r} = 0, \;\; v_y = v_r = 0, \;\; \frac{\partial T}{\partial y} = \frac{\partial T}{\partial r} = 0 \tag{7}$$

where v_x is the velocity in x direction ($m \cdot s^{-1}$),
v_y is the velocity in y direction ($m \cdot s^{-1}$),
v_r is the velocity in radial direction ($m \cdot s^{-1}$),
T_∞ is the outside temperature (K),
T_w is the wall temperature (K),
q_w is the heat flux ($W \cdot m^{-2}$).

On the basis of the Fourier and Newton law, the local Nusselt numbers based on the local heat transfer coefficients were being evaluated alongside the channel length. The local heat transfer coefficient is defined as [3]:

$$h_x = -\lambda \frac{dT}{dn}\bigg|_{y=\frac{H}{2}=\frac{D}{2}} \frac{1}{T_w - T_b} \tag{8}$$

where n is the normal direction to the wall (-),
H is the channel height (H = 0.05 m),
D is the channel diameter (D = 0.05 m).

The bulk temperature is defined as:

$$T_b = \frac{\int_A T v_x dA}{\int_A v_x dA} \tag{9}$$

The local Nusselt number for the rectangular duct is defined as:

$$Nu_x^R = \frac{2 h_x H}{\lambda} \tag{10}$$

The local Nusselt number for the circular tube is defined as:

$$Nu_x^c = \frac{h_x D}{\lambda} \tag{11}$$

For each simulation, the representative value of the local Nusselt number is taken from the area where a fully developed flow is reached and subsequently compared with the exact one that can be achieved when solving equations (1) – (3) analytically. According to Han [4] and Erdogan and Imrak [5], the Nusselt number for the rectangular duct with infinite width and circular tube under the constant wall heat flux and temperature are shown in Table 1.

Table 1 The exact Nusselt number for investigated channels
Tabuľka 1 Exaktné hodnoty Nusseltovho čísla pre vyšetrované kanály

	Rectangular Duct (parallel plates)	Circular Tube
Wall Heat Flux	140/17	48/11
Wall Temperature	7.541	3.658

Since the Nusselt number depends on the mesh distribution, 5 different values for each channel and load combination were achieved and subsequently approximated by a power function in the form:

$$Nu = ar^b + c \tag{12}$$

where r is the number of elements (-),
a, b, c are unknown coefficients to be determined.

Considering the asymptotical function, it is possible to calculate the exact Nusselt number when the variable equals infinity. Hence, the coefficient c determines a theoretically exact value. The unknown coefficients are searched for by the least square method.

RESULTS AND DISCUSSION

When performing the computations, the temperature fields are evaluated to obtain the temperature distribution alongside the vertical lines and calculate the bulk temperature. A part of the temperature field in a developed flow area is shown in Fig. 2.

A dependence of the Nusselt number on the number of the half-vertical edge elements is shown in Fig. 3. Undoubtedly, all values increase with the number of elements and get closer to a certain value that might be the exact one for infinite number of elements. The most suitable approximation of the points is achieved by Eq. 12 where the coefficients were determined by the least square method. Subsequently, the Nusselt number at infinite number of edge elements is calculated that is represented by the coefficient c. Discrepancies between the coefficient c and exact values are 0.02% and 0.03% for the rectangular duct at constant wall heat flux and rectangular duct at constant wall temperature respectively. For the circular tube at constant wall heat flux and circular tube at constant wall temperature, discrepancies were achieved as 0.05% and 0.08% respectively.

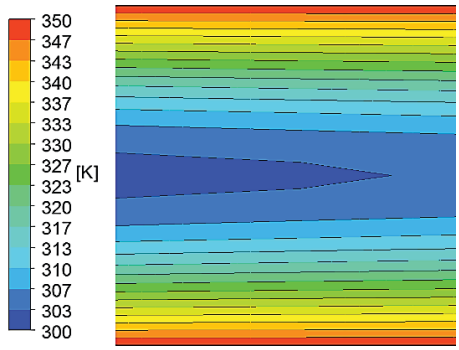

Fig. 2 Temperature field in the domain
Obr. 2 Teplotné pole v kanáli

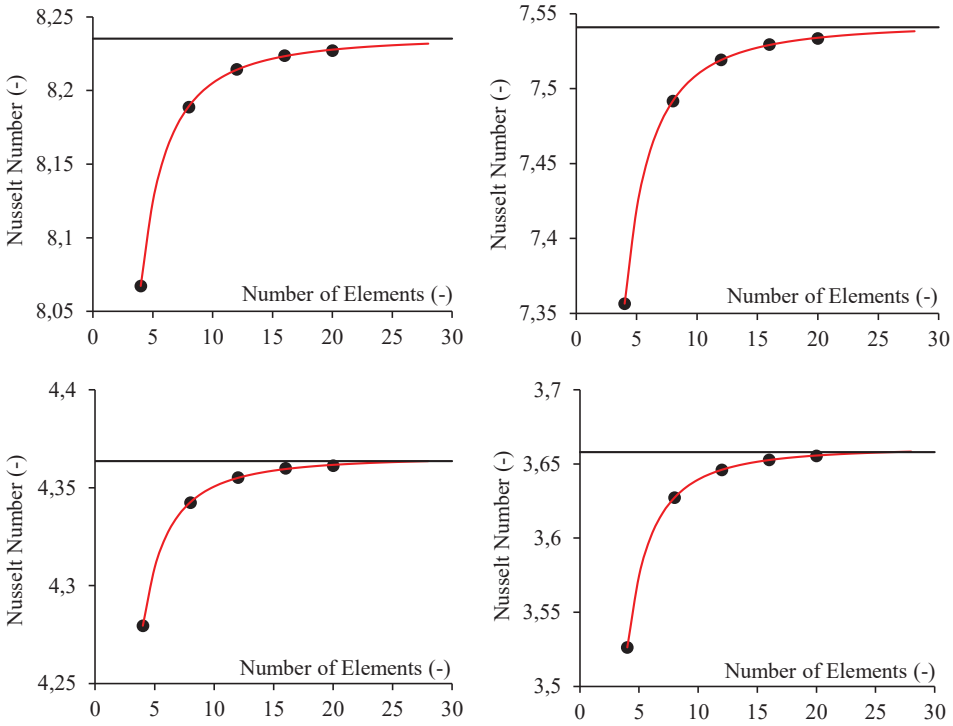

Fig. 3 Dependence of the Nusselt number on the mesh size
Obr. 3 Závislosť hodnoty Nusseltovho čísla na veľkosti siete

Using the least square method, the power functions were created that describe the data from the CFD computations as follows:
- rectangular duct with constant wall heat flux

$$Nu = -2.152r^{-1.834} + 8.236 \tag{13}$$

- rectangular duct with constant wall temperature

$$Nu = -2.467r^{-1.862} + 7.543 \quad (14)$$

- circular tube with constant wall heat flux

$$Nu = -1.199r^{-1.899} + 4.366 \quad (15)$$

- circular tube with constant wall temperature

$$Nu = -2.149r^{-1.998} + 3.661 \quad (16)$$

The power function according to Eq. 12 might be uniquely defined by three points. Let us consider three mesh distributions with the smallest number of elements and determine the coefficient c that achieves the following values:

- rectangular duct with constant wall heat flux c = 8.239
- rectangular duct with constant wall temperature c = 7.544
- circular tube with constant wall heat flux c = 4.367
- circular tube with constant wall temperature c = 3.661

The maximum discrepancy of the coefficient c between the approximation with five points and the approximation with three points is 0.02%, which can be considered as negligible.

CONCLUSION

The effect of element mesh size on the Nusselt number in a channel flow was studied in the paper where a significance of the edge element distribution on the heat transfer parameter was proved. When performing the CFD computations, two different channel shapes and two different heat loads were considered while five different mesh distributions were used for each combination. The dependence of the Nusselt number on the number of vertical edge elements was approximated by a power function that allows the calculation of the Nusselt number for theoretically infinite number of elements. Since three points are necessary to create the function only, three mesh distributions with the smallest number of elements were used. The discrepancies between the exact value of the Nusselt number and the coefficient that represents the Nusselt number for theoretically infinite number of elements were achieved in the range of 0.04% to 0.09%, which is considered as negligible. It is important information from the computational time point of view, since the less number of elements the lower computational time is required. The mentioned approach can be conducted for different domains and heat transfer conditions where similar behavior can be noticed.

ACKNOWLEDGMENT

The paper was funded by the Cultural and Educational Grant Agency under the project KEGA no. 002TU Z-4/2023 “Innovation of the Educational Process by Applying New Didactic Approaches Focusing on the Field of Mechanisms in Transport and Handling as Tools Increasing the Quality of Professional Knowledge and Critical Thinking” and by the EU NextGenerationEU through the Recovery and Resilience Plan for Slovakia under the project No. 09I03-03-V05-00016.

REFERENCES

MOHANTY, R. L., SWAIN, A., DAS, M. K. 2018. Thermal Performance of Mixed Tube Bundle Composed of Circular and Elliptical Tubes. In Thermal Science and Engineering Progress, vol. 5, pp. 492-505. ISSN 2451-9049.

MASSOUD, M. 2005. Engineering Thermofluids – Thermodynamics, Fluid Mechanics, and Heat Transfer. Springer-Verlag Berlin Heidelberg 2005, pp. 1119. ISBN 978-3-540-22292-7.

YILMAZ, A., KURU, M. N., ERDINC, M. T., YILMAZ, T. 2016. Numerical Calculation of Heat Transfer and Pressure Drop in In-Line Axially-Finned Tube Banks. 1st International Mediterranean Science and Engineering Congress, 2016, pp. 2634-2647. ISBN 978-607-67067-0-7

HAN, J. Ch. 2012. Analytical Heat Transfer. Taylor & Francis Group, Boca Raton, 2012, pp. 314. ISBN 978-1-4398-6196-7.

ERDOGAN, M. E., IMRAK, C. E. 2005. The Effects of Duct Shape on the Nusselt Number. In Mathematical and Computational Applications, no. 1, vol. 10, pp. 79-88. ISSN 2297-8747.

Corresponding author:
Stanislav Kotšmíd, tel. +421 45 5206 036, e-mail: stanislav.kotsmid@tuzvo.sk

EFFECT OF RAM-AIR ON THE COOLING PROCESS OF HEAT TRANSFER FLUID IN THE COOLING CIRCUIT OF AN AUTOMOBILE ENGINE

VPLYV NÁPOROVÉHO VZDUCHU NA PROCES CHLADENIA TEPLONOSNEJ KVAPALINY V CHLADIACOM OKRUHU MOTORA AUTOMOBILU

Marek Lipnický[1], Zuzana Brodnianská[2], Pavel Beňo[3]

[1] *Department of Mechanics, Mechanical Engineering and Design, Faculty of Technology, Technical University in Zvolen, Studentska 26, 960 0, Zvolen, Slovak Republic, xlipnicky@tuzvo.sk*
[2] *Department of Mechanics, Mechanical Engineering and Design, Faculty of Technology, Technical University in Zvolen, Studentska 26, 960 01, Zvolen, Slovak Republic, zuzana.brodnianska@tuzvo.sk*
[3] *Department of Mechanics, Mechanical Engineering and Design, Faculty of Technology, Technical University in Zvolen, Studentska 26, 960 01, Zvolen, Slovak Republic, pavel.beno@tuzvo.sk*

ABSTRACT: The paper deals with the investigation of the influence of the ram-air on the cooling process of the heated coolant circulating in the cooling circuit of the automobile engine. The axial drum fan located upstream of the heat exchanger is used to simulate the flow of the impingement air at average velocities 6, 8 and 10 m/s. Simultaneously, a manufacturer's fan is mounted on the cooler in order to compare the time required to dissipate excess heat using only ram-air and forced cooling using the fan on the cooler. The coolant mixture consists of ethylene glycol and water in a 1:1 ratio. To record the coolant temperatures in the circuit and the temperature distribution on the cooler, thermistors and thermal imaging technology are used. The shortest cooling time of the hot coolant was recorded at a ram-air velocity of 10 m/s, when the thermostatic valve released the hot coolant into the long circuit for 20 seconds. Heat transfer from the coolant to the ambient increases with increasing volume and airflow through the cooler core, which positively affects the efficiency of engine operation.

Key words: engine cooler, coolant, fan, ram-air, temperature

ABSTRAKT: Príspevok sa zaoberá skúmaním vplyvu náporového vzduchu na proces chladenia ohriatej chladiacej kvapaliny cirkulujúcej chladiacim okruhom motora automobilu. Axiálny bubnový ventilátor umiestnený pred výmenníkom tepla slúži pre simuláciu prúdu náporového vzduchu pri stredných rýchlostiach 6, 8 a 10 m/s. Zároveň, na chladiči je osadený továrenský ventilátor za účelom porovnania času potrebného pre odvod prebytočného tepla len pomocou náporového vzduchu a núteným chladením pomocou ventilátora na chladiči. Zmes chladiacej kvapaliny pozostáva z etylénglykolu a vody v pomere 1:1. Pre záznam teplôt chladiacej kvapaliny na vstupe a výstupe chladiča a rozloženia teplôt na chladiči sú použité termistory a termovízna technika. Najkratšia doba chladenia horúcej chladiacej kvapaliny bola zaznamenaná pri rýchlosti náporového vzduchu 10 m/s, kedy termostatický ventil prepúšťal horúcu chladiacu kvapalinu do veľkého okruhu po dobu 20 sekúnd. Prenos tepla z chladiacej kvapaliny do okolia stúpa spolu s narastajúcim objemom a prietokom prúdiaceho vzduchu jadrom chladiča, čo pozitívne ovplyvňuje efektivitu prevádzky motora.

Kľúčové slová: chladič motora, chladiaca kvapalina, ventilátor, náporový vzduch, teplota

INTRODUCTION

Today's automobiles are equipped with highly efficient and powerful engines (Dwivedi & Rai 2015). It also affects the life of engine components (Thantla et al. 2023). Engine performance and efficiency are affected by various systems such as the air intake system, fuel system, lubrication system, cooling system, etc. (Channankaiah & Arunpandiyan 2016). The cooling system is one of the most important systems within the car. It plays an important role in maintaining the operating temperature of the engine (Chastain et al. 2010; Pang et al. 2012). It removes the waste heat produced during engine operation to ensure optimum combustion in the cylinder (Wang et al. 2014; Amrutkar & Patil 2013). Waste heat is dissipated through the engine cooler (heat exchanger), which ensures the transfer of heat from the engine components to the surrounding environment (Mounika et al. 2016). Typically, it is a cross heat exchanger transferring heat from the hot coolant coming out of the engine to the air flowing through it, either naturally (air rush when the car is moving) or forced (cooler fan) (Shah & Gaurvadkar 2023). The coolant flows through the cooler when its temperature exceeds its operating value and the heat needs to be transferred to cooler air (Fatigati et al. 2021). During this process, cooled coolant is circulated in the engine to reduce its temperature (Muller et al. 2023). The performance of the cooling system is influenced by 2 factors. One is the mass flow through the cooler and the other is the air distribution at the inlet surface of the cooler (Zhang et al. 2018). Authors (Salehi et al. 2023) stated in their paper that increasing the mass flow of air passing over the surface of the cooler increases heat transfer, which results in an increase in cooling performance. Mass flow and flow distribution depend on ambient air velocity, vehicle movement speed, radiator fan performance and geometric parameters.

Ambient air at a lower temperature is an important part of the heat transfer process as it removes excess heat from the heat exchange surfaces of coolers and engine component surfaces. The air in the hot core cooler environment is heated in a relatively short time. In order for the cooler to efficiently dissipate heat back into the ambient air, the continuously heated air must be replaced with cool air to ensure that the heat exchange process continues. Coolers are therefore predominantly placed at the front of the vehicle, where the heat is continuously extracted by the ram-air. Ram-air is the flow of air through and around the bodywork caused by movement between the vehicle and the air surrounding the vehicle. Ram-air can also be applied to a stationary vehicle (idling) when the heat exchange surfaces of the radiators are cooled by the ambient wind. The amount and velocity of the ram-air passing to the cores of vehicle coolers are influenced by the size of the openings in the front end, the design of the body elements, the elements used to direct the airflow, and the radiator support wall. Up to 95 % of the cooling of the coolant inside the cooling circuit takes place by means of ram-air. At the moment when a sufficient flow of charge air through the coolers is not ensured, an additional device is put into operation. The volume of air passing through the cooler core is increased in modern vehicles by an electric fan or a pair of electric fans. These are axial fans, installed to the heat exchange surface of the cooler on the air side (Hussein et al. 2014). They blow air between the fins and tubes of the heat exchange surface which provides temperature control of the engine and also prevents it from overheating (Razak et al. 2017).

Authors (Manat et al. 2022) investigated the effect of three types of coolants and charge air on radiator performance. The fan generating the air pressure was fitted to the front of the cooler. As part of the experimental tests, the cooler temperature was monitored at different air velocities. The results showed that an increase in fan velocity (increase in air flow) in front of the cooler will improve heat dissipation from the heat exchange surface. Authors (Gemicioglu & Demircan 2021) investigated the effect of using different ethylene glycol/water mixture ratios on the performance of the engine cooler. A fan mounted in front of the heat exchange surface generated a cooling air stream with a velocity of 1 ÷ 4 m/s. The best cooling effect was achieved using pure water only, with a coolant inlet temperature of 80 °C, a flow rate of 22 l/min and an airflow velocity of 4 m/s. Again, the increase in cooling air flow and velocity has been shown to provide more efficient heat transfer.

In the present study is investigated the effect of ram-air on the cooling time of the heated coolant and the temperature drop of the automotive cooling circuit. The cooling process was accomplished by a factory cooler fan mounted to the heat exchange surface and an axial drum industrial fan used to simulate the vehicle‘s ride. The coolant temperature was sensed using thermistors in the inlet and outlet pipes of the vehicle cooler. The distribution of temperature fields on the heat exchange surface, inlet and outlet pipes of the cooler was captured by the FLIR E5-XT thermal imaging camera.

MATERIAL AND METHODS

Experimental setup of the automobile engine cooling circuit inspired by Ali et al. 2015; Cuevas et al. 2011; Goudarzi et al. 2017; Heris et al. 2014; Vasudevan et al. 2015; Wang et al. 2017; Yadav & Singh 2011 is shown in Fig. 1, with the principle of operation. The size of the experimental cooling circuit and the volume of coolant contained plays a key role in simulating the heating and cooling process (Singh et al. 2017). In the experimental cooling circuits used so far, the volume of coolant contained exceeded the standard volume of coolant contained in a real car engine cooling circuit. The increase in coolant volume can negatively affect the duration of the heating and cooling process, leading to a distortion of the acquired data from the experimental tests. For this reason, an experimental cooling circuit was constructed according to a real car cooling circuit with a total cooling charge volume of 6 liters.

Even though there is no combustion process in the cylinder block (5), the coolant temperature reaches 80 °C, which represents the optimum operating temperature of a real engine. The necessary heat required to monitor changes in the thermal parameters of the cooling circuit is generated by a heating coil (11) with an output of 1.5 kW located in the heating element (12). The heater (12) is connected in the cooling circuit to a pipe which originally served for the supply and discharge of heated coolant into the cabin (interior) of the vehicle.

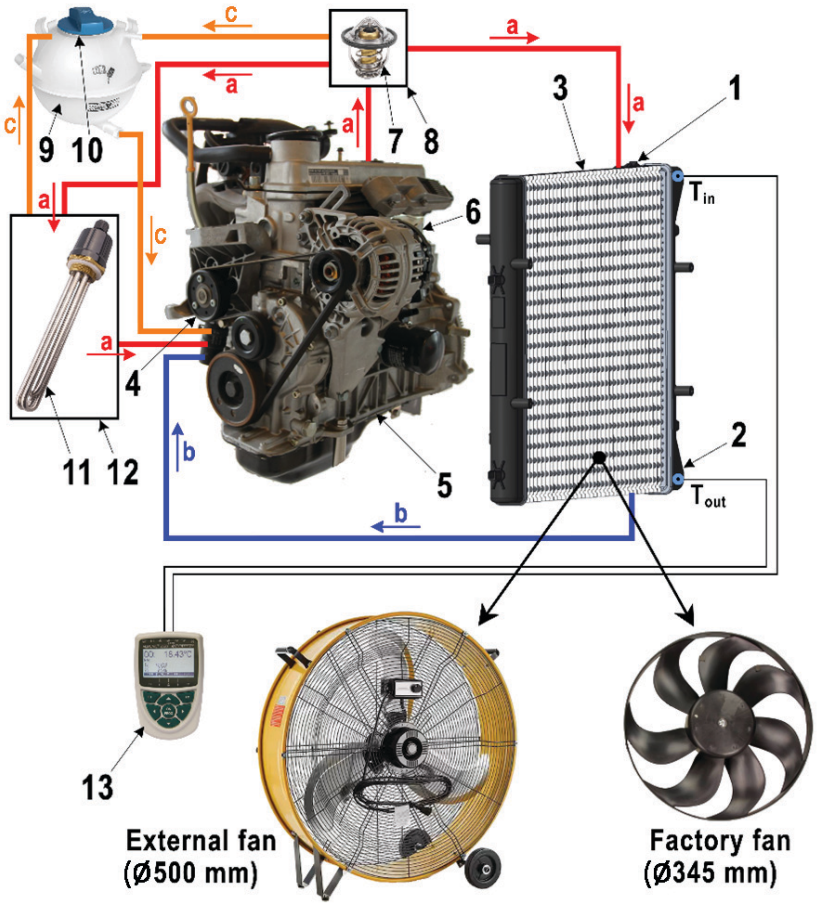

Fig. 1 The scheme of experimental set-up

1 – inlet cooler pipe, 2 – outlet cooler pipe, 3 – heat exchange surface (cooler core), 4 – water pump, 5 – cylinder block, 6 – cylinder head, 7 – thermostatic valve, 8 – thermostatic valve body, 9 – expansion tank, 10 – overpressure plug, 11 – heating spiral, 12 – heating spiral body, 13 – datalogger, a – hot coolant (up 80 °C), b – cooled coolant (below 80 °C), c – coolant operating temperature (80 °C)

Obr. 1 Schéma experimentálneho zariadenia

1 – vstupné potrubie chladiča, 2 – výstupné potrubie chladiča, 3 – teplovýmenná plocha (jadro chladiča), 4 – vodné čerpadlo, 5 – blok valcov, 6 – hlava valcov, 7 – termostatický ventil, 8 – teleso termostatického ventilu, 9 – expanzná nádobka, 10 – pretlaková zátka, 11 – ohrevná špirála, 12 – teleso ohrevnej špirály, 13 – záznamník hodnôt, a – horúca chladiaca kvapalina (nad 80 °C), b – ochladená chladiaca kvapalina (pod 80 °C), c – prevádzková teplota chladiacej kvapaliny (80 °C)

The cooling system is flooded with coolant through the expansion vessel (9). By starting the electric motor using the frequency converter, start the water pump (4). The electric

motor is connected to the water pump by a V-belt, which is tensioned by a mechanism. The experimental cooling system assembly has two cooling circuits (small and large). the cooling medium flows in a small cooling circuit at a temperature of up to 80 °C. It consists of a water pump (4) which drives the coolant through the cylinder block (5), the cylinder head (6) and subsequently into the thermostat body (8). From there, the coolant is driven to the inlet of the heater. In the heating spiral body (12), the coolant is heated by a heating spiral (11). In the case of aeration or flooding of the heating element (12), a return pipe (d) is led from its upper part to the expansion vessel (9). The outlet of the heating element is connected by a pipe to a water pump. The coolant flows in a small circuit until the temperature rises above 80 °C. Subsequently, the thermostatic valve housed in the thermostat body (8) starts to open and the hot refrigerant flows to the inlet of the cooler (1). In the event that the hot liquid cannot flow under pressure through the cooler (3), a part of it flows through the return pipe (d) into the expansion vessel. Through the cooler outlet pipe (2), the cooled medium flows back to the water pump and from there back to a small circuit until the coolant temperature drops below 80 °C. If the coolant cannot be cooled by the engine cooler itself, the fan is activated, which more intensively removes heat from the pipes and fins of the cooler.

The distribution and circulation of the cooling air volume to the heated cooler core was provided by a Master DF 20 P fan placed in front of the cooler. An axial fan takes in and blows out air parallel to the axis of the drive (increasing the pressure of the air flowing through it). This type of fan provides an airflow of 6,600 m^3/h and has an ideal outer diameter (ø 500 mm), which is identical in size to the built-up engine cooler from the Skoda Fabia 1.4 (Fig. 2). Outlet airflow can be set in three stages (stage 1: 6 m/s, stage 2: 8 m/s, stage 3: 10 m/s). The fan can be rotated both horizontally and vertically to simulate side airflow.

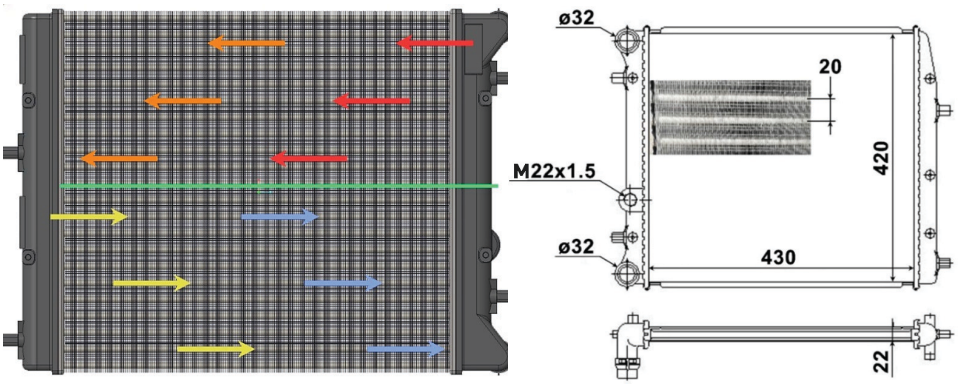

a) b)

Fig. 2 Skoda Fabia 1.4 cooler used in the research, a) direction of coolant flow, (b) basic dimensions

Obr. 2 Chladič Škoda Fabia 1.4 použitý pri výskume, a) smer toku chladiacej kvapaliny, b) základné rozmery

The arrangement of the tubes in this type of cooler is consecutive, the fluid flow is transverse, and the tubes are divided by a dividing chamber into an upper and a lower part (two-way cooler). The radiator from the Skoda Fabia 1.4 engine consists of 44 tubes, which are arranged in two rows of 22 pieces in each row. The spacing between each ø 5 mm diameter pipe is 20 mm and the spacing between the first and second rows is 10 mm. Along the entire length of the cooler tubes 430 mm, fins are fitted on the tubes for intensive heat dissipation.

The experimental measurements were carried out while the coolant in the large engine coolant circuit was cooling down until the thermostat was closed (below 80 °C). Cooling process of the G12 coolant lasted experimentally for 180 seconds after the fans were started. During heating and cooling, the temperatures of the coolant in the pipes at the inlet (Fig. 3a) and outlet (Fig. 3b) of the cooler, were recorded by means of two NTC ZA 9040-FS thermistors (accuracy ±0.01 °C). Temperature values from the course of measurements were recorded by the ALMEMO 2590-4S datalogger. The temperature distribution on the surface of the cooler was non-contactless recorded by a thermal imaging camera FLIR E5-XT (accuracy ±2% of the recorded value, detector resolution 160×120 points, measured temperature range from -20 °C to +250 °C, field of view 45°×34°), (Fig. 3c).

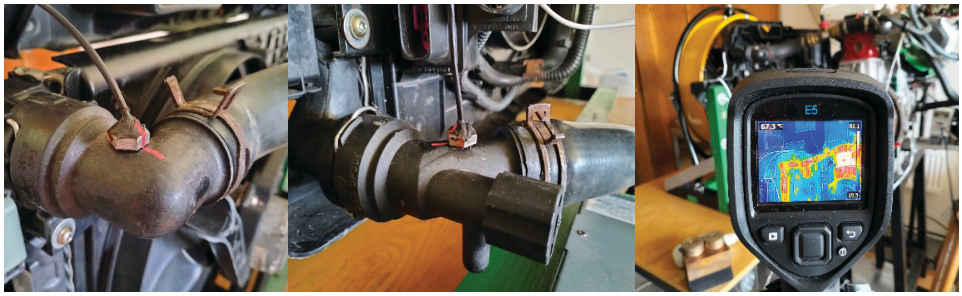

a) b) c)

Fig. 3 Sensors and instruments for recording temperatures, (a) thermistor in the inlet pipe of the cooler, (b) thermistor in the outlet pipe of the cooler, (c) thermal imaging camera

Obr. 3 Snímače a prístroje pre záznam teplôt, a) termistor vo vstupnom potrubí chladiča, b) termistor vo výstupnom potrubí chladiča, c) termovízna kamera

RESULTS AND DISCUSSION

Coolant inlet temperatures (Fig. 4) and coolant outlet temperatures (Fig. 5) were recorded while monitoring the cooling process. To determine the difference in cooling efficiency, a measurement was first made using the engine cooler fan. Subsequently, an industrial fan was mounted in front of the cooler and after heating the coolant in the circuit to the operating temperature (80 °C), the industrial fan was started with an initial air velocity of 26.6 km/h (6 m/s). This was followed by an increase in air velocity to 28.8 km/h (8 m/s) and the highest possible velocity that the fan can generate to 36 km/h (10 m/s).

Within the inlet manifold of the cooler, the industrial fan with all tested airflow velocity initially achieved better temperature values by time 0:01:30. This is because the ram-air does not have to first suck the hot air through the heat exchange surface (causing

the heat exchange to slow down) and divert it towards the engine compartment, as is the case with a fan. The ram-air passes directly through the heat exchange surface at ambient temperature, which is usually a few tens of degrees lower (in this case 20 °C). The reversal occurred at time 0:02:00, when the engine cooler fan achieved better heat dissipation compared to the intake air by 0.5 °C on average, with this value rising to 1.5 °C at the end of the measurements (time 0:03:00). This is because the ram-air passing through the heat exchange surface of the cooler hits the plastic cover of the cooler fan, which prevents the ram-air from cooling individual hoses or components of the cooling system or engine. The only possible path of the ram-air passing through the heat exchange surface is between the individual fan blades, thus the heat dissipation from the components located behind the cooler is relatively limited. However, this problem does not occur when the cooler fan is running as it initially draws in hot air from in front of the cooler and discharges it into the engine compartment, which at the same time lowers the temperature of the engine. In real engine operation, however, the measured difference in fan and charge air efficiency is negligible because the temperature drop during the cooling process is usually below the operating temperature and cooling lasts only a few seconds.

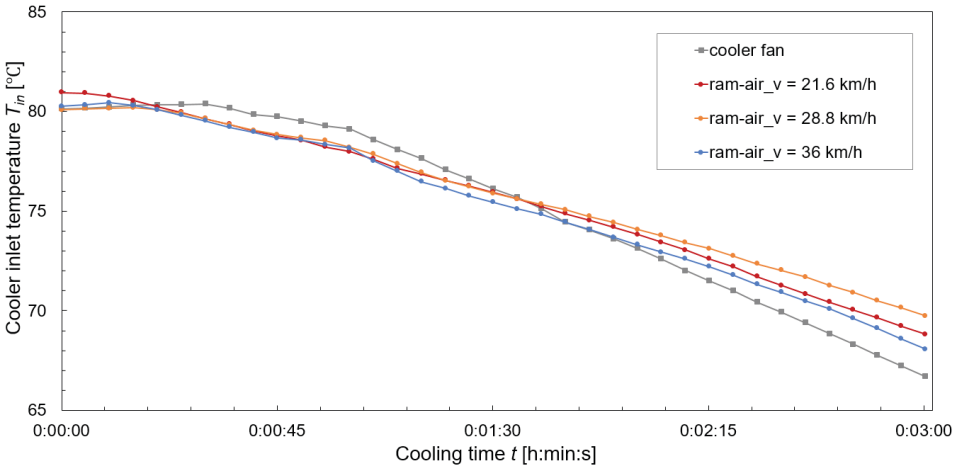

Fig. 4 Comparison of cooling times at the cooler inlet when using a cooler fan and an external fan (ram-air)

Obr. 4 Porovnanie časov ochladzovania na vstupe do chladiča pri použití ventilátora chladiča a externého ventilátora (nápor vzduchu)

For efficient operation of an internal combustion engine, it is essential to maintain its temperature within the optimum temperature range (coolant 80 ÷ 90 °C, lubricating oil 80 ÷ 120 °C). If the engine does not achieve it, this leads to increased wear of components (moving parts), increased exhaust gas pressure, degradation of the operating cartridges, increased fuel consumption and loss of power.

Table 1 Coolant inlet temperatures drop during the cooling process by the cooler fan and the external fan (ram-air)
Tabuľka 1 Pokles teplôt chladiacej kvapaliny na vstupe do chladiča pri procese chladenia ventilátorom chladiča a externým ventilátorom (nápor vzduchu)

Cooling time t (h:min:s)	Cooler fan	External fan v = 6 m/s (26,6 km/h)	External fan v = 8 m/s (28,8 km/h)	External fan v = 10 m/s (36 km/h)
	T_{in} (°C)	T_{in} (°C)	T_{in} (°C)	T_{in} (°C)
0:00:00	80.1	81.0	80.1	80.3
0:00:05	80.2	80.9	80.1	80.3
0:00:10	80.2	80.8	80.1	80.4
0:00:15	80.3	80.5	80.2	80.3
0:00:20	80.3	80.2	80.1	80.1
0:00:25	80.4	80.0	79.9	79.8
0:00:30	80.4	79.7	79.6	79.5
0:01:00	79.1	78.0	78.2	78.2
0:02:00	73.1	73.8	74.1	73.3
0:03:00	66.7	68.8	69.7	68.1

For the engine to operate in optimum condition, it is essential to ensure that the cooled coolant is transported from the cooler outlet to the thermostatic valve in the shortest time. The comparison of the coolant temperatures during the cooling process flowing from the thermostatic valve into the cooler inlet pipe and the subsequent break in coolant flow through the cooler core (thermostatic valve closure due to temperature drop below 80 °C) is shown in the Table 1.

The forced cooling process in the small cooling circuit of the car engine does not usually exceed 30 seconds. When the engine and its components function properly during this time, the large cooling circuit will be closed by the thermostatic valve. The faster the coolant temperature drops slightly below the operating temperature, the faster the engine runs efficiently. From the curve plot of Fig. 4, during the cooling process by the cooler fan, the coolant temperature did not drop below 80 °C within 30 seconds of start-up. The thermostatic valve closed the coolant supply to the cooler at 0:00:40 when the temperature reached T_{in} = 79.9 °C. In the process of cooling the coolant with an external fan, the temperature dropped below the operating value of 80 °C at the same time (0:00:25) for all 3 airflow rates tested. The lowest inlet coolant temperature T_{in} = 79.5 °C was recorded at 0:00:30 from the start of the fan with an airflow velocity of 10 m/s.

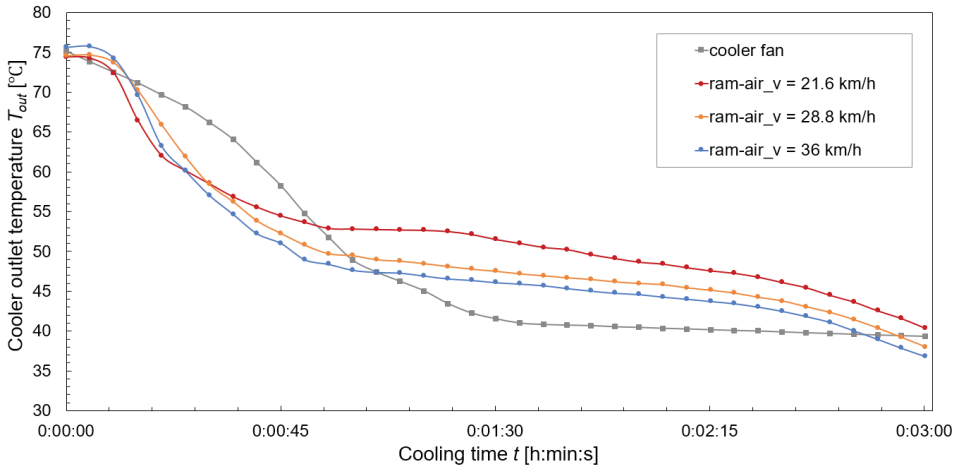

Fig. 5 Comparison of cooling times at the cooler outlet when using the cooler fan and the external fan (ram-air)

Obr. 5 Porovnanie časov ochladzovania na výstupe z chladiča pri použití ventilátora chladiča a externého ventilátora (nápor vzduchu)

The curve plot of Fig. 5 for the cooler fan cooling process shows that after 30 seconds, the coolant temperature value dropped to T_{out} = 66.2 °C. In the process of cooling the cooler core with ram-air (external fan), lower coolant temperatures were recorded for the same time compared to the cooler fan for all tested air velocities.

A comparison of the coolant temperature drops in the cooler during the cooling process by the factory fan and the external fan (ram-air) is shown in Table 2. The temperature drop ΔT represents the difference between the inlet temperature T_{in} and the outlet temperature T_{out} of the coolant. The maximum temperature drop reaches during the first 30 seconds from the start of the cooling process by the cooler fan was ΔT = 14.2 °C. As the volume of air passing through the core of the cooler increases in a shorter time, the temperature difference between the inlet and outlet temperature of the coolant increases - making the cooling process more efficient. This also applies in the case of the external fan cooling process where the largest temperature drops (ΔT = 22.5 °C) was within 30 seconds of the fan start at a forced air velocity of 10 m/s.

Table 2 Outlet coolant temperature at the cooler outlet during the cooling process by the cooler fan and the external fan (ram-air)
Tabuľka 2 Teploty chladiacej kvapaliny na výstupe z chladiča pri procese chladenia ventilátorom chladiča a externým ventilátorom (nápor vzduchu)

Cooling time t (h:min:s)	Cooler fan		External fan v = 6 m/s (26,6 km/h)		External fan v = 8 m/s (28,8 km/h)		External fan v = 10 m/s (36 km/h)	
	T_{out} (°C)	ΔT (°C)	T_{out} (°C)	ΔT (°C)	T_{out} (°C)	ΔT (°C)	T_{out} (°C)	ΔT (°C)
0:00:00	75.1	5.0	74.4	6.5	74.6	5.5	75.6	4.6
0:00:05	73.8	6.4	74.3	6.7	74.7	5.4	75.7	4.6
0:00:10	72.5	7.8	72.4	8.4	73.7	6.4	74.3	6.2
0:00:15	71.2	9.2	66.5	14.1	70.3	9.9	69.7	10.6
0:00:20	69.6	10.7	62.0	18.2	65.9	14.2	63.2	16.8
0:00:25	68.1	12.2	60.1	19.8	61.9	18.1	60.1	19.7
0:00:30	66.2	14.2	58.5	21.2	58.4	21.2	57.1	22.5
0:01:00	48.9	30.3	52.8	25.2	49.5	28.7	47.7	30.5
0:02:00	40.4	32.7	48.7	25.2	46.0	28.1	44.6	28.7
0:03:00	39.3	27.4	40.4	28.5	38.0	31.7	36.8	31.2

Thermal images of the temperature fields during the cooling process by the cooler fan (Fig. 6) and the external fan (Fig. 7) were recorded at a time interval of 30 seconds.

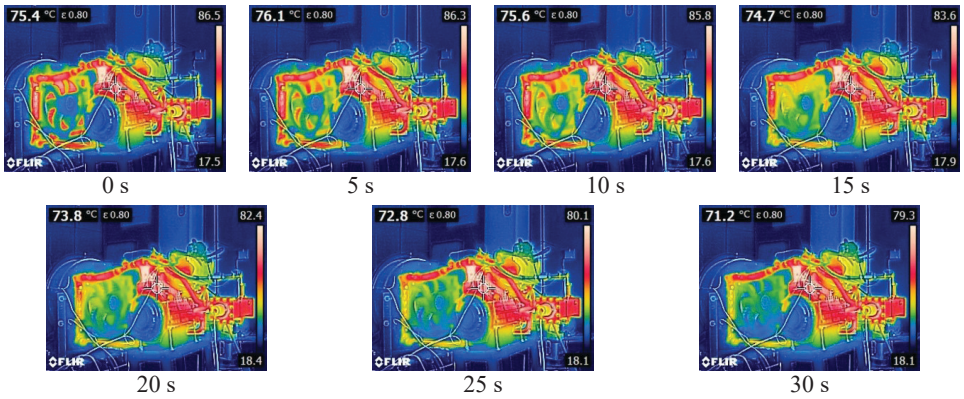

Fig. 6 Thermal images during the cooling process by the cooler fan (fan located behind the cooler)

Obr. 6 Termovízne snímky počas procesu chladenia ventilátorom chladiča (ventilátor za chladičom)

Among the most heat-exposed components in an internal combustion engine during operation are the cylinder head and cylinder block, where high temperatures are generated because of the combustion process of the mixture in the cylinder. During the experimental tests, the thermal imaging camera imaged the surface of the cylinder block where, as in the real engine, the greatest heat accumulation occurred.

From the comparison of the sensed surface temperatures, the temperature drop of the cylinder block surface during the external fan cooling process (air velocity of 10 m/s) for 30 seconds was 4.2 °C. In the process of cooling by the cooler fan, the surface temperature of the cylinder block dropped by 11.5 °C in 30 seconds. The three-fold reduction in surface temperature by the cooler fan is due to its location. The cooler fan is attached to the heat exchange surface by means of a wreath. This shroud is full except for the cut-out for the fan mounting and allows the distribution of the ram-air further to the engine only between the fan blades. In contrast, the airflow generated by the cooler fan blades has no obstacle in its path, it flows directly onto the individual surfaces of the engine components, thus cooling them at the same time.

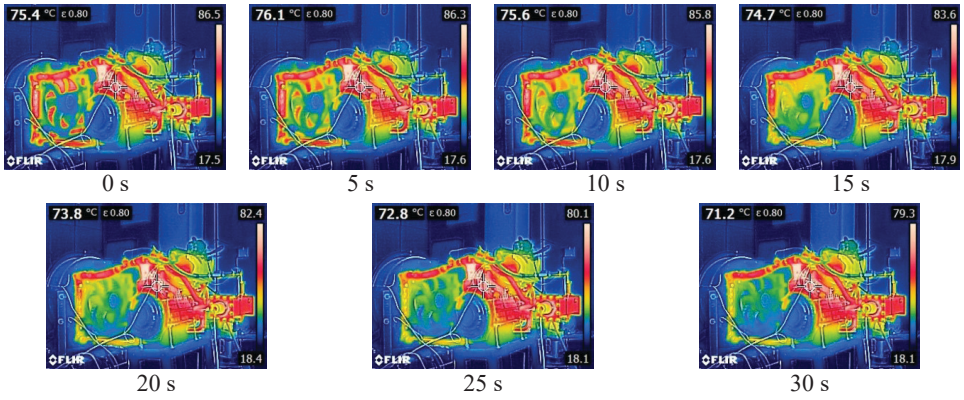

Fig. 7 Thermal images during the external fan cooling process
(ram-air: fan located in front of the cooler)

Obr. 7 Termovízne snímky počas procesu chladenia externým ventilátorom
(náporový vzduch: ventilátor umiestnený pred chladičom)

However, more meaningful than the surface temperature of the components is the temperature inside the engine. Compared to the cooler fan, the external fan provided a higher coolant temperature drop (from an operating value of 80 °C) at the cooler outlet of 9.1 °C. In the case of correct operation of the engine and its groups, the ram-air (driving of the vehicle) reliably ensures intensive dissipation of excess heat and maintenance of the optimum temperature. The cooler fan is started only rarely and for a short period of time (15 ÷ 30 seconds on average) when there is insufficient flow of ambient air at a lower temperature through the heat exchange surface.

CONCLUSION

For the efficient operation of an internal combustion engine, it is necessary to maintain it within the optimum operating temperature range. In a real car engine cooling circuit, excess heat from the coolant is removed from the 95 % during operation by the forward movement of the vehicle (ram-air) or by the airflow from the cooling fan. In the vehicle driving simulation of the experimental tests, the process of cooling the G12 coolant with 10 m/s ram-air achieved a higher temperature drop of 0.8 °C at the cooler inlet pipe after 30 seconds. At this point, the inlet temperature was T_{in} = 79.5 °C, indicating a break in the coolant flow from the small circuit. During the cooling process by the cooler fan, the inlet coolant temperature did not drop below 80 °C (T_{in} = 80.4 °C) and the hot liquid inflow from the small circle continued. The faster the flow of coolant is break (a slight drop in temperature below the operating value of 80 °C − thermostatic valve closure), the faster the engine will be able to work more efficiently.

The cooling process with an external fan (ram-air) achieved a higher temperature drop even within the monitored outlet pipe of the cooler. After 30 seconds, the G12 coolant reached a temperature of T_{out} = 57.1 °C at the outlet, which is an improvement of 9.1 °C compared to the cooler fan.

Based on the measured data, the fact was confirmed that the larger the volume and flow rate of the air flowing through the heat exchanger surface of the cooler, the more efficient the dissipation of excess heat, resulting in an increase in the efficiency of engine operation.

ACKNOWLEDGMENT

This research was funded by the EU NextGenerationEU through the Recovery and Resilience Plan for Slovakia under the project No. 09I03-03-V05-00016.

REFERENCES

ALI, H. M., ALI, H., LIAQUAT, H., MAQSOOD, H. T. B., NADIR, M. A. 2015. Experimental investigation of convective heat transfer augmentation for car radiator using ZnO-water nanofluids. In Energy, Elsevier, vol. 84, pp 317-324. DOI: 10.1016/j.energy.2015.02.103.

AMRUTKAR, P. S., PATIL, S. R. 2013. Automotive Radiator Performance – Review. In IJEAT International Journal of Engineering and Advanced Technology, vol. 2, no. 3, pp 563-565. ISSN: 2249-8958.

CUEVAS, C., MAKAIRE, D., DARDENNE, L. NGENDAKUMANA, P. 2011. Thermo-hydraulic characterization of a louvered fin and flat tube heat exchanger. In Experimental Thermal and Fluid Science, vol. 35, pp 154-164. ISSN: 0894-1777.

DWIVEDI, V. D., RAI, R. 2015. Modelling and Fluid Flow Analysis of Wavy Fin Based Automotive Radiator. In Journal of Engineering Research and Applications, vol. 5, no. 1, pp 17-26. ISSN: 2248-9622.

FATIGATI, F., BATTISTA, D. D., CIPOLLONE, R. 2021. Design improvement of volumetric pump for engine cooling in the transportation sector. In Energy, vol. 231, pp 1-18. DOI: 10.1016/j.energy.2021.120936.

GEMICIOGLU, B., DEMIRCAN, T. 2021. Experimental analysis of the effects of using different water-ethylene glycol mixture rates on heat transfer performance in a heat exchanger. In J ESOGU Engin Arch Fac., vol. 29, no. 2, pp 145-157. DOI:10.31796/ogummf.870256.

GOUDARZI, K., JAMALI, H. 2017. Heat transfer enhancement of Al_2O_3-EG nanofluid a car radiator with wire coil inserts. In Applied Thermal Engineering, vol. 118, pp 510-517, DOI: 10.1016/j.applthermaleng.2017.03.016.

HERIS, S. Z., SHOKRGOZAR, M., POORPHARHANG, S., SHANBEDI, M., NOIE, S. H. 2014. Experimental Study of Heat Transfer of a Car Radiator with CuO/Ethylene Glycol-Water as a Coolant. In Journal of Dispersion Science and Technology, vol. 35, no. 5, pp 677-684, ISSN: 0193-2691.

HUSSEIN, A. M., BAKAR, R. A., KADIRGARGAMA, K., SHARMA, K. V. 2014. Heat transfer enhancement using nanofluids in an automotive cooling system. In International Communications in Heat and Mass Transfer, vol. 53, pp 195-202. DOI: 10.1016/j.icheatmasstransfer. 2014.01.003.

CHANNANKAIAH, Dr., ARUNPANDIYAN, D. 2016. A Review of Automotive Radiator Performance. In IJIRST International Journal for Innovative Research in Science & Technology, vol. 2, no. 10, pp 166-169. ISSN: 2349-6010.

CHASTAIN, J., WAGNER, J., EBERTH, J. 2010. Advanced Engine Cooling – Components, Testing and Observations. In IFAC Proceedings Volumes, vol. 43, no. 2, pp 294-299. DOI:10.3182/20100712-3-DE-2013.00007.

MANAN, A. N. A., ANUAR, DZ., KHALID, M. L. A., ISMAIL, A. K., AZID, I. A. 2022. Overall Heat Transfer Coefficient of Different Coolants and Frontal Air Velocity in Automotive Radiators. In Advanced Structured Materials, vol. 169, pp 139-146. ISSN: 1869-8441.

MOUNIKA, P., SHARMA, R. K., KISHORE, P. S. 2016. Performance Analysis of Automobile Radiator. In IJRMEE International Journal on Recent Technologies in Mechanical and Electrical Engineering, vol. 3, no. 5, pp 35-38. ISSN: 2349-7947.

MULLER, J., BESSER, N., HERMSEN, P., PISCHINGER, S., KNAUF, J., BAGHERZADE, P., FRYJAN, J., BALAZS, A., GOTTORF, S. 2023. Virtual Development of Advanced Thermal Management Functions Using Model-in-the-Loop Applications. In Energies, vol. 16, no. 7, pp 1-26. DOI:10.3390/en16073238.

PANG, S. C., KALAM, M. A., MASJUKI, H. H., HAZRAT, M. A. 2012. A review on air flow and coolant flow circuit in vehicles – cooling system. In International Journal of Heat and Mass Transfer, vol. 55, pp 6295-6306. ISSN: 0017-9310.

RAZAK, N. F. D., SANI, M. S. M., AZMI, W. H., ZHANF, B. 2017. Noise and vibration analysis for automotive radiator cooling fan. In IOP Conf. Ser.: Mater. Sci. Eng., vol. 257, pp 1-10. DOI:10.1088/1757-899X/257/1/012083.

SALEHI, H., BASIR, H., BIDHENDI, H. M., FARHANI, F., ROSEN, M. A. 2023. Experimental and simulation study of an automobile cooling system: Performance improvement using passive flow control. In Int. Commun. Heat Mass Transf., vol. 149, pp 1-16. DOI: 10.1016/j.icheatmasstransfer.2023. 107168.

SHAH, A. P., GAURVADKAR, A. 2023. Design and development of automotive radiator for better cooling efficiency. In Materials Today: Proceedings, vol. 72, no. 3, pp 1028-1034. DOI: 10.1016/j.matpr.2022.09.153.

SINGH, S., KUMAR, A., KHAN, F. 2017. Experimental study for heat transfer enhancement of car radiator using twisted inserts with coolants. In International Journal of Interdisciplinary Research, vol. 3, no. 1, ISSN: 2455-1600.

THANTLA, S., ASPFORS, J., GHANBARPOUR, M., FRIDH, J. 2023. Performance analysis of a dual-loop organic Rankine cycle system for waste heat recovery from engine coolant and exhaust of a heavy-duty truck. In Appl. Therm. Eng, vol. 219, pp 1-15. DOI: 10.1016/j.applthermaleng.2022.119203.

VASUDEVAN NAMBESAN, K. P., PARTHIBAN, R., RAM KUMAR, K., ATHUL, U. R., VIVEK, M., THIRUMALINI, S. 2015. Experimental study of heat transfer enhancement in automobile radiator using Al_2O_3/water-ethylene glycol nanofluid coolants. In IJAME International Journal of Automotive and Mechanical Engineering, vol. 12, pp 2857-2865, ISSN:2229-8649.

WANG, T. T., JAGARWAL, A., WAGNER, J. R., FADEL, G. 2014. Optimization of an Automotive Radiator Fan Array Operation to Reduce Power Consumption. In IEEE/ASME transactions on mechatronics, vol. 20, no. 5, pp 1-11. DOI:10.1109/TMECH.2014.2377655.

WANG, H., CAI, Y., WANG, W., A. 2017. A dynamic thermal-mechanical model of the spindle-bearing system. In Mechanical Sciences, vol. 8, no. 2, pp 277-288. DOI:10.5194/ms-8-277-2017.

YADAV, J. P., SINGH, B. R. 2011. Study on performance evaluation of automotive radiator. In A Journal of Physical Sciences, Engineering and Technology, vol. 2, no. 2, pp 47-56. ISSN: 2229-7111.

ZHANG, CH., UDDIN, M., ROBINSON, A. C., FOSTER, L. 2018. Full vehicle CFD investigations on the influence of front-end configuration on radiator performance and cooling drag. In Appl. Therm. Eng, vol. 130, pp 1328-40. DOI: 10.1016/j.applthermaleng.2017.11.086.

Corresponding author:

Ing. Marek Lipnický, PhD. tel.: +421455206 871, e-mail: marek.lipnicky@tuzvo.sk

TESTING AND EVALUATION OF THE ADHESION PROPERTIES OF MOTORCYCLE TIRES

TESTOVANIE A HODNOTENIE ADHÉZNYCH VLASTNOSTÍ MOTOPNEUMATÍK

Martin Krasňanský[1], Ivan Janoško[2]

[1] *Institute of Agricultural Engineering, Transport and Bioenergetics, Department of Transport and Handling, Faculty of Engineering, Slovak University of Agriculture in Nitra, Tr. A. Hlinku 2, 949 76 Nitra, Slovak Republic, email: xkrasnansky@uniag.sk*
[2] *Institute of Agricultural Engineering, Transport and Bioenergetics, Department of Transport and Handling, Faculty of Engineering, Slovak University of Agriculture in Nitra, Tr. A. Hlinku 2, 949 76 Nitra, Slovak Republic, email: ivan.janosko@uniag.sk*

ABSTRACT: The main objective of this research is to test the adhesion properties of motorcycle tires and brakes with Nankang Sportiac WF-2 tires using deceleration. Nowadays, the probability of a traffic accident is increased with the ever-increasing number of vehicles on our roads, while most accidents can be prevented by improving the condition and driving characteristics of the vehicle and training the driver in critical situations. It is also necessary to improve the driving characteristics of the motorcycle with the ever-increasing power of motorcycles. Our measured motorcycle is equipped with a sports exhaust and on the front pair of brakes it is equipped with Brembo brake pads with a sintered compound. At the time of measurement, the front tire had approximately 3,000 km and the rear approximately 1,000 km. We used the device XL MeterTM Pro Alfa designed to measure the acceleration or deceleration of the vehicle needed to calculate tire adhesion while the device must be positioned such way that its attachment is perpendicular to the road and the axis of the measuring device is parallel to the axis of the vehicle. Another device was a digital rollmeter used to measure ground distances and to check the results of the braking distance. Before the measurements themselves, it was necessary to fix the measuring device and to perform test rides to evaluate the road quality and warm up the test motorcycle. Measurements on the said motorcycle were carried out at three different speeds of 50, 70 and 100 $km.h^{-1}$, while at each speed braking was measured either with only the front brake, the rear brake or both brakes together. In all measurements with only the rear brake, the rear wheel skidded, while when braking with the rear brake from speeds of 75 and 98 $km.h^{-1}$ and when braking from speeds of 67 and 102 $km.h^{-1}$, the rear wheel lifted into the air. The highest deceleration was achieved at a speed of 79 $km.h^{-1}$ at a value of 9.77 $m.s^{-2}$ when braking with only the front brake, which corresponds to an adhesion of 0.99, while the lowest adhesion values were achieved at braking with the rear brake only in the value of 0.34 due to the low load on the rear wheel and dynamic load transfer. During limit braking with the front brake, the entire gravitational force is dynamically transferred to the front wheel, which makes it possible to use the entire weight for braking power, thus this phenomenon has a great influence on the resulting deceleration. The given method of determining the limit adhesion can be considered technically acceptable and

correct. From the resulting measurement values, it follows that braking with the rear brake is very difficult due to the rapid occurrence of wheel locking and the subsequent threat of loss of stability.

Key words: motorcycle, tires, deceleration, adhesion,

ABSTRAKT: Hlavným cieľom tohto výskumu je testovanie adhéznych vlastností a bŕzd pomocou spomalenia na motocykle s pneumatikami Nankang Sportiac WF-2. V dnešnej dobe s neustále sa zvyšujúcim počtom vozidiel na našich cestách je zvýšená pravdepodobnosť dopravnej nehody, pričom väčšine nehôd sa dá predísť zlepšením stavu a jazdných vlastností vozidla a školením vodiča v kritických situáciách. S neustále sa zvyšujúcim výkonom motocyklov je potrebné zlepšovať aj jazdné vlastnosti motocykla. Náš meraný motocykel je vybavený športovým výfukom a na prednom páre bŕzd je vybavený brzdovými doštičkami Brembo so sintrovanou zmesou. V čase merania mala predná pneumatika najazdených približne 3000 km a zadná približne 1000 km. Pri meraniach sme použili prístroj XL MeterTM Pro Alfa určený na meranie zrýchlenia alebo spomalenia vozidla potrebného na výpočet adhézie pneumatík pričom zariadenie musí byť umiestnené tak, aby jeho upevnenie bolo kolmé na vozovku a os meracieho zariadenia bola rovnobežná s osou vozidla. Ďalší použitý prístroj bol digitálny rollmeter určený na meranie vzdialeností od zeme a na kontrolu výsledkov brzdnej dráhy. Pred samotnými meraniami bola potrebné upevnenie meracieho zariadenia a vykonanie testovacích jázd na vyhodnotenie kvality vozovky a zahriatie testovaného motocykla. Merania na uvedenom motocykli boli realizované pri troch rôznych rýchlostiach 50, 70 a 100 km.h^{-1}, pričom pri každej rýchlosti bolo merané brzdenie buď len prednou brzdou, zadnou brzdou alebo oboma brzdami spolu. Pri všetkých meraniach len so zadnou brzdou došlo k šmyku zadného kolesa pričom pri brzdení zadnou brzdou z rýchlosti 75 a 98 km.h^{-1} a pri brzdení z rýchlosti 67 a 102 km.h^{-1} sa zadné koleso zdvihlo do vzduchu. Najvyššie spomalenie bolo dosiahnuté pri rýchlosti 79 km.h^{-1} pri hodnote 9,77 m.s^{-2} pri brzdení len prednou brzdou, čo zodpovedá adhézii 0,99, pričom najnižšie hodnoty adhézie boli dosiahnuté pri brzdení so zadnou brzdou len v hodnote 0,34 z dôvodu nízkej záťaže zadného kolesa a dynamického prenosu záťaže. Pri limitnom brzdení prednou brzdou sa celá gravitačná sila dynamicky prenáša na predné koleso, čo umožňuje využiť celú hmotnosť na brzdnú silu, tým pádom tento jav má veľký vplyv na výsledné dosiahnuté spomalenie. Daný spôsob stanovenia limitnej adhézie možno považovať za technicky prijateľný a správny. Z výsledných hodnôt merania vyplýva, že brzdenie zadnou brzdou je veľmi náročné z dôvodu rýchleho vzniku zablokovania kolies a následnej hrozby straty stability.

Kľúčové slová: motocykel, pneumatiky, spomalenie, adhézia

INTRODUCTION

Nowadays, with the ever-increasing number of vehicles on our roads, there is an increased chance of a traffic accident, while most accidents can be prevented by improving the condition and driving characteristics of the vehicle and by training the driver in critical situations. With the ever-increasing performance of motorcycles, it is also necessary to improve the driving characteristics of the motorcycle. The tire has several important functions, mainly ensuring the transmission of driving forces and braking forces, indicating the direction of the vehicle and also providing the initial suspension of the vehicle. The gas in the tire can be filled either directly between the tire and the wheel rim in the case of tubeless tires or into the tube of the tire, while the gas is mostly air or pure nitrogen used mainly in sports vehicles. Tires are made of several materials, the main ones being rubber and steel. The tire is fixed on the rim. Disks can be of different types. The most

commonly used are metal or light alloy, with older vehicles or motorcycles, spoked wheels are also used. The main requirements for wheel discs are low weight, mechanical and chemical resistance, flexibility and strength. In the case of motorcycles as well as in other vehicles, it is necessary that their brakes are sufficiently dimensioned for the use of the given vehicle (Hugo, 1994; Dočkal et al., 1998). Different types of brake systems are used in motorcycles. There are drum and disc brakes. Drum brakes were often used in the past on all types of motorcycles, nowadays they are used on cheap vehicles and exclusively on the rear wheel. Their main disadvantage is insufficient cooling compared to modern disc brakes. Disc brakes system is more modern than drum brakes. Its main advantage is better heat dissipation and smaller size with the same braking effect. Disc brakes consist of three basic parts namely brake shoes, brake discs and brake segment. Just as cars are equipped with various auxiliary systems for the protection of the driver and the vehicle‘s crew, so are motorcycles (Vernanec, 2006; Kolektív autorov, 2008; Sloboda, 2008). The most used such device for braking is ABS. Another auxiliary system is traction control, the task of which is to compare the speed of the wheels, and if the system evaluates a discrepancy, the power transmitted to the driven axle is reduced. In the case of powerful machines, the anti-wheelie system prevents the front wheel from lifting during sharp acceleration. In this work, we will focus on testing the adhesion properties and brake system of the Honda CB600S motorcycle at different speeds on the selected surface (Kulhánek, 1997; Liščák, 2004; Hudák, Vrábeľ, 2010).

MATERIAL AND METHODS

Characteristic of used material

For the measurement, we used a Honda motorcycle with year of manufacture 2003 and type designation CB600S. The motorcycle is equipped with a sports exhaust pipe and on the front pair of brakes it is equipped with Brembo brake pads with sintered compound. The mentioned motorcycle does not contain any auxiliary elements either for braking or acceleration. The motorcycle was measured with Nankang Sportiac WF-2 tires. At the time of measurement, the front tire had travelled approximately 3000 km and the rear approximately 1000 km. Other characteristics and parameters of the motorcycle are shown in Tab. 1.

Tab. 1 Parameters and properties of motorcycle
Tabuľka 1 Parametre a vlastnosti motocykla Honda CB600S 2003

Motorcycle Honda CB600S 2003	
Brand[1)]	Honda
Type[2)]	motorcycle
Category[3)]	L3e
Engine capacity[4)] [cm^3]	599
Motor (type)[5)]	PC34/4/1
Maximum engine power [kW] / revolutions [min^{-1}][6)]	70 / 12 000

Maximum torque [Nm] / revolutions [min^{-1}][7)]	67 / 10 000
Operational weight[8)] [kg]	197
The size of front tire[9)]	120/70ZR 17 (58W)
The size of rear tire[10)]	180/55ZR 17 (73W)

[1)]Značka, [2)]Typ, [3)]Kategória, [4)]Objem motora, [5)]Motor, [6)]Maximálny výkon /otáčky, [7)]Maximálny krútiaci moment / otáčky, [8)]Prevádzková hmotnosť, [9)]Rozmer prednej pneumatiky, [10)]Rozmer zadnej pneumatiky

Fig. 1 Tested motorcycle Honda CB600S 2003
Obr. 1 Testovaný motocykel Honda CB600S 2003

Characteristic of used devices

The first used device was the XL Meter™ Pro Alfa designed to measure the acceleration or deceleration of the vehicle needed to calculate tire adhesion. The device displays data such as maximum speed or the deceleration achieved during the measurement, the length of the braking distance and the braking time. The device must be placed in such a way that its attachment is perpendicular to the road and the axis of the measuring device must be parallel to the axis of the vehicle. Next, we used a digital rollmeter to measure ground distances and to check the results of the braking distance. The measuring range of this device is in the range from 0 to 9999 meters with an accuracy of 0.10 meters.

Fig. 2 Digital rollmeter
Obr. 2 Digitálny rollmeter

Characteristics of work procedures

- Production of a handle for attaching the measuring device to the vehicle and fixing the measuring device to the holder, recording the parameters of the measured vehicle, tires and measurement conditions
- During the measurement the ambient temperature was 27 °C and the road temperature 30.2 °C.
- Carrying out test rides to evaluate the quality of the road and warm up the tested motorcycle
- Performing measurement nine times at speeds of 50, 80, 100 km.h^{-1}. and using different combinations of braking with either the front brake only, the rear brake or both at the same time
- Recording and evaluation of measured values with the XL MeterTM Pro device and measuring the length of the braking distance with a rollmeter
- Based on the measured deceleration values, it is possible to calculate the tire adhesion values.

The adhesion coefficient calculation:

$$\mu = \frac{a}{g} \tag{1}$$

where a is measured deceleration [m.s^{-2}],
g is gravitational deceleration [m.s^{-2}]

RESULTS

In all measurements with the rear brake only, the rear wheel skidded, while the rear wheel lifted into the air when braking from speeds of 75 and 98 km.h^{-1}. Tab. 2 shows the results of measuring the braking distance when braking with the rear brake only, and Fig. 3 shows the characteristics of the deceleration of the motorcycle using the rear brake only. When braking from speeds of 67 and 102 km.h^{-1}, the rear wheel rose again into the air. Tab. 3 shows the results of measuring the braking distance when braking only with the front brake, and Fig. 4 shows the characteristics of motorcycle deceleration using only the front brake.

Table 2 Measurement the braking distance when braking with the rear brake only
Tabuľka 2 Meranie brzdnej dráhy pri brzdení len zadnou brzdou

Measurement	1.	2.	3.
Speed[1)] [km.h^{-1}]	49	65	79
Values measured by rollmeter			
Beginning of the braking track[2)] [m]	57,5	44,7	118,5
End of the braking track[3)] [m]	71,4	77,4	164,5
The length of the braking track[4)] [m]	27,5	32,7	44
Values obtained from the XL-meter			
Length of braking distance[5)] [m]	27,7	47,52	60,2
Braking time[6)] [s]	4,26	5,34	7,13
Deceleration value[7)] [m.s^{-2}]	3,4	3,2	3,3

[1)] Rýchlosť, [2)]Začiatok brzdnej stopy, [3)]Koniec brzdnej stopy, [4)]Dĺžka brzdnej stopy, [5)] Dĺžka brzdnej dráhy, [6)]Čas brzdenia, [7)]Hodnota spomalenia

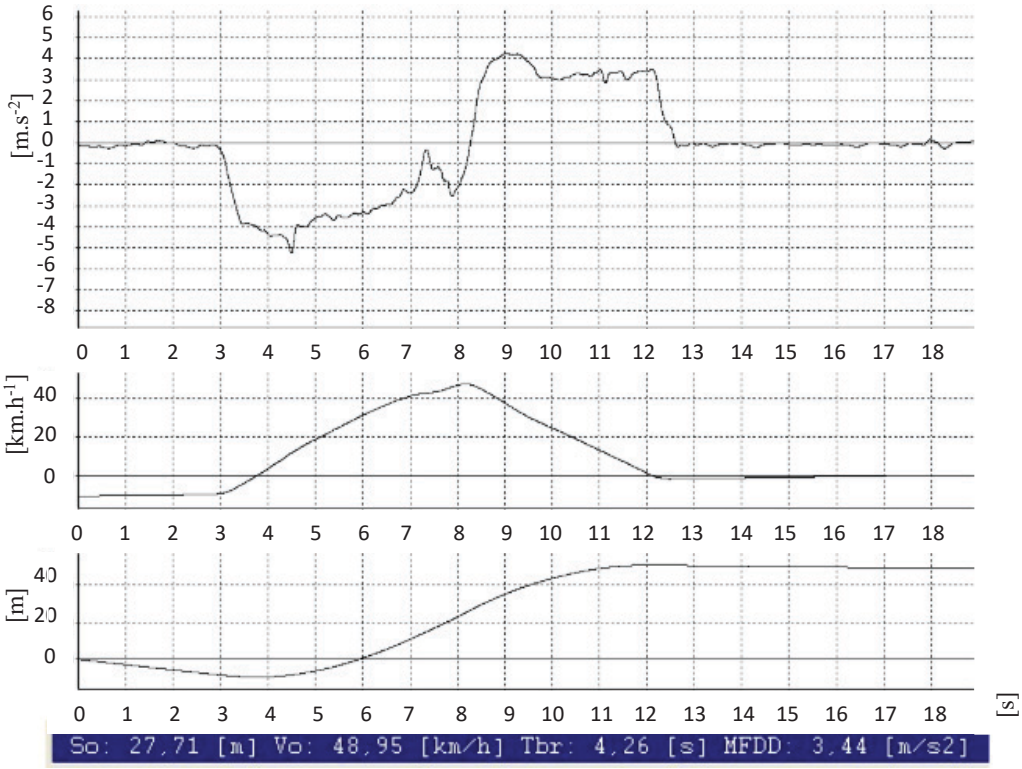

Fig. 3 Characteristics of deceleration of the Honda CB600S using the rear brake, on dry asphalt at a speed of 49 km.h^{-1}, braking time 4,26 s and braking deceleration 3,44 m.s^{-2}
Obr. 3 Charakteristika spomalenia Hondy CB600S zadnou brzdou, na suchom asfalte pri rýchlosti 49 km.h^{-1}, brzdný čas 4,26 s a brzdné spomalenie 3,44 m.s^{-2}

Tab. 3 Measurement of the braking distance when braking with the front brake only
Tabuľka 3 Meranie brzdnej dráhy pri brzdení len prednou brzdou

Measurement	4.	5.	6.
Speed[1)] [km.h^{-1}]	55,6	79,57	102,2
Values measured by rollmeter			
Beginning of the braking track[2)] [m]	36,7	79,0	111,9
End of the braking track[3)] [m]	49,5	104,0	157,1
The length of the braking track[4)] [m]	12,7	25,0	47,1
Values obtained from the XL-meter			
Length of braking distance[5)] [m]	19,5	39,68	57,60
Braking time[6)] [s]	2,12	2,96	3,56
Deceleration value[7)] [m.s^{-2}]	8,8	9,77	9,2

[1)] Rýchlosť, [2)]Začiatok brzdnej stopy, [3)]Koniec brzdnej stopy, [4)]Dĺžka brzdnej stopy, [5)]Dĺžka brzdnej dráhy, [6)]Čas brzdenia, [7)]Hodnota spomalenia

[m.s-

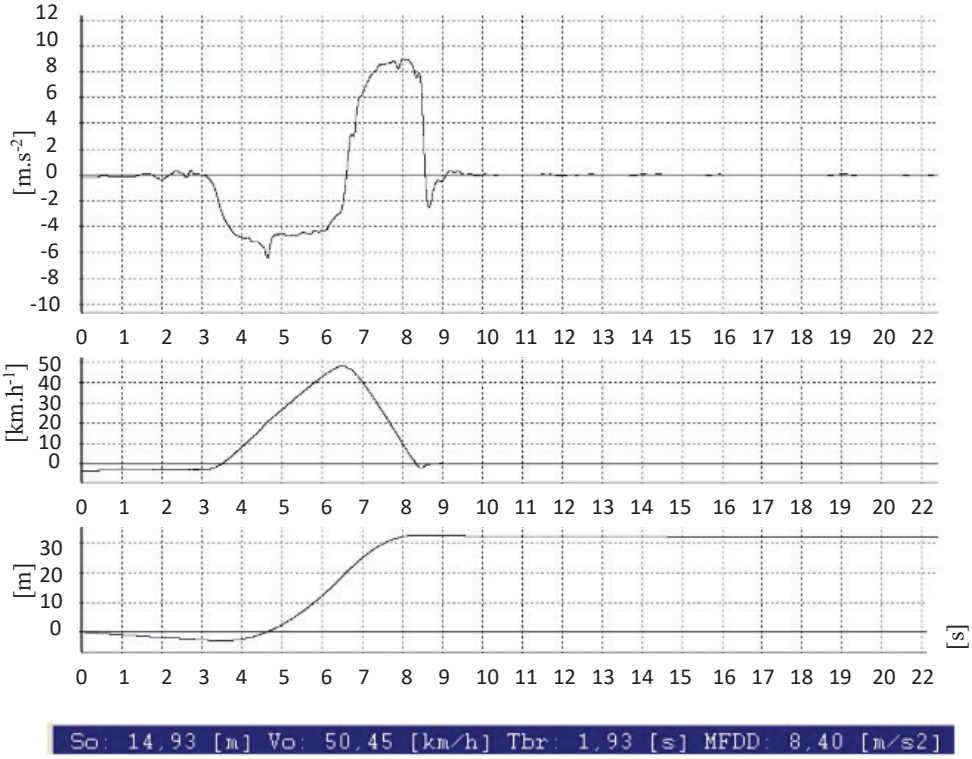

Fig. 4 Characteristics of deceleration of the Honda CB600S using the front brake, on dry asphalt at a speed of 50 km.h^{-1}, braking time 1,93 s and braking deceleration 8,40 m.s^{-2}
Obr. 4 Charakteristika spomalenia Hondy CB600S pomocou prednej brzdy, na suchom asfalte pri rýchlosti 50 km.h^{-1}, brzdný čas 1,93 s a brzdné spomalenie 8,40 m.s^{-2}

Tab. 4 Measurement of the braking distance when braking with both brakes
Tabuľka 4 Meranie brzdnej dráhy pri brzdení oboma brzdami

Measurement	7.	8.	9.
Speed [km.h^{-1}]	50,6	67,1	102,2
Values measured by rollmeter			
Beginning of the braking track [m]	21,0	50,7	122,2
End of the braking track [m]	34,4	67,7	155,9
The length of the braking track [m]	13,4	17,0	33,7
Values obtained from the XL-meter			
Length of braking distance [m]	14,9	28,5	50,8
Braking time [s]	1,93	2,52	3,35
Deceleration value [m.s^{-2}]	8,3	9,6	9,4

[1)]Rýchlosť, [2)]Začiatok brzdnej stopy, [3)]Koniec brzdnej stopy, [4)]DÍžka brzdnej stopy, [5)]DÍžka brzdnej dráhy, [6)]Čas brzdenia, [7)]Hodnota spomalenia

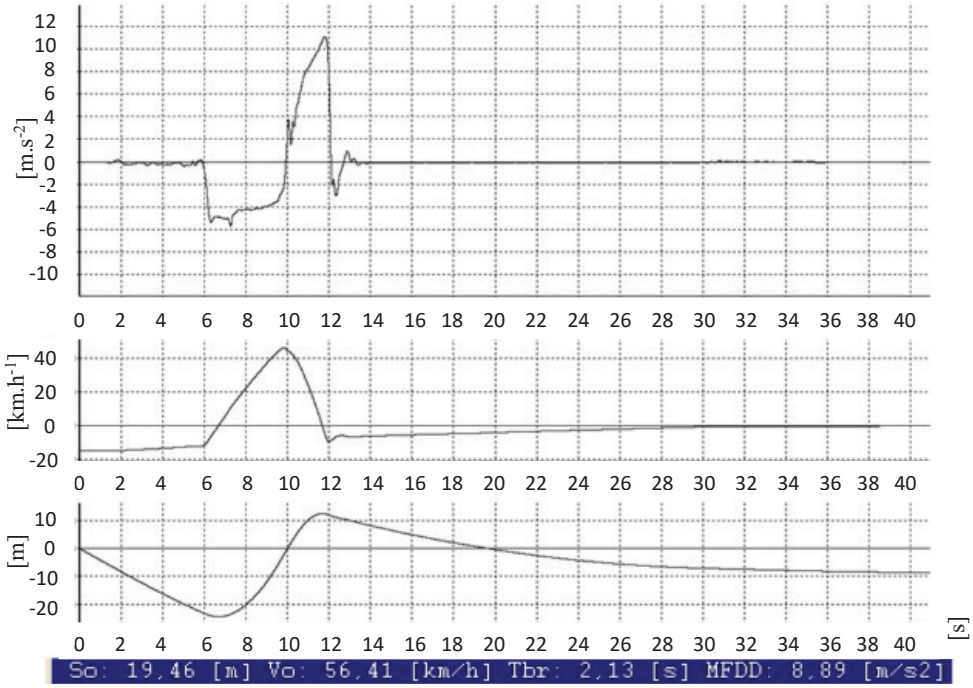

Fig. 5 Characteristics of deceleration of the Honda CB600S using the both brakes, on dry asphalt at a speed of 50,6 km.h^{-1}, braking time 2,13 s and braking deceleration 8,89 m.s^{-2}
Obr. 5 Charakteristika spomalenia Hondy CB600S pomocou obidvoch bŕzd, na suchom asfalte pri rýchlosti 50,6 km.h^{-1}, brzdný čas 2,13 s a brzdné spomalenie 8,89 m.s^{-2}

In Tab. 4 are shown the results of measuring the braking distance when braking with both brakes, and Fig. 5 shows the characteristics of motorcycle deceleration using both brakes. For each measurement, we calculated the adhesion coefficient values, which can be seen in Tab. 5 together with the corresponding deceleration value for the individual speeds and used motorcycle brakes.

Tab. 5 Results of measurements
Tabuľka 5 Výsledky meraní

Speed [km.h^{-1}]	Brakes	Deceleration value [m.s^{-2}]	Gravitational acceleration [m.s^{-2}]	Coefficient of adhesion	Average coefficient of adhesion
49	Rear	3,4	9,81	0,35	0,34
65		3,2		0,33	
57		3,3		0,34	
55.6	Front	8,8		0,90	0,94
79,57		9,77		0,99	
102,2		9,2		0,94	
50,6	Both	8,3		0,85	0,93
67,1		9,6		0,98	
102,2		9,4		0,96	

When braking with the front brake only and with both brakes, the detected values are almost the same, while the highest deceleration was achieved at a speed of 79 km.h^{-1} at a value of 9.77 m.s^{-2} when braking with the front brake only, which corresponds to an adhesion of 0.99, while the lowest adhesion values were achieved at braking with the rear brake only in the value of 0.34. This value cannot be considered the maximum, because when braking with the rear brake only, the weight is transferred to the front wheel and according to relation (1), the entire weight falling on the rear wheel is not used for deceleration, which significantly reduces the braking force from the pad. When braking at the limit with the front brake, the entire gravity force is dynamically transferred to the front wheel, which makes it possible to use the entire weight for braking force, which means that this phenomenon has a great influence on the resulting deceleration achieved. The given method of determining limit adhesion can be considered technically acceptable and correct.

If a cruiser type vehicle or a touring motorcycle were measured, it can be assumed that the adhesion values would be greater on the rear wheel. From the resulting measurement values, it follows that braking with the rear brake is very difficult due to the rapid occurrence of wheel locking and the subsequent threat of loss of stability. Therefore, braking with the rear brake requires greater experience and better dosing of the braking force by the rider himself.

DISCUSSION

Similar measurements and results were achieved by the author Kotek (2017), who also dealt with the evaluation of the adhesion properties of tires they noticed that the braking distance increases with increasing speed and also brake deceleration results increased with increasing speed. They found a braking distance of 31 m at an initial speed of 100 km.h^{-1} with a braking deceleration of 9.8 m.s^{-2}. In his work, the author Novosad (2017) similarly focused on the adhesion properties of road vehicle tires and after evaluating the results he came to similar conclusions. The author found that at an initial speed of 100 km.h^{-1}, the braking distance was 46.3 m with a braking deceleration of 8.9 m.s^{-2} and coefficient of an adhesion 0,907. An author which confirmed the claim of the manufacturers and experts, which speaks of better adhesion properties of summer tires at a temperature higher than 7 °C. Author Očovay (2013) carried out a similar measurement where he observed and tested selected tires on different surfaces and found that winter tires have higher braking deceleration values than summer tires, which is due to the softer winter tire compound used. This was also reflected in the shorter braking distance. The measured braking deceleration values were different, which was caused by different road characteristics and different temperature in each measurement. The author measured the highest value at a speed of 46 km.h^{-1} and found out that the braking deceleration increases with increasing speed due to the greater effect of the ABS system. Similar research was carried out by author Zálešák (2016) who dealt with the issue of investigating summer and winter properties of tires. When measuring summer tires, an author found that at an initial speed of 94.53 km.h^{-1}, the braking distance was 39 m with a braking deceleration of 9.26 m.s^{-2} and an adhesion coefficient of 0.94.

CONCLUSION

This research was focused on measuring the adhesion properties of tires on a test motorcycle of the brand and type Honda CB600S. Within the motorcycle, we used Nankang tires of the Sportiac WF-2 type with size 120/60 R17 on the front wheel and size 180/55 R17 on the rear wheel. We achieved the highest deceleration when braking with the front brake only in the value of 9.77 $m.s^{-2}$ at a speed of 79 $km.h^{-1}$ and with an achieved adhesion of 0.99, on the contrary, we achieved the lowest deceleration values when braking with the rear brake only due to the low load on the rear wheel and dynamic load transfer. From the resulting measurement values, it follows that braking with the rear brake is very difficult due to the rapid occurrence of wheel locking and the subsequent threat of loss of stability. Therefore, braking with the rear brake requires greater experience and better dosing of the braking force by the rider himself. After comparing the results with other authors, we can conclude that our measurement was correct and we fulfilled the research objective and the given method of determining limit adhesion can be considered technically acceptable and correct.

REFERENCES

DOČKAL, V. – KOVANDA, J. – HRUBEC, F. 1998. Tires. Praha: ČVUT. [In Czech: Pneumatiky]. pp 71. ISBN 80-01-01882-2

HUDÁK, A. – VRÁBEĽ, J. 2010. Factors affecting the safety of tire-road contact. In Doprava a spoje, vol. 6, no. 1. [In Slovak: Faktory ovplyvňujúce bezpečnosť styku pneumatiky a vozovky] pp. 99-106. ISSN 1336-7676

HUGO, W. 1994. The big book about motorcycles. Bratislava: Gemini. 191 pp. (In Slovak: Veľká kniha o motocykloch). ISBN 80-7161-096-8

KOLEKTÍV AUTOROV. 2008. The perfect ride on a motorcycle. České Budějovice: Kopp. 212 pp. (In Czech: Dokonalá jízda na motocyklu). ISBN 8072323474

KOTEK, F. 2017. Adhesion properties of tires on the selected surface. Diploma thesis. Nitra: Slovak University of Agriculture, Faculty of Engineering. [In Slovak: Adhézne vlastnosti pneumatík na vybranom povrchu]. pp. 62. Dostupné na: https://opac.crzp.sk/?fn=docview2ChildATLMU&record=DF521320909666631F7BE2F290DD&seo=CRZP-Prehliadanie-pr%C3%A1c

KULHÁNEK, J. 1997. Motor vehicles. Bratislava: Príroda. 4. edition. 248 pp. ISBN 80-07-00973-6.

LIŠČÁK, Š. 2004. Operating characteristics of vehicles. Žilina: EDIS. 177 pp. [In Slovak: Prevádzkové charakteristiky vozidiel]. ISBN 80-8070-247-0.

NOVOSAD, J. 2017. Adhesion properties of road tires. Bachelor thesis. Nitra: Slovak University of Agriculture, Faculty of Engineering. [In Slovak: Adhézne vlastnosti cestných pneumatík]. pp. 48. Dostupné na: https://opac.crzp.sk/?fn=docview2ChildQV9KN&record=998D604438B59F55B68053FC0D22&seo=CRZP-Prehliadanie-pr%C3%A1c

OČOVAY, Ľ. 2013. Testing of selected tires and vehicles. Diploma thesis. Nitra: Slovak University of Agriculture, Faculty of Engineering. 50 pp. [In Slovak: Testovanie vybraných pneumatík a vozidiel. Dostupné na: https://opac.crzp.sk/?fn=docview2ChildA1633A&record=BF2E02CB30820396AAE2356A3158&seo=CRZP-Prehliadanie-pr%C3%A1c

SLOBODA, A. 2008. Construction of wheeled and tracked vehicles. Košice: Vienala. 552 pp. [In Slovak: Konštrukcia kolesových a pásových vozidiel]. ISBN 978-80-89232-28-45.
VERNAREC, Jozef. 2006. Construction and maintenance of vehicles. Nitra: Slovak University of Agriculture. 134 pp. [In Slovak: Konštrukcia a údržba vozidiel]. ISBN 80-8069-693-4.
ZÁLEŠÁK, T. 2016. Adhesion properties of tires and their finding out. Diploma thesis. Nitra: Slovak University of Agriculture, Faculty of Engineering. [In Slovak: Adhézne vlastností pneumatík a ich zisťovanie]. pp. 45. Dostupné na: https://opac.crzp.sk/?fn=docview2ChildK15IUD&record=6CC5FEA37B0036024CF632918D04&seo=CRZP-Prehliadanie-pr%C3%A1c

Corresponding author:
Martin Krasňanský, tel. +421917566904, e-mail: xkrasnansky@uniag.sk

ACTA FACULTATIS TECHNICAE
ZVOLEN – SLOVAKIA

XXIX
2024

SELECTED POSSIBILITIES OF ARTIFICIAL INTELLIGENCE SYSTEMS USE IN MANUFACTURING TECHNOLOGY – A REVIEW

VYBRANÉ MOŽNOSTI VYUŽITIA ALGORITMOV UMELEJ INTELIGENCIE V OBLASTI VÝROBNEJ TECHNIKY – PREHĽAD

Tomáš Čuchor, Peter Koleda

Department of Manufacturing and Automation Technology, Faculty of Technology, Technical University in Zvolen, T. G. Masaryka 24, 960 01, Zvolen, Slovakia, xcuchor@is.tuzvo.sk

ABSTRACT: The use of artificial intelligence algorithms and their properties makes it easier to analyse data and then, based on it, find out the factors that affect it the most. This paper summarizes basics of the algorithm, inner principes of algorithms with examples and usage in terms of problem solving. In this overview several algorithms are mentioned such as: genetic algorithm, decision tree, artificial neural network etc. Each algorithm is suitable for a different type of problem, the article briefly presents their uses for manufacturing and automation. In the conclusion, general recommendations for choosing a suitable algorithm are summarized.
Artificial neural network algorithms and their modifications are used in the modelling of production and machining processes based on the amount of real measured data of these processes. Such models then enable the prediction and trend of monitored variables in real time, e.g. prediction of tool wear and the related quality of the created surface.
Optimization algorithms such as particle swarm or ant colony optimisation, and other genetic algorithms are used in the search for the optimal solution as the shortest sizes (distances) between manufacturing systems. This optimization does not have to be only in terms of time, but e.g. also the costs necessary for the implementation of material flows, energy consumption. When choosing a specific algorithm, the type of measured quantity (e.g. acoustic emission, vibration, power consumption, cutting force) and thus the nature of the output signal of a specific sensor must be considered. It is also necessary to consider the computational complexity and accuracy of the algorithm within the requirements of a specific application, where e.g. algorithms such as decision trees are relatively fast, but not as accurate as algorithms using artificial neural networks.

Key words: artificial intelligence, machine learning, manufacturing technology

ABSTRAKT: Využívanie algoritmov umelej inteligencie a ich vlastností zjednodušuje analyzovanie dát a potom na základe nich zistenie faktorov, ktoré ich najviac ovplyvňujú. Tento článok sumarizuje základné algoritmy umelej inteligencie, ich vnútorné princípy s príkladmi na ich využitie v oblasti výrobnej techniky a obrábania. V tomto prehľade je spomenutých niekoľko algoritmov

ako: genetický algoritmus, rozhodovací strom, umelá neurónová sieť a ďalšie. Každý algoritmus je vhodný pre iný typ problému, v článku sú stručne uvádzané ich použitia pre výrobu a automatizáciu. V závere sú sumarizované všeobecné odporúčania pre výber vhodného algoritmu.
Algoritmy na princípe umelej neurónovej siete a ich modifikácie sa využívajú pri modelovaní výrobných a obrábacích procesov na základe množstva reálnych nameraných údajov týchto procesov. Takéto modely potom umožňujú predikciu a trend sledovaných premenných v reálnom čase, napr. predikcia opotrebovania nástroja a s tým súvisiacej kvality vytvoreného povrchu.
Pri hľadaní optimálneho riešenia ako najkratšie veľkosti (vzdialenosti) medzi výrobnými systémami sa využívajú optimalizačné algoritmy ako optimalizácie zhlukom častíc alebo kolóniou mravcov a ďalšie genetické algoritmy. Táto optimalizácia nemusí byť len z časového hľadiska, ale napr. aj náklady potrebné na realizáciu materiálových tokov, spotrebu energie. Pri výbere konkrétneho algoritmu treba brať do úvahy typ meranej veličiny (napr. akustická emisia, vibrácie, príkon, rezná sila) a tým aj charakter výstupného signálu konkrétneho snímača. Taktiež je potrebné zvážiť výpočtovú náročnosť a presnosť algoritmu v rámci požiadaviek konkrétnej aplikácie, kde napr. algoritmy ako rozhodovacie stromy sú relatívne rýchle, ale nie také presné ako algoritmy využívajúce umelú neurónovú sieť.

Kľúčové slová: umelá inteligencia, strojové učenie, výrobná technika

INTRODUCTION

Finding suitable solution to a problem arising in technical practice is not always an easy task. In order to find a solution to a problem is imperative that we know all factors that relate to and affect it. After rigorous analysis we can determine the appropriate solution. Not always we have resources necessary to analyse and solve the issue, while using algorithms can save time and resources. Machine learning and algorithms of machine learning are tools that are most suitable for finding optimal solution not only for manufacturing process. This article describes some algorithms used to solve problems aimed at technical practice, with a particular focus on manufacturing technology. Coming forth are indirect methods of measuring machining parameters. Measured data can be used to create models. These algorithmic models offer subsequent advantage in adaptive and predictive control.

The purpose of this article is to describe the basic principles and method of artificial intelligence algorithms used for purpose in manufacturing sector. Selection of algorithms is made on the basis of their spread especially for machining and related control and automation.

Article is divided into two main sections Machine learning and Neural network. In the conclusion section, recommendations for choosing a suitable algorithm are summarized.

MACHINE LEARNING

Machine learning (ML) is a branch of artificial intelligence (AI) that focuses on the using data and algorithms to enable AI to imitate the way that humans learn without being programmed explicitly (Pimenov *et al*. 2023), gradually improving its overall accuracy. Machine learning can be divided into three main parts such as decision process, an error function and model optimization process.

- Decision Process: Overall machine learning algorithms are used to make a prediction or classification. Based on some of input data, algorithm will produce an estimate about a pattern in the data.
- Error Function: Function that evaluates the prediction of the model. If there are known examples, an error function can make a comparison to assess the accuracy of the model.
- Model Optimization Process: In case that model can fit better to the data points in the training set, then weights are adjusted to reduce the discrepancy between the known examples and the model estimates. The algorithm will repeat this iterative "evaluate and optimize" process, updating weights autonomously until a threshold of set accuracy has been met (IBM 2021).

Machine learning can be also divided to fall to categories according to supervision of learning.

- Supervised machine learning – defined by its use of labelled datasets to train algorithms to classify data or predict outcomes accurately. As input data is put into the model, the model adjusts its weights until it has been fitted appropriately. This occurs as part of the cross-validation process to ensure that the model avoids overfitting (resulting in a model that cannot make accurate predictions or conclusions) or underfitting (unable to capture the relationship between the input and output variables accurately) Supervised learning helps organizations solve a variety of real-world problems at scale.
- Unsupervised machine learning uses machine learning algorithms to analyse and cluster unlabelled datasets (subsets called clusters). These algorithms discover hidden patterns or data groupings without the need for human intervention. This method's ability to discover similarities and differences in information make it ideal for exploratory data analysis, cross-selling strategies, customer segmentation, and image and pattern recognition. Two common approaches for this are principal component analysis (PCA) and singular value decomposition (SVD).
- Semi-supervised learning offers a medium between supervised and unsupervised learning. During training, it uses a smaller labelled data set to guide classification and feature extraction from a larger, unlabelled data set. Semi-supervised learning can solve the problem of not having enough labelled data for a supervised learning algorithm (Zhang et al. 2010).

In order to utilize algorithms for problem solving we need to know about all available information about data in order to predict adequate solution as written by Hastie *et al.* (2011). Machine learning offers advantages in manufacturing sector. From predictive maintenance, quality control, customer personalization, supply and demand gives competitive advantage to company. Implementation purpose of machine learning and its advantages are shown in Fig 1.

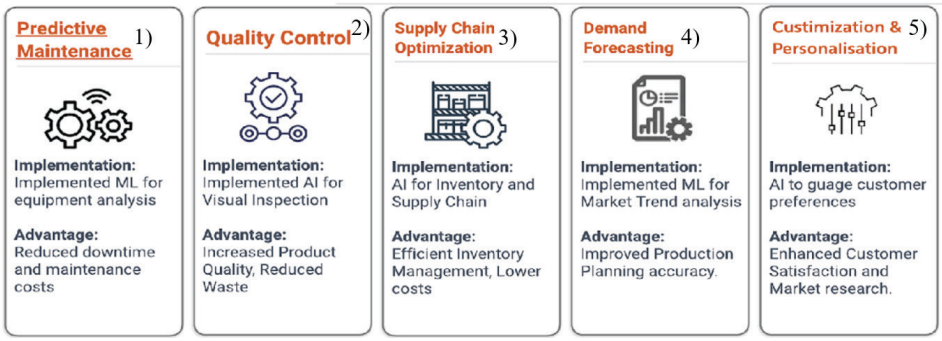

Fig. 1 Advantage of machine learning in manufacturing (Sanapala 2023)
Obr. 1 Výhody strojového učenia vo výrobe
[1)]prediktívna údržba, [2)]Kontrola kvality, [3)]Optimalizácia dodávateľov, [4)]Predpoveď požiadaviek, [5)] Prispôsobenie

Practical examples of machine learning can already be found in our daily life whenever it's a facial recognition of security systems, product recommendation or automated filtering of spam. As machine learning gets better so does its incorporation in everyday life. Same thing can be said about manufacturing sector. For every manufacturing process that can be automated, shortened or improved leads to increase in productivity or quality.

DEEP LEARNING

The way in which deep learning and machine learning differ is in how each algorithm learns. "Deep" machine learning can use labelled datasets, also known as supervised learning, to inform its algorithm, but it does not necessarily require a labelled dataset. The deep learning process can ingest unstructured data in its raw form, and it can automatically determine the set of features which distinguish various categories of data from one another (IBM, 2024). Figure 2 shows scope of deep learning.

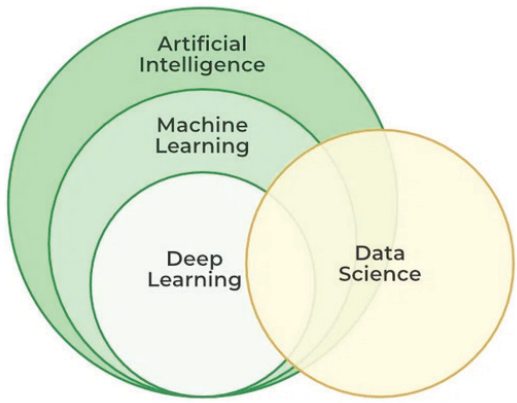

Fig. 2 Scope of Deep learning (Introduction to Deep learning, 2024)
Obr. 2 Obsah hlbokého učenia

Modern monitoring, diagnostic and prediction procedures are based on the collection of a large amount of data from various sensors. Their processing uses the methods of deep learning, especially in the form of artificial neural networks, also due to the penetration of Industry 4.0 into all production sectors (Serin *et al*. 2020).

As mentioned by Hosain at al. deep learning has led to notable progress in enhancing the interpretability of AI systems enabling users to understand the decision-making processes of complex models (Hosain *at al.* 2024).

Deep learning can practically learn everything given time and data. Range of learning is enormous it can generate translation of language in real time to complex decision making in manufacturing processes. As working with machines precision on two machines of same product can be achieved with slightly different manufacturing parameters. In order to utilize machine to its fullest potential its needed to learn about every machine individually, time required to boost production of these machine is not worth the investment with parameters changing over time. With integration of deep learning into manufacturing we can let machine to decide production parameters. It cost little in terms of time which would person investigating issue take.

REINFORCEMENT MACHINE LEARNING

Reinforcement machine learning is a machine learning model that is like supervised learning, but the algorithm isn't trained using sample data. This model learns as it goes by using trial and error. A sequence of successful outcomes will be reinforced to develop the best recommendation or policy for a given problem. Simplified example can be seen in the fig. 3 where robot is trying to find diamond and avoid fires while finding shortest route. If the robot finds a path, the value of the fields through which the path leads to the destination is increased. Otherwise, this value is reduced. The result is a sequence of fields with the highest values.

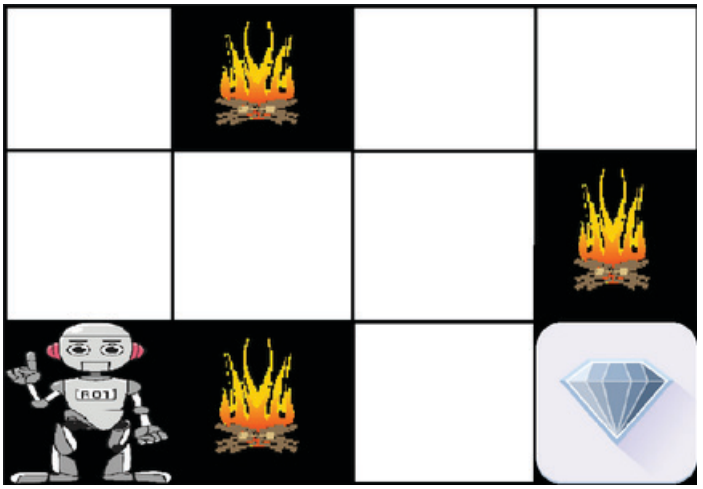

Fig. 3 Graphical explanation of reinforcement machine learning (Reinforcement learning, 2023)
Obr. 3 Grafické vysvetlenie spätnoväzobného strojového učenia

Reinforcement learning can optimize production scheduling, predictive maintenance, defect detection, inventory levels, quality forecasting, and automated process control - all leading to improved manufacturing efficiency.

Reinforcement learning systems learn optimal policies over time by analysing production data. They adapt dynamically to minimize bottlenecks, downtime, waste, and costs while maximizing throughput and quality. The key benefit is continuous self-improvement. As reinforcement learning experience more data, they get smarter at boosting efficiency across the whole manufacturing system.

Mentioned by Mahesh (2020) reinforcement learning is one of three basic machine learning paradigms and best choice is determined by amount of data in dataset. The reinforcement learning method is modelled as a Markov decision process, what means that the most important feature is to work with a reward and penalty system (Sutton *et al*. 2018). Trial and error is sometime one of the best ways to achieve results. As humans the more we fail more we learn same thing can be said about algorithms. Practical examples are in automotive industry. Driving assistants interacts with an environment, receives feedback and, based on that, adjusts its decision-making strategy. Sensor on parking camera detects something in back and driver is trying to back up, computer makes decision, so it does not allow car backup.

GLOBAL MACHINING PREDICTION AND OPTIMIZATION

Finding solutions that maximize or decrease certain criteria is called optimalization. Important in optimalization is decreasing expenses with production of a thing or a service, while maximizing profits and decreasing number of materials needed to create goods or services. Optimization is today commonly used in many various fields ranging from engineering applications such as program optimalization, coding, software to management in stores used for logistics. In short optimalization is making processes or part of process more efficiently or consume less resources. There are many ways to make manufacturing processes more efficient. Use of algorithms to analyse process is fundamental. Most used algorithms nowadays are artificial neural network (ANN), adaptive neuro-fuzzy logic (ANFL), genetic algorithms (GA), whale optimization algorithm (WAO), ant lion optimization algorithm (ALOA), grasshopper optimization algorithm (GOA). Global optimalization techniques are applied to optimize manufacturing process of mechanical components by optimalization of production parameters. Current trend in optimization is hybrid formulation and application. (Okokpujie 2023)

ARTIFICIAL NEURAL NETWORKS (ANN) AS GLOBAL PREDICTION TECHNIQUE

Artificial neural network is a biological inspired nonlinear algorithm-based model that compresses artificial neurons linked to brain cells. This neural system can be taught and learn to execute tasks such as classification, decision making and prediction. In short, an artificial neuron network is a computational model that mimics the way nerve cells work in the human brain. In principle neural network is given input information and output in-

formation than network tries to establish connection between input and output parameters. Neural network has three layers: input layer, hidden layer and output layer (Fig. 4). Input layer receives input data from outside and sends it to hidden layer. This data is at hidden layer where it interacts with assigned weight of each hidden layer. After computing in neural network data is transferred to output layer.

There are several types of neural networks used for prediction analysis they are as follows:

- Radiant basis function Neural Network,
- Recurrent Neural Network (RNN),
- Convolutional Neural Network,
- Kohonen Self Organizing Neural Network,
- Long/Short term Memory,
- Modular Neural Network,
- Feedforward Neural Network- Artificial neuron.

Seven steps to train model using Artificial Neural Network according to (Aravindpai 2024):

- Model approximate solution,
- Set up data,
- Decide on network architecture,
- Neural network training,
- Boost generalization abilities of neural network,
- Test outcome of neural network,
- Create functional model.

Models of neural network depends on number of factors, including training procedures, network architecture and activation function. Performance of neural network also depends on these factors. Image bellows shows factors and training process of neural networks.

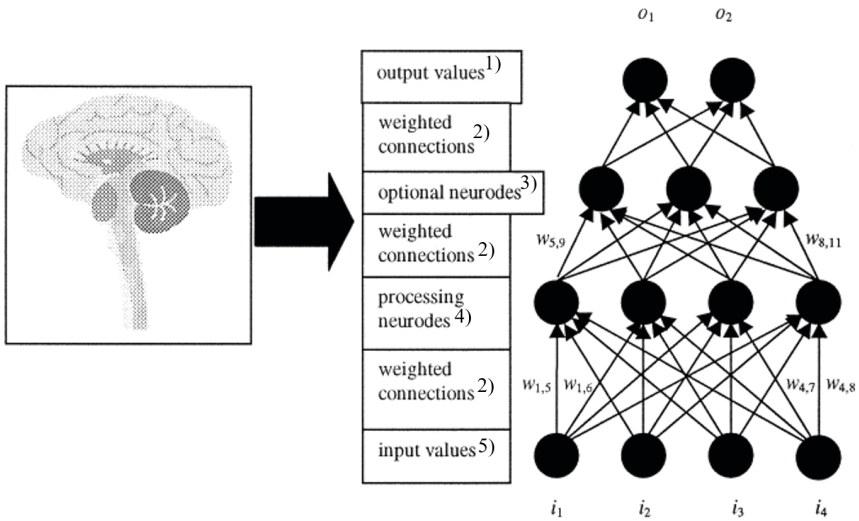

Fig. 4 Sample artificial neural network architecture (Jinia *et al*. 2021)

Obr. 4 Vzorka architektúry umelej neurónovej siete

[1)]výstupné hodnoty, [2)]váhové prepojenia, [3)]voliteľné neuróny, [4)]spracúvajúce neuróny, [5)]vstupné hodnoty

ARTIFICIAL NEURAL NETWORKS

Artificial neural network can be used for data analysis in applications such as pattern recognition, prediction, system identification and control as written by Dongare et al. (2012).

Practical examples of neural network can be seen in autonomous cars detecting traffic sighs and lanes and driving within the lanes with adequate speed limit with safe breaking distance. Many works in the field of manufacturing are focused on the prediction of tool wear with various ANN modifications (Sun *et al.* 2020, Cai *et al.* 2020). Huang *et al.* (2019) used convolutional neural network to process the vibration and cutting force data for tool prediction during milling.

NEURAL NETWORK

Neural network is revolutionizing computing with their ability to "think". Capability of interpreting data and accounting are some of smart solutions. Four steps that neural network uses to operate effectively are:

- Associating or training enables neural networks to 'remember' patterns. If the computer is shown an unfamiliar pattern, it will associate the pattern with the closest match present in its memory.
- Classification or organizing data or patterns into predefined classes.
- Clustering or the identification of a unique aspect of each data instance to classify it even without any other context present.
- Prediction, or the production of expected results using a relevant input, even when all context is not provided upfront.

Neural networks require high throughput to carry out these functions accurately in near real-time. This is achieved by deploying numerous processors to operate parallel to each other, which are arranged in tiers.

The neural networking process begins with the first tier receiving the raw input data. After that, each consecutive tier gets the results from the preceding one. This goes on until the final tier has processed the information and produced the output. Every individual processing node contains its database, including all its past learnings and the rules that it was either programmed with originally or developed over time. These nodes and tiers are all highly interconnected.

Neural network application areas are quite wide as written by Abiodun Oludare *et al.*(2018). AI but undoubtedly will be extremely important in the future. Benardos and Vosniakos (2002) proposed a NN modelling approach for face milling operations to predict surface roughness (Ra) (Benardos, Vosniakos, 2002). Shrivastava and Singh (2018) used the ANN model for cutting zone prediction in CNC machining.

ADAPTIVE NEURO-FUZZY INTERFERENCE SYSTEM

Adaptive neuro-fuzzy interference system (ANFIS) is framework that combines benefits of fuzzy logic (FL) and artificial neural networks (ANNs). Fuzzy logic is a heuristic approach that allows for more advanced decision-tree processing and better integration

with rules-based programming. Models ANFIS offer rapid learning capacity and adaptive interpretation skills in order to fulfil needs of complicated patterns and comprehend non-linear interactions. Adaptive neuro-fuzzy interference system was created in 1993 by J. S. Roger Jang and is commonly recognized as universal estimator. In system final output is weighted average of the output of all logic rules, and rule outputs are linear combination of input variables and constants.(Jang 1993)

As mentioned by Salleh *et al.* (2017) various structural and parameters optimization techniques have been proposed, however, there is enough room of improvement in ANFIS architecture. ANFIS can easily handle nonlinear functions and predict with great accuracy (Jang, 1993). Many researchers specially in machining field reported the application of ANFIS.

Veluchamy *et al.* (2021) predict the surface roughness values with ANFIS model during turning Al7075. Sharma *et al*. (2020) studied wet turning of AISI D3 steel and measured and influence of machining parameters. Mohd *et al*. (2017) stated that to reduce computational complexity by architectural modifications as well as effizrning ofcient training procedures need improvement.

GENETIC ALGORITHM

Principe of genetic algorithm (GA) is based on natural selection, meaning that the mechanism propel biological evolution is adapt to environment. Search technique known as GA is used to address optimalization issues in machine learning. Methods of algorithms are crucial because it resolves challenging issues that would otherwise take lot of time. These algorithms have lot of real-world application such as data centres, electronic circuits design, code breaking picture processing and artificial creativity. As mentioned by Gill and Kaur fuzzy genetic approach in which the system log files are analysed to detect the user behaviour of the system. (Gill & Kaur 2013). The generational genetic algorithm (GGA), steady state genetic algorithm (SSGA), steady-generational genetic algorithm (SGGA) are different forms of GA . GA belongs to the larger class of evolutionary algorithms (EA) (Albadr *et al*. 2020).

Manufacturing processes show the capabilities of GA to work on different kind of neural networks. Kumar *et al.* (2020) applied the GA during hard turning of EN 24 steel . They studied various parameters like as material removal rate, surface roughness, temperature and forces. Finally, they performed optimized using GA. Durairaj and Gowri (2013) optimized the tool life and surface roughness with the application of genetic algorithm.

Genetic algorithms can be used in production scheduling to optimize the allocation of resources and minimize production costs. Genetic algorithms choose current best population and uses them as parents for next generation this process is looping till adequate solution is found. Graphical example of principle of genetic algorithm can be seen in Fig. 5.

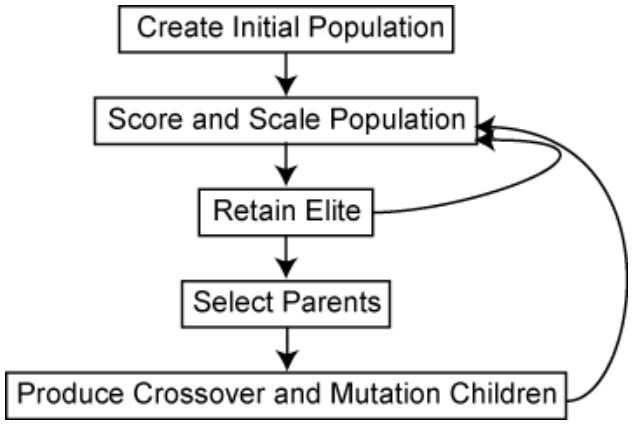

Fig. 5 Principle of genetic algorithm (Matlab 2024)
Obr. 5 Princíp genetického algoritmu

PARTICLE SWARM OPTIMIZATION

Particle Swarm Optimization (PSO) was proposed by Kennedy and Eberhart in 1995. Sociobiologists believe a school of fish or a flock of birds that moves in a group "can profit from the experience of all other members".

Suppose there is a swarm (a group of birds). Now, all the birds are hungry and are searching for food. These hungry birds can be correlated with the tasks in a computation system which are hungry for resources. Now, in the locality of these birds, there is only one food particle. This food particle can be correlated with a resource. As we know, tasks are many, resources are limited. So this has become a similar condition as in a certain computation environment. Now, the birds don't know where the food particle is hidden or located. In such a scenario, how the algorithm to find the food particle should be designed. If every bird will try to find the food on its own, it may cause havoc and may consume a large amount of time. Thus on careful observation of this swarm, it was realized that though the birds don't know where the food particle is located, they do know their distance from it. Thus the best approach to finding that food particle is to follow the birds which are nearest to the food particle.

In other words, while a bird flying and searching randomly for food, for instance, all birds in the flock can share their discovery and help the entire flock get the best food. While we can simulate the movement of a flock of birds, we can also imagine each bird is to help us find the optimal solution in a high-dimensional solution space and the best solution found by the flock is the best solution in the space. Particle swarm optimalization is bio-inspired algorithm; its purpose is search for best solution in problem area. It differs from other optimization techniques. Its difference is that it does not have dependence on gradient or any differential form of objective it simply requires objective to function. This is a heuristic solution because proving that optimal overall position is in some cases impossible to reach. However, solution found by Particle Swarm Optimization is quite close to the optimal parameters. Another property of Particle Swarm Optimization is that it can be

parallelized easily. As manipulating multiple parameters to find the optimal solution, each parameter can be updated in parallel (Liu *et al*. 2022).

Lim and Isa (2015) put forward a hybrid PSO algorithm which introduced the fuzzy reasoning and a weighted particle to construct a new search behavior model to increase the search ability of the conventional PSO algorithm. Besides the information of the global best and individual best particles, Shin and Kita (2014) took advantage of the information of the second global best and second individual best particles to promote the search performance of the original PSO.

The PSO algorithm is often used as an improved or in combination with other algorithms. Xu *et al*. (2020) proposed a reasoning system for milling process, where they also used the vibration particle swarm optimization algorithm, where input parameters were tool wear and cutting condition and output power consumption and cutting vibration.

WHALE OPTIMIZATION ALGORITHM

The Whale Optimization Algorithm (WOA) is a novel intelligent optimization algorithm proposed by Australian researchers in 2016. It is inspired by the collective hunting behaviour of whales in the natural world (Nadimi-Shahraki *et al*. 2023).

This algorithm offers advantages such as simplicity in principles, fewer parameters, and ease of implementation. It has successfully been applied to solve a variety of problems in fields such as image retrieval, image segmentation, medicine, energy, neural networks, feature selection, wind speed prediction, key recognition, and sentiment analysis, among others. However, WOA still faces challenges when applied to nonlinear, high-dimensional, and complex optimization problems, including issues related to low optimization precision, slow convergence, and susceptibility to local convergence. To address these challenges, researchers have proposed various strategies to enhance WOA. Improvements to WOA primarily fall into two categories: enhancing WOA through improvements in initialization, parameter settings, and algorithm structure; and leveraging the complementary strengths of WOA with other algorithms. Chart of whale optimization algorithm can be seen in Fig. 6. It shows steps by step of algorithm from start to finish.

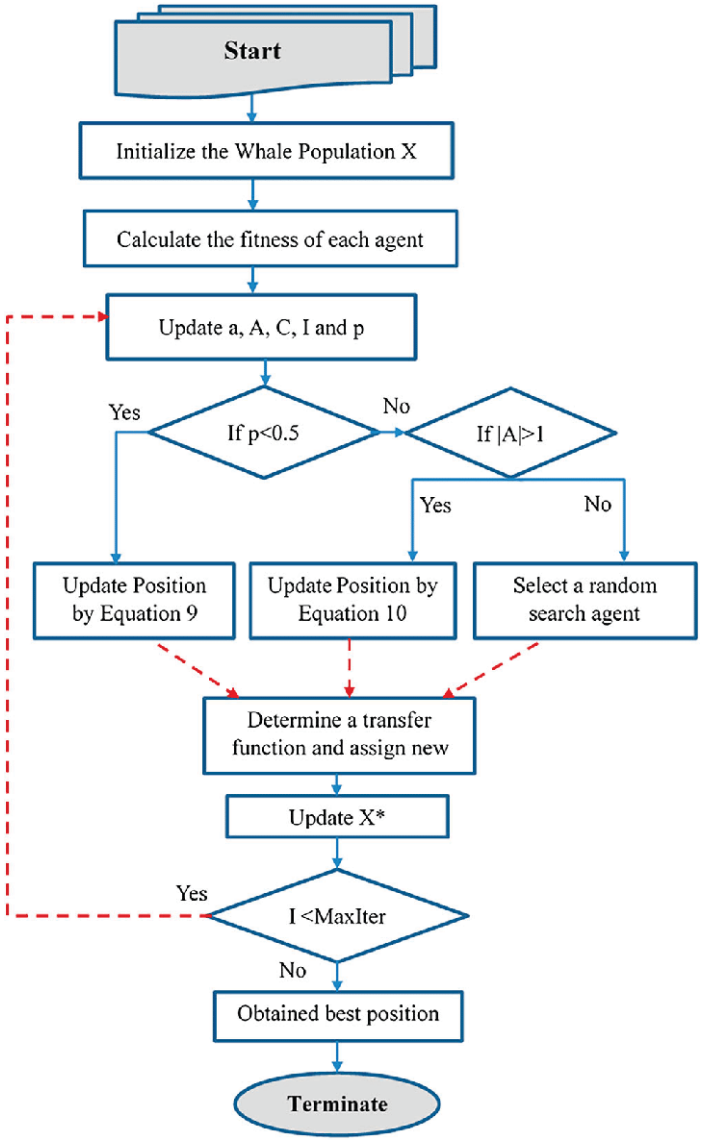

Fig. 6 Whale optimization algorithm chart
Obr. 6 Graf algoritmu optimalizácie veľrýb

Direct inspiration for a Whale Optimisation Algorithm was special hunting method of humpback whales which is called bubble-net feeding method. It is a hunting method unique for this species written by Mirjalili and Lewis (2016). An extensive study was conducted on 29 mathematical benchmark functions to analyse exploration, exploitation, local optima avoidance, and convergence behaviour of the algorithm. WOA is most commonly used with allocation of resources.

ANT COLONY OPTIMIZATION ALGORITHM

Ant colony optimization (ACO) is inspired by the foraging behaviour of ants. At core is communication between parameters to find shortest path. ACO algorithm has strong robustness as well as good dispersed calculative mechanism. ACO can be combined easily with other methods, it shows well performance in resolving the complex optimization problem. ACO optimizes a problem by having an updated pheromone trail and moving these ants around in the search space according to simple mathematical formulae over the transition probability and total pheromone in the region. At each iteration, ACO generates global ants and calculates their fitness. Update pheromone and edge of weak regions. If fitness is improved, then move local ants to better regions, otherwise select new random search direction. Update ant pheromone and evaporate ant pheromone. The continuous ACO is based on both local and global search. Local ants have the capability to move toward latent region with best solution with respect to transition probability of region (Dorigo 2004). Graphical explanation of Ant colony optimization can be seen in Fig. 7. ACO searched for best available parameters in manufacturing in order to find suitable parameters for production.

As study of combination effective strategies, a multi-strategy adaptable ant colony optimization algorithm was proposed to improve the deficiencies of Ant colony optimization by Cui *at a*l. (2024). Zhang et al. (2020) proposed multi-role adaptive collaborative mechanism with two communication strategies: elite attribute learning strategy and pheromone balancing strategy. ACOs are applied to many combinatorial optimization problems for finding the shortest distances of configurable elements. Maniraj *et al*. (2017) used this algorithm for minimizing the capital cost of the reconfigurable manufacturing systems.

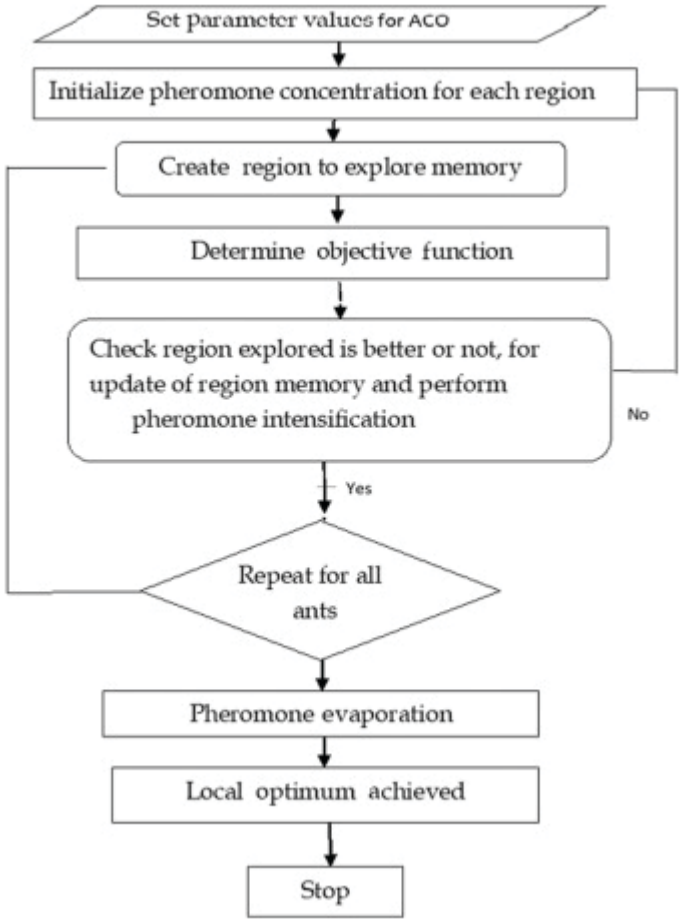

Fig. 7 Graphical explanation of Ant colony optimization
Obr. 7 Grafické vysvetlenie optimalizácie kolóniou mravcov

DECISION TREE

Decision tree has a hierarchical tree structure consisting of a root node, branches, internal nodes, and leaf nodes. Decision trees are used for classification and regression tasks, providing easy-to-understand models. A decision tree is one of the most powerful tools of supervised learning algorithms. It builds a flowchart-like tree structure where each internal node denotes a test on a factor of criteria, each branch represents an outcome of the test, and each leaf node (terminal node) holds a class label. It is constructed by recursively splitting the training data into subsets based on the values of the attributes until a stopping criterion is met, such as the maximum depth of the tree or the minimum number of samples required to split a node (Saini 2024).

During training, the Decision Tree algorithm selects the best criteria to split the data based on a metric such as entropy or "Gini impurity", which measures the level of impurity or randomness in the subsets. The goal is to find the criteria that maximizes the information gain or the reduction in impurity after the split. Graphical illustration of nodes is shown in figure bellow. Fig. 8 shows each node as parent that has to choose between nodes bellow them. Child is selected based on criteria defined in parent node.

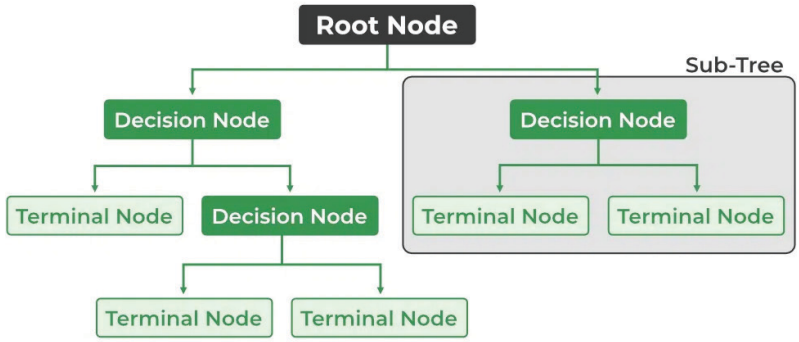

Fig. 8 Nodes in Decision tree (Decision Tree 2024)
Obr. 8 Uzly v rozhodovacom strome

As parameters for splitting decision trees are crucial it's important to choose most optimal parameters as mentioned by Rokach and Maimon (2005).

Both categorical and numerical data can be handled easily by Decision trees. Sofuoglu *et al.* (2019) optimized the different turning processes using ANN, classification and regression tree (CART) and SVM. They optimized surface roughness depth of cut and tool temperature with these methods. The results depicted that the CART method gave better results as compared with other methods.

Decision trees are highly flexible and suitable for a wide array of problems such as decision making, quality control or predicting customer behaviour. According to Kuncheva random forest and boosting trees are the most common ensemble models applied to tool's monitoring. Random Forest makes use of variation of Decision Trees called Random Tree, whereas Boosting allows the use of an extensive sort of base models (Kuncheva, 2014).

CONCLUSION

Choice of most suitable algorithms depends on the initial inputs and overall accuracy of the objective. Each algorithm suited for different conditions and manufacturing processes Elements of AI are mainly used in the prediction, modeling and monitoring of various machining processes, especially milling, turning, grinding, and to a lesser extent others.

However, there are few available works that would be devoted to the machining of wood-based materials in this way and scope.

ANN algorithms and their modifications are used in the modelling of production and machining processes based on the amount of real measured data of these processes. Such

models then enable the prediction and trend of monitored variables in real time, e.g. prediction of tool wear and the related quality of the created surface.

Optimization algorithms such as PSO or ACO and other genetic algorithms are used in the search for the optimal solution as the shortest sizes (distances) between manufacturing systems. This optimization does not have to be only in terms of time, but e.g. also the costs necessary for the implementation of material flows, energy consumption. When choosing a specific algorithm, the type of measured quantity (e.g. acoustic emission, vibration, power consumption, cutting force) and thus the nature of the output signal of a specific sensor must be taken into account. It is also necessary to consider the computational complexity and accuracy of the algorithm within the requirements of a specific application, where e.g. Algorithms such as decision trees are relatively fast, but not as accurate as algorithms using ANNs.

ACKNOWLEDGMENT

This research was funded by APVV-20-0403 „FMA analysis of potential signals suitable for adaptive control of nesting strategies for milling wood-based agglomerates“ and the EU NextGenerationEU through the Recovery and Resilience Plan for Slovakia under the project No. 09I03-03-V05-00016

REFERENCES

ABIODUN O. I., JANTAN A. , OMOLARA A. E.,. DADA K. V, ABD N., MOHAMED E., ARSHAD H., 2018 State-of-the-art in artificial neural network applications: A survey.

ALBADR, M. TIUN S., AYOB M.,AL-DHIEF F., 2020, Genetic Algorithm Based on Natural Selection Theory for Optimization Problems. Symmetry. Available on: http://dx.doi.org/10.3390/sym12111758

ARAVINDPAI P.,2024, Analyzing types of neural network in deep learning , Available on: https://www.analyticsvidhya.com/blog/2020/02/cnn-vs-rnn-vs-mlp-analyzing-3-types-of-neural-networks-in-deep-learning/

BENARDOS P., VOSNIAKOS, G.C., 2002. Prediction of surface roughness in CNC face milling using neural networks and Taguchi‘s design of experiments. Robotics and and Computer-Integrated Manufacturing.

CAI, W., ZHANG, W., HU, X., LIU, Y. 2020. A hybrid information model based on long short--term memory network for tool condition monitoring. Journal of Intelligent Manufacturing, 31, 1497–1510.

CUI J., WU L., HUANG X., XU D., LIU C., XIAO W., 2024, Multi-strategy Adaptable Ant Colony Optimization Algorithm and Its Application in Robot Path Planning, Volume 288, ISSN 0950-7051, Available on: https://www.sciencedirect.com/science/article/pii/S0950705124000947

Decision Tree, 2024. [online] [cit. 2024-04-23]. Available on https://www.geeksforgeeks.org/decision-tree/

DONGARE A.D., KHARDE R.R., KACHARE A. D., 2012 Introduction to Artificial Neural Network, vol 2, issue 1available on: https://citeseerx.ist.psu.edu/document?repid=rep1&type=pdf&doi=04d0b6952a4f0c7203577afc9476c2fcab2cba06

DORIGO M., STÜTZLE T., 2004, Ant Colony Optimization, MIT Press. ISBN 0-262-04219-3

DURAIRAJ, M., GOWRI, S., 2013, Parametric optimization for improved tool life and surface finish in micro turning using genetic algorithm. Procedia Engineering, 64, 878–87. Available on:

https://doi.org/10.1016/j.proeng.2013.09.164
GILL N., KAUR H., 2013, Host based Anomaly Detection using Fuzzy Genetic Approach (FGA) available on: https://www.researchgate.net/publication/260973150_Host_based_Anomaly_Detection_using_Fuzzy_Genetic_Approach_FGA
HASTIE T., TIBSHIRANI R., FRIEDMAN J., 2011, The Elements of Statistical Learning: Data Mining, Inference, and Prediction (Springer, New York, 2011).
HOSAIN MD.T., JIM J. R., MRIDHA M.F., KABIR MD. M., 2024, Explainable AI approaches in deep learning: Advancements, applications and challenges, Computers and Electrical Engineering, Volume 117, ISSN 0045-7906, available on: https://www.sciencedirect.com/science/article/pii/S0045790624001745
HUANG, Z., ZHU, J., LEI, J., LI, X., TIAN, F. 2019. Tool wear predicting based on multi-domain feature fusion by deep convolutional neural network in milling operations. Journal of Intelligent Manufacturing, 31, 953–966.
IMB, 2024, *What is Machine Learning (ML)*? [online] [cit. 2024-04-23]. Available on: <https://www.ibm.com/topics/machine-learning>
Introduction to Deep Learning, 2024 [online] [cit. 2024-04-23]. Available on: https://www.geeksforgeeks.org/introduction-deep-learning/
JANG, J.S. 1993. ANFIS: Adaptive-network-based fuzzy inference system. IEEE Transactions on Systems, Man, and Cybernetics, 23, 665–685
JINIA, A. J., MAURER, T. E., MEERT, Ch. A., HUA, M. Y. CLARKE, S. D., KIM, H., WENTZLOFF, D. D., POZI, S. A., 2021. An Artificial Neural Network System for Photon-Based Active Interrogation Applications. In IEEE Access, vol. 9, pp. 119871-119880, doi: 10.1109/ACCESS.2021.3108406.
KENNEDY J. EBERHART R., 1995 "Particle swarm optimization," Proceedings of ICNN'95 International Conference on Neural Networks, Perth, WA, Australia, , pp. 1942-1948 vol.4, doi: 10.1109/ICNN.1995.488968.
KUNCHEVA, L. I. 2014. Combining pattern classifiers: methods and algorithms. John Wiley & Sons. 350 p. ISBN:9780471210788
KUMAR, A., PRADHAN, S. K., JAIN, V., 2020, Experimental investigation and optimization using regression genetic algorithm of hard turning operation with wiper geometry inserts. Materials Today Proceedings, 27, 2724–2730. Available on: https://doi.org/10.1016/j.matpr.2019.12.191
LIM H.W., ISA N.A.M., 2015, Adaptive division of labor particle swarm optimization. Expert Systems with Applications Volume 42, Issue 14, 15 August 2015, Pages 5887-5903 available on: https://doi.org/10.1016/j.eswa.2015.03.025
LIU Z., SUN Y., XING C., LIU J., HE Y., ZHOU Y., ZHANG G., 2022, Artificial intelligence powered large-scale renewable integrations in multi-energy systems for carbon neutrality transition: Challenges and future perspectives, Energy and AI, Volume 10, ISSN 2666-5468, Available on: https://doi.org/10.1016/j.egyai.2022.100195
MAHESH B:, 2020, Machine Learning Algorithms - A Review Available on: https://www.researchgate.net/publication/344717762_Machine_Learning_Algorithms_-A_Review
MANIRAJ, M., PAKKIRISAMY, V., JEYAPAUL, R. 2017. An ant colony optimization–based approach for a single-product flow-line reconfigurable manufacturing systems. *Proceedings of the Institution of Mechanical Engineers, Part B: Journal of Engineering Manufacture*. Vol. 231, no. 7, pp. 1229-1236. doi:10.1177/0954405415585260
Mathworks Help Center, 2024. *What Is the Genetic Algorithm? [online] [cit. 2024-04-23].* Available on: https://uk.mathworks.com/help/gads/what-is-the-genetic-algorithm.html
MIRJALILI S., LEWIS A., 2016,The Whale Optimization Algorithm, Pages 51-67, ISSN 0965-9978, Available on: https://www.sciencedirect.com/science/article/pii/S0965997816300163
MOHD N., TALPUR N., HUSSA K. ,2017, Adaptive Neuro-Fuzzy Inference System: Overview, Strengths, Limitations, and Solutions, 527-534

https://link.springer.com/chapter/10.1007/978-3-319-61845-6_52
NADIMI-SHAHRAKI, M., ZAMANI, H., ASGHARI VARZANEH, Z.,2023, A Systematic Review of the Whale Optimization Algorithm: Theoretical Foundation, Improvements, and Hybridizations. Available on: https://doi.org/10.1007/s11831-023-09928-7
OKOKPUJIE, I.P., TARTIBU, L.K. (2023). Global Machining Prediction and Optimization. In: Modern Optimization Techniques for Advanced Machining. Studies in Systems, Decision and Control, vol 485. Springer, Cham. https://doi.org/10.1007/978-3-031-35455-7_4
PIMENOV, D. Y, BUSTILLO, A., WOJCIECHOWSKI, S., SHARMA, V. S., GUPTA, M. K. 2023. Artificial intelligence systems for tool condition monitoring in machining: analysis and critical review. In *Journal of Intelligent Manufacturing*, no. 34, pp. 2079-2121. https://doi.org/10.1007/s10845-022-01923-2
Reinforcement learning, 2023 [online] [cit. 2024-04-23]. Available on https://www.geeksforgeeks.org/what-is-reinforcement-learning/
ROKACH L., MAIMON O., 2005, Top-down induction of decision trees classifiers-a survey, IEEE Transactions on Systems Man and Cybernetics Part C: Applications and Reviews, vol. 35, no. 4, pp. 476-487,
SAINI A., 2024, What is Decision Tree? Available on: https://www.analyticsvidhya.com/blog/2021/08/decision-tree-algorithm/
SALLEH, M.N.M., TALPUR, N., HUSSAIN, K., 2017, Adaptive Neuro-Fuzzy Inference System: Overview, Strengths, Limitations, and Solutions. In: Tan, Y., Takagi, H., Shi, Y. (eds) Data Mining and Big Data. DMBD 2017. Lecture Notes in Computer Science(), vol 10387. Springer, Cham. https://doi.org/10.1007/978-3-319-61845-6_52
SANAPALA, P., 2023. AI/ML Advantage in Manufacturing. Linkedin.com. Available on https://www.linkedin.com/pulse/aiml-advantage-manufacturing-padma-sanapala-vrqtc
SERIN, B., SENER, B., OZBAYOGLU, A. M., UNVER, H. O. 2020. Review of tool conditon monitoring in machining and opportunities for deep learning. In *The International Journal of Advanced Manufacturing Technology*, no. 109, pp. 953-974. https://doi.org/10.1007/s00170-020-05449-w
SHRIVASTAVA, Y., SINGH, B. POSSIBLE, 2018, Way to Diminish the Effect of Chatter in CNC Turning Based on EMD and ANN Approaches. Arab J Sci Eng 43, 4571–4591. https://doi.org/10.1007/s13369-017-2993-1
SHARMA, V., KUMAR, P., PRAKASH MISRA J., 2020, Cutting force predictive modelling of hard turning operation using fuzzy logic. Materials Today Proceedings, 26, 740–740. Available on: https://doi.org/10.1016/j.matpr.2020.01.018.
SHIN Y., KITA E., 2014, Search performance improvement of particle swarm optimization by second best particle information. Applied Mathematics and Computation Volume 246, 1 November 2014, Pages 346-354 available on: https://doi.org/10.1016/j.amc.2014.08.013
SOFUOGLU, M. A., ÇAKIR, F. H., KUSHAN, M. C., ORAK, S., 2019, Optimization of different non-traditional turning processes using soft computing methods. Soft Computing, 23, 5213–5231. Available on: https://doi.org/10.1007/s00500-018-3471-8
SUN, H., ZHANG, J., MO, R., ZHANG, X. 2020. In-process tool condition forecasting based on a deep learning method. Robotics and Computer-Integrated Manufacturing, 64, p. 101924. Available on: https://doi.org/10.1016/j.rcim.2019.101924
SUTTON, R. S., BARTO A. G., BACH, F. 2018. Reinforcement learning and introduction. The MIT Press. 552 p. ISBN 9780262039246
VELUCHAMY B., KARTHIKEYAN N., RADHA KRISHNAN B., MATHALAI SUNDARAM C., 2021, Surface roughness accuracy prediction in turning of Al7075 by adaptive neuro-fuzzy inference system, Materials Today: Proceedings, Volume 37, Part 2, Pages 1356-1358, ISSN 2214-7853, Available on: https://www.sciencedirect.com/science/article/pii/S2214785320350410
ZHANG D., YOU X., LIU S., PAN H., 2020,Dynamic Multi-Role Adaptive Collaborative Ant Co-

lony Optimization for Robot Path Planning , IEEE Access, vol. 8, pp. 129958-129974, Available on: https://ieeexplore.ieee.org/document/9141250
ZHANG Y.,2010, New Advances in Machine Learning. InTech. Available on: http://dx.doi.org/10.5772/225.
XU, L., HUANG, C., LI, C., WANG, J., LIU, H., WANG, X. 2020. Estimation of tool wear and optimization of cutting parameters based on novel ANFIS-PSO method toward intelligent machining. In *Journal of Intelligent Manufacturing*, no. 32, pp. 77–90.

Corresponding author:
Tomáš Čuchor, xcuchor@is.tuzvo.sk